NTNU

Norwegian University of
Science and Technology

Rational analysis of Nordlaks' "Havfarm" aquastructure concept for exposed waters

Lars Sunde Gjengseth

Marine Technology
Submission date: June 2017
Supervisor: Jørgen Amdahl, IMT
Co-supervisor: Nicolas Marchal, Bureau Veritas Norway

Norwegian University of Science and Technology
Department of Marine Technology

MASTER THESIS 2017

For

Stud. Techn. Lars Sunde Gjengseth

Rational analysis of Nordlaks' "Havfarm" aquastructure concept for exposed waters

Rasjonelle analysemetoder anvendt påNorlaks' "Havfarm" havbrukskonsept for eksponerte farvann

Marine fish farming is in rapid development. Dimensions are expected to increase and locations are being moved to areas exposed to more energetic waves and stronger currents. This leads to several challenges: Strong currents can cause large net deformations and affect largely the hydroelastic behavior of the cage. Wave overtopping may occur in during extreme waves, so nonlinear effects matter. Viscous effects are essential for the loading on the net structures, as well as the wake inside the cage. Another issue is the effect of biofouling on the net loading. Waves and currents are of concern for the volume within the fish cage and thedesign of mooring lines. Operations with a wellboat moored to the fish farm become challenging. For example the ship propeller can suck the net and this can partially break the net and cause fish escape.

Collapse of fish farms, with large-scale fish escape to the level experienced in the past, will not be tolerated by the society. New and extreme loading scenarios need to be properly designed for by means of "first principles" methods to meet required safety levels and performance.

Rational design requirements for aquaculture structures must be developed based on simulations of the governing physical phenomena, structural load effects and

structural resistance. That is, the motion of the fish farm in irregular seas must be simulated, along with accurate assessment of load effects (stresses) in the load carrying structures. Fatigue, ultimate strength and accidental limit state conditions should be addressed. Simplified design oriented load cases, e.g. static load cases, should be developed and calibrated against fundamental numerical simulations.

The intention of this work is to contribute to this development by analysing a realistic new concept proposed for exposed waters; the **Nordlaks**' "Havfarm" structure. Havfarm, which will be deigned for operation in significant wave height in the range of 5 m, may be installed outside the island Hadsel in Vesterålen. The design of the Havfarm concept is carried out by **NSK Ship design AS**.

The work, which will be carried out in collaboration with **Bureau Veritas Norway**, is proposed carried out in the following steps:

1. Describe the Havfarm concept, the rational behind the concept and discuss briefly how it differs form other proposed concepts for exposed waters.
2. Perform a model of a typical transverse section in Mars and verify the strength of the transverse section
3. Investigate the structural drawings and arrangement to see what will be the main dimensioning parameters of the Havfarm concept
4. Based on the updated information form Nordlaks/N ship design establish a finite element model for global analysis with BV software. If a net model is available, the net shall be included in the finite element model. Initially, the analysis shall be carried out in the frequency domain. Perform eigenvalue analysis.
5. Establish transfer function for global loads and selected key response quantities for the main dimensioning parameters (hull girder loads, for example). Estimate the characteristic extreme response levels to the extent possible. Investigate whether it is possible to establish an equivalent design wave to determine the characteristic ultimate limit state (ULS) response quantities
6. Compare the results with those obtained by NSK Ship design, if available.
7. If time permits perform a sensitivity study of the net model and how it affects the key response quantities.
8. Conclusions and recommendations for further work in the master thesis project.

Literature studies of specific topics relevant to the thesis work may be included.

The work scope may prove to be larger than initially anticipated. Subject to approval from the supervisor, topics may be deleted from the list above or reduced in extent.

In the thesis the candidate shall present his personal contribution to the resolution of problems within the scope of the thesis work.

Theories and conclusions should be based on mathematical derivations and/or logic reasoning identifying the various steps in the deduction.

The candidate should utilise the existing possibilities for obtaining relevant literature.

Thesis format

The thesis should be organised in a rational manner to give a clear exposition of results, assessments, and conclusions. The text should be brief and to the point, with a clear language. Telegraphic language should be avoided.

The thesis shall contain the following elements: A text defining the scope, preface, list of contents, summary, main body of thesis, conclusions with recommendations for further work, list of symbols and acronyms, references and (optional) appendices. All figures, tables and equations shall be numerated.

The supervisor may require that the candidate, in an early stage of the work, presents a written plan for the completion of the work. The plan should include a budget for the use of computer and laboratory resources, which will be charged to the department. Overruns shall be reported to the supervisor.

The original contribution of the candidate and material taken from other sources shall be clearly defined. Work from other sources shall be properly referenced using an acknowledged referencing system.

The report shall be submitted in two copies:

- Signed by the candidate
- The text defining the scope included
- In bound volume(s)

- Drawings and/or computer prints which cannot be bound should be organised in a separate folder.
- The report shall also be submitted in pdf format along with essential input files for computer analysis, spreadsheets, MATLAB files etc in digital format

Ownership
NTNU has according to the present rules the ownership of the thesis. Any use of the thesis has to be approved by NTNU (or external partner when this applies). The department has the right to use the thesis as if the work was carried out by a NTNU employee, if nothing else has been agreed in advance.

Thesis supervisor
Prof. Jørgen Amdahl

Supervisor Bureau Veritas Norway
Nicolas Marchal

Contact person at NSK Ship Design:
Håkon Ådnanes

Deadline:, June 10 2017

Trondheim, January 11, 2017

Jørgen Amdahl

Preface

This master thesis is part of my 5 year study at Norwegian University of Sience and Technology (NTNU) by the Department of Marine Technology.

The master thesis is carried out in collaboration and supervision with Bureau Veritas Norway as well as NSK Ship Design which is the designer of the Havfarm structure

In association with the work done in this master thesis there are people I would like to thank. Their help and guidance have been very helpful and valuable.

First of all I would like to thank Nicolas Marchal in Bureau Veritas for guidance and discussions. I would also tank you for giving me the opportunity to do my master thesis in collaboration with Bureau Veritas Norway and with you as a supervisor. Your guidance have been motivational and highly appreciated.

I would also like to thank my supervisor Professor Jørgen Amdahl. Your guidance and efforts to arrange this master thesis in collaboration with Bureau Veritas and NSK Ship Design is much appreciated.

Lastly I would like to thank Håkon Ådnanes and NSK Ship Design for openly and willingly sharing information regarding the design and development of the Havfarm project. This master thesis would not be possible to do without it.

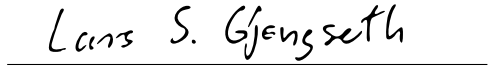

Lars Sunde Gjengseth

Trondheim, June 10, 2017

Summary

A global analysis of Nordlaks' Havfarm concept has been conducted. In order to do so three equivalent design waves targeting the ultimate limit state response of the vertical bending, horizontal bending and torsional moment have been established. There have been built both a hydro and a structural model of the Havfarm in order to be able to perform a seakeeping analysis and to evaluate the capacity of the structure. The modelling process has by far been the most time consuming part of this thesis. Models have been subjected to continues updates. Best engineering judgment have been used during the modelling of the Havfarm in order to best be able to represent the real physics of the structure while still trying to include special characteristics of the structure. That is the lice skirts and the nets of the Havfarm. The lice skirts was neglected at an early stage as it was clear that there was no good way to include them in the seakeeping analysis. However, an effort was made to include the lice skirts, unfortunately it turned out that the only way to model them would change the hydrodynamic properties such as the water plane area and the GM_L in a way that the model no longer would represent the physical case in a god way. Thus the lice skirts was also neglected.

The hydro and the FE model have been modelled as detailed as possible according to the structural drawnings provided by NSK Ship Design. This for both main dimensions, scantlings and weight distribution of steel weight and ballast tanks.

Bureau Veritas software have been used to preform the seakeeping analysis and to transfer loads from the hydrodynamic model to the FE model. The seakeeping analysis was performed in the frequency domain with headings ranging from 0^o - 180^o with 15^o increment and periods ranging form 3 - 30 second. Based on the seakeeping analysis RAOs for internal loads were established which in turn was used to determine the ULS response of the internal loads. The results was used to establish the following three EDWs used to evalueate the strucutres ULS capacity.

Design Wave	Target Load	Wave Height	Wave Heading	Wave Period
1	VBM	3.93[m]	135$[^o]$	13.4[s]
2	HBM	5.76[m]	105$[^o]$	6.3[s]
3	TM	6.19[m]	105$[^o]$	6.3[s]

When subjected to the EDWs the FEA results of the Havfarm indicates that the top and bottom pontons will experience von Mises stresses exceeding 400[MPa] over large areas, and high stress concentrations in sharp connectiuons exceeding 600 [MPa]. This indicates that the Havfarm do not have sufficient capacity.

Sammendrag

En global analyse av Nordlaks Havfarm-konsept er utført. For å gjøre det, er tre ekvivalente designbølger rettet mot det ultimate grenseforholdsresponsen av den vertikale bøynings-, horisontal bøynings- og vridningsmoment blitt etablert. Det har vært bygget både en hydro og en struktur modell av Havfarm for å kunne utføre en sjødyktighetsanalyse og å evaluere kapasiteten til strukturen. Modelleringsprosessen har langt på vei vært den mest tidkrevende delen av denne oppgaven vært. Modellene har blitt gjenstand for kontinuerlige oppdateringer. Konstruksjonsvurdering har vært brukt under modelleringen av Havfarmen for best å avgjøre hvordan den virkelige fysikken i strukturen best kan representeres, samtidig som det er forsøket å inkludere spesielle egenskaper av strukturen. Dette er da spesielt lusskjørtene og nettene på Havfarm. Lusskjørtene ble forsømt på et tidlig stadium, da det var klart at det ikke var mulig åinkludere dem i sjødyktighetsanalysen på en god måte. Imidlertid ble det gjort en innsats for å inkludere lusskjørtene, men det viste seg dessverre at den eneste måten å modellere dem ville endre de hydrodynamiske egenskapene som vannplanområdet og GM_L på en måte som gjorde at modellen ikke lenger ville representere den virkelige fysikken i strukturen på en god måte. Lusskjørtene ble dermed også forsømt.

Hydro- og FE-modellen er modellert så detaljert som mulig i henhold til strukturelle tegninger levert av NSK Ship Design. Dette for både hoveddimensjoner, stivere, tverrammer og vektfordeling av stålvekt og ballasttanke.

Bureau Veritas-programvare har blitt brukt til å gjennomføre sjødyktighetsanalysen og å overføre laster fra den hydrodynamiske modellen til FE-modellen. sjødyktighetsanalysen ble utført i frekvensdomenet med innkommende bølge retninger som varierte fra 0^o til 180^o med 15^o inkrement og perioder som varierer fra 3 til 30 sekunder. Basert på sjødyktighetsanalysen ble det etablert RAOer for interne belastninger, som i sin tur ble brukt til å bestemme ULS-responsen for de interne belastningene. Resultatene ble brukt til å etablere følgende tre EDWer som ble brukt til å evaluere strukturens ULS kapasitet.

Design Bølge	Kritisk last	Bølge Høyde	Bølge retning	Bølge Periode
1	VBM	3.93[m]	$135[^o]$	13.4[s]
2	HBM	5.76[m]	$105[^o]$	6.3[s]
3	TM	6.19[m]	$105[^o]$	6.3[s]

Når FEA-resultatene fra Havfarm blir utsatt for EDWs, indikerer det at topp- og bunnpontoner vil oppleve von Mises spenninger over 400 [MPa] over store om-

råder, og høye spenningskonsentrasjoner i skarpe forbindelser som overstiger 600 [MPa]. Dette indikerer at Havfarm ikke har tilstrekkelig kapasitet.

Contents

List of Tables

List of Figures

List of Abbreviations

α	Angle between the flow direction and the net normal vector in the direction of the flow
β	Initial angle against the flow
κ	Pressure drop coefficient
λ	Mesh size of the net
ρ	Density of water
θ	Angle between the current direction and the normal vector of the net panel
A^F	Tube area
A^N	Area of the net panel normal to the flow direction
A^P	Area of net panel parallel to the flow
$c(x, \dot{x})$	damping coefficient associated with the motion degree of freedom
C_D	
C_D^F	Drag coefficient for the tube
C_D	Drag coefficient as function of angle between net normal and flow direction
C_L	Lift coefficient as function of angle between net normal and flow direction
e_T	Unit tangential vector defined in the direction from the upper end to the lower end point of the net panel

$f_{H_sT_p}(h.t)$ long term distribution of the sea state characteristics, h_s and t_p

$F_{X_{3h}}(x)$ long term distribution of the 3-hour maximum response, X_{3h}

$k(x, \dot{x})$ stiffness coefficient associated with the motion degree of freedom

N_c Number of cages in direction to the flow

N_N Number of cages in direction normal to the flow

U_∞ Free current velocity

A Area of net panel

D Twine diameter

F(t) external loading action on the mass in the direction of the selected degree of freedom

m mass of the system

Sn The ratio between the area covered by the threads in the screen and the total area of the screen

U Current velocity

u mean flow through the net

x Generalized motion, can be a translation or a rotation

Chapter 1

Introduction

During the past 50 years a very efficient food production of Atlantic Salmon without any agricultural subsidies has arisen in Norway. In 2013 Norway produced 1,3 million tones of salmon and trout and exported sea food worth 61 billion NOK. Production of salmon and trout make almost 42,3 billion of the exported sea food[15]. Both current and earlier governments as well as the industry it self have expressed their ambitions of increased production. Central reports have suggested that an increase three times of today's production by 2030 and five times of today's production by 2050 is possible[15]. To realize these ambitions of increased productions some problems needs to be solved. Where the physical expansion should take place, how to eliminate the lice and sickness problems we have in the conventional industry today and lastly how to avoid large-scale fish escape in the future are all questions that need to be answered.

This master thesis will review and perform a globla analysis of Nordlaks' promising HAVFARM concept which seems to give a good solution to the mentioned problems above. The design of the "Havfarm" structure is carried out by NSK Ship Design AS. A thorough description of the "Havfarm" concept will follow in the later chapters but to give the reader an idea of the scope of the structure an illustration of the structure is given in figure 1.1.

1.1 Problem Definition

The problem definition of this thesis was made by professor Jørgen Amdahl with some changes made by Nicolas Marchal in Bureau Veritas Norway. The Master thesis text can be found in the front of this thesis, however with reference to the same numeration as in the problem text, the points addressed in this project thesis

Figure 1.1: Concept illustration of Nordlaks' offshore fish farm together with a wellboat on port side and a feed carrier on starboard side (Illustration by NSK Ship Design AS)

will be listed here:

1. The whole point is included.
2. Not included, this should be done, and is suggested as further work. This will be a good way to also make a control of FEA results.
3. This point in not spesifically included, however it is performed as a process of the evaluation of the structural drawings during the modelling of the FE model.
4. Included.
5. Included
6. Iincluded, motion RAOs established in the master thesis is compared with RAOs made available from NSK Ship Design.
7. Not included as elements needed to model the lice skirts and nets in Hydrostar was not made available yet. This point is suggested for furhter work when these elments are ready.
8. Included

1.2 Challanges in the Conventional Fish Farming Industry

Figure 1.2 shows the development of the amount of Norwegian farmed salmon sold over the past few years. As can be clearly seen form the figure there has been an enormous increase in tones of salmon sold. As the government and the industry aims to five double the production of salmon within 2050, it is clear that more farming locations are needed [15]. Traditionally farm sites have been located close to shore where the sea-cages have been sheltered. As a result of this the water exchange in the cage have been limited [16]. As the farms will increase in numbers as well as the size of the farms, it is clear we are running out of good suitable locations. Thus we need to look to more offshore locations. This will also ensure greater water exchange in the cage [16]. Another challenge as the farms are getting

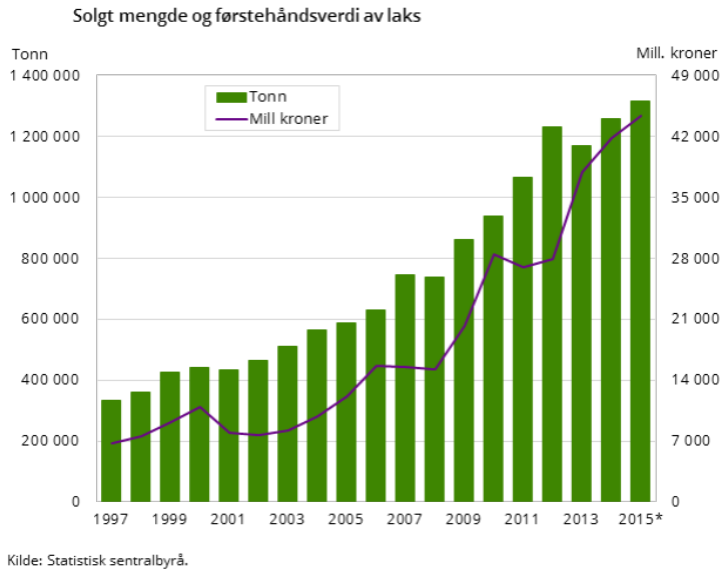

Figure 1.2: Development of sale of Norwegian farmed salmon in tonnes and billion NOK (Figure: Statistics Norway) [27]

bigger is the imminent risk of a large scale fish escape. The amount of salmons held at one location increased by 50% through out the industry during 2005 to 2009. As the amount of fish increases in each cage, the potential consequences of a breakdown of the fish cage and a large-scale fish escape also increases. If a single cage contains hundreds of thousands of cultured salmon a potential collapse of the structure can result in an escape where the cultured fish easily will outnumber the wild populations, which in turn may cause ecological and genetic impacts on the wild population [16].

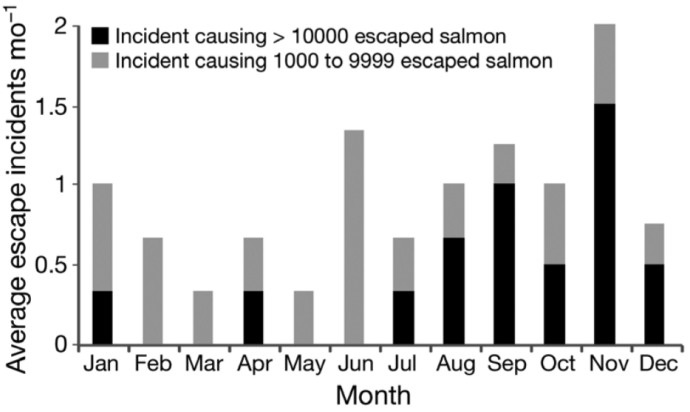

Figure 1.3: Seasonal escape of Atlantic salmon reported to the Norwegian Fisheries Directorate between 1 September 2006 and 31 December 2009. Figure taken from [16]

According to [16] 68% of the reported fish escapes in Norway between 2006 to 2009 are due to structural failure of equipment. These failures are typically caused by severe environmental forces in combination with fatigue or installation or operational errors (human errors). From figure 1.3 it can also observed that most of the large-scale escapes occur during the autumn months when storms are frequent along the coast. This could suggest that a thorough analysis of the design before it is built is well worth the time and money and could prevent large-scale fish escape.

Lastly the industry is facing challenges regarding lice and general health problems among the cultured salmon. In 1986 an experiment was conducted at Karlshamn in Sweden to detect differences between inshore manually fed and offshore automatically fed rainbow trout. From the experiment Tore Sveälv conclude that (1) the mortality was reduced by over 50% among the offshore farmed rainbow trout, (2) that there exists a relationship between an offshore environment and high quality fish and lastly (3) as a result of the increased swimming activity in the offshore cage gives the rainbow trout a slimmer body shape with less viscera fat[1] [34]. However these results may be promising it should be noted that due to the way the experiment was conducted it is impossible to determine that the improved water quality and higher fish activity were the only reason to the reduced mortality, for further details about the experiment the reader is referred to Sveälvs article [34].

If a fishfarm is properly designed to resist the harsh offshore environment it looks like the answer to the fish-farming industry's problem would be to move the farm sites offshore.

[1] Defined as viscera (stomach emptied of feed) including fat but excluding kidney

1.3 Fish Farm Designs

A brief review of different fish farm designs will be given in this section. Different designs will be suitable for different locations and will also affect the farming environment which in turn can affect whether or not the fish will thrive in the cages.

1.3.1 Traditional Design

Due to Norways long coastline with multiple fjords and islands there is lots of locations sheltered from wind and waves. This has resulted in the most common design in Norway which consist of a floating framework with a net cage suspended underneath with weights to ensure tension in the net. Figure 1.4 shows a typical traditional fish farm site. The design is typically located in shallow and sheltered areas and moored with multiple mooring lines to keep it in place. These kind of fish farms are dependent on natural current and tidal water ti ensure sufficient water exchange on the site [34]. The floating structure is typically made of plastic material, but also wood, steel, aluminum or fiberglass. Several of these structures may be located together in one location and sometimes also with a with a raft housing an office, feeding control unit and feed storage to increase the scale and reducing cost of operations.[1]. They can also be of a circular or a squared shape, however according to Sveälv a circular shape will give the cultured fish a more natural environment which it will utilize more effectively [34].

A limitation of this design is if it is subjected to large current forces the net deformations may become large and reduce the volume of the cage. SINTEF Fisheries and Aquaculture conducted a study of two full-scale comercial Atlantic salmon farms conducted of deformations in relation to incoming current. At one farm for a critical current speed of $0.13m^{-1}$ the volume of the net was reduces by 20%, while for the other a critical current speed of $0.35m^{-1}$ reduced the volume by 40%. This will affect how the fish will thrive in the farm [19].

1.3.2 Closed Cage at Sea

Hauge Aqua has developed a closed system concept. An illustration of the concept is shown in figure 1.5. The ambition of this concept is to provide an alternative platform for production compared to the traditional designs. The key idea to this concept is to have complete control of everything going into and out from the system. By keeping the fish in a closed system it will be easier to keep control over what goes into and out of the system. This will make it easier to keep the lice on the outside, which is one of the biggest problems in the conventional industry today. Since the system is closed and complete control of water intake and outflow infection pressure between pens and sites is dramatically reduced. The risk of

Figure 1.4: Traditional fish farm design (http://www.floroby.no)

fish escape will also be greatly reduced as a result of the robust and closed unit. Such a system also opens up for new locations as the system isn't depending on high current for water flow since the all the water is pumped. This opens for new sheltered locations as well as traditional locations. However, this concept is still in development phase and not ready for production [2].

1.3.3 The Havfarm Concept

The Havfarm concept is a design developed by NSK Ship Design in conjunction with Nordlaks. The concept is shown in figure 1.1. The intentions of the Havfarm concept is to move fish farming to offshore locations. NSK Shipdesign describes the Havfarm concept as "an aquaculture ship that could be the beginning of a sustainable revolution in the fish farming industry".

Although the structure looks like a ship it would be more accurate to describe it as a floating truss structure with the nets suspended beneath. With an over all length of 431 meters, a breadth of 54 meters and nets going to a depth of 60 meters the structure will be able to contain 10 000 tonnes of salmon in six nets. The Havfarm will be equipped with steel lice skirts which will prevent contamination of lice from outside the Havfarm. Unlike other fish farm concepts the Havfarm Structure will only be moored at one point, in the bow. This single point mooring allows for weather vaning, and it will also increase the spreading area for waste products 27 times compared to an ordinary pens [9]. This is illustradetd in figure 1.6. The vessel is characterized by submerged pontoons providing buoyancy and a small

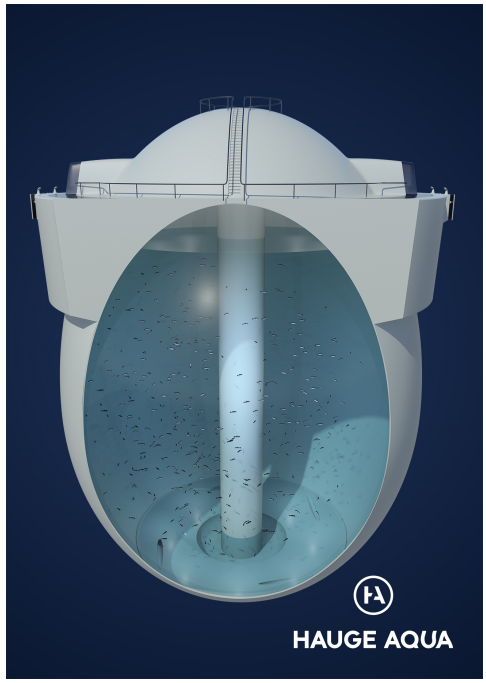

Figure 1.5: Hauge Aqua has developed a closed system concep figure taken from (http://www.haugeaqua.com/Technology/)

water plane, this would imply large natural periods in heave, pitch and roll.

1.3.4 Other Offshore Fish Farm Designs

Ocean Farming AS, a subsidiary of SalMar Group are currently working on a design of an offshore fish farm. The concept is illustrated in figure 1.7. The technical design is performed by Global Maritime. This concept is the one which is closest to completion. Construction of a pilot project started March 2016 and will be completed in the third quarter of 2017. Although this structure is of a completely different design compared to the Havfarm, the idea of this concept is much the same, namely to provide a design which is suitable to move offshore for new and better fish farming locations. The structure is intended for offshore installation in water depths of 100-300 meters. The main dimensions will be a total height of 68 meters and a diameter of 110 meters[29]

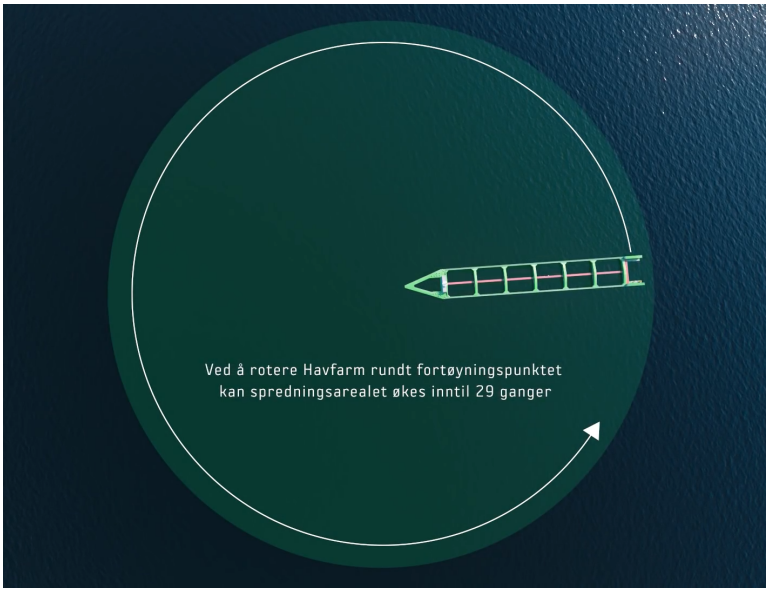

Figure 1.6: Havfarm vaneing possibilities(Screen shot of NSK Ship Designs info video - http://www.nskshipdesign.com/ designs/aquaculture/fish-farm/)

Figure 1.7: Global Maritimes exposed fishfarm concept. Illustration taken from http://subseaworldnews.com

Aker Solutions is also working on developing a new fish pen on request from Norway Royal Salmon. An illustration of the concept is shown in figure 1.8. This

concept is able to hold 3000 tonnes of salmon. The structure consist of two pontoon rings distanced with 10 meters. The net is suspended form the bottom pontoon ring. The idea of the concept is that the structure will be submersible. When the accessing the fish pen for maintenance the structure may be raised such that the lower pontoon is at the sea surface. During production the structure will be lowered such that the upper pontoon will be at sea surface. In this condition the top of the fish net will be submerged at a dept of 10m, meaning that the salmon in the pen will for most of the time be located at a depth below 10 meters. The main reason for this is to eliminate the lice problem. In submerged condition there will be an air pocket in the lower pontoon so that the fish sill have access to air to adjust the swim bladder . This concept is still in development but small scale tests shows that this concepts is promising [33]. A study of how the long term growth, condition and behaviour of Altantic Salmon is affected by submerging the cages is conducted by SINTEF Fisheries and Aquaculture, Institute of Marine Research and Department of Zoology University of Melbourne. In this study it is concluded that continuous submergence below 10 m for longer than 2 weeks reduces the welfare and performance of Atlantic salmon, for further reading about this topic the reader is refered to the article [17].

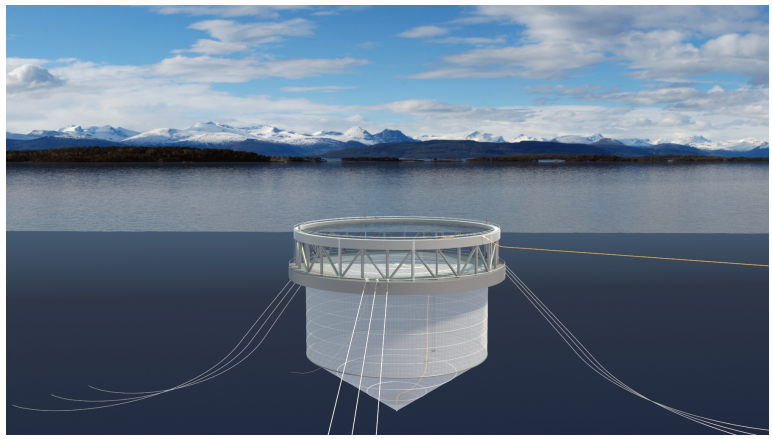

Figure 1.8: Aker Solutions offshore fish farm concept. The fish cage is submersible. (Illustration taken from www.tu.no)

1.4 Current Rules and Regulations

The Norwegian Ministry of Fisheries and Coastal Affairs have developed the NYTEK regulation which applies to floating aquaculture structures. This regulation is a legislative body by law and at the top of the hierarchy, and all floating aquaculture structures must be designed to satisfy this regulation. The objective of this regula-

tion is to prevent fish escape by giving sound technical standards for the aquaculture structures [12]. In this regulation it is referred to the the Norwegian Standard 9415:2009 which sets requirements regarding design of marine fish farms and how it shall be documented, including calculation and planning rules [28]. According to Jensen et al. the number of reported escaped salmon was significantly reduced when this standard, NS-9415, was first introduced in 2004. Jensen et al. further claims that within Norway, NS-9415 technical standard has perhaps been the most useful tool at an industry-wide scale to prevent escapes [16].

Although the NYTEK regulation and NS-9415 have proven to have great effect on reducing the number of escaped salmon, this regulation might not give sufficien guidence as the aquaculture structures are moving further offshore and into harsher conditions.

For the activities within petroleum industry the International (ISO/IEC) and European standards (CEN/CENELEC) form the basis. In addition to these the NORSOK standards developed by the Norwegian petroleum industry are the legislative bodies by law in Norway, in the same way as the NYTEK regulation for the aquaculture [32]. The intentions of the NORSOK standards are to ensure adequate safety, value adding and cost effectiveness for petroleum industry developments and operations. Perhaps the most relevant NORSOK standards are N-001, N-003 and N-004.

The N-001 standard, Integrity of offshore structures, specifies general principles and guidelines for the design and assessment of offshore facilities, and the verification of load bearing structures and related maritime systems subjected to foreseeable actions [24]. The N-003 standard, Actions and action effects, specifies general principles and guidelines for determination of actions and action effects for the structural design and the design verification of structures.. Both the N-001 and N-003 standard is applicable to all types of offshore facilities used in the petroleum activities, including bottom founded facilities as well as floating facilities [25]. The N-004, Design of steel structures, standard specifies guidelines and requirements for design and documentation of offshore steel structures [26].

These three standards provides a thorough guidance of the design requirements for offshore structures intended for use in the petroleum industry. Since as of now there are no unique regulation for offshore aquaculture farms facing harsh weather conditions, in my opinion, it would be best to base the design of future offshore aquaculture structures on the NYTEK regulation and the NORSOK standards. The best of judgement will have to be used to adopt the petroleum industry intended regulations to application in the aquaculture industry.

1.4.1 Bureau Veritas Rules

There also exist a tentative issue of a rule set for classification and certification of fish farms in the Bureau Veritas rules.

1.5 How the litterature research is conducted

To search for relevant information mainly the university library has been used, both online (through oria.no) as well as the Marine Technology Library located at Tyholt. In addition Google Scholar has also been used to search for relevant articles. As much is happening within this topic general browsing for interesting offshore aquaculture concepts have proven usefull for the introduction part of this thesis.

1.6 Preview of following chapters

A literature review is presented in chapter two. This literature was conducted during my project thesis, and more or less included directly.

Chapter three gives a brief review of ULS loads and load effects theory. Also this part was created during my project thesis, and more or less included directly.

Chapter four gives a review of the software used for the global analysis performed in the master thesis.

The hydro and structural FE model established and which is used for the global analysis is thoroughly described in chapter 5.

Hydro and FE analysis results are presented and evaluated in chapter six.

Chapter seven contains end remarks and suggestions for further work.

Chapter 2

Literature Review

The literature was performed during the project thesis and have been included here as well. The literature review has been limited to literature relevant to moving the aquaculture offshore. Although the search for relevant literature was challenging some work on this field have been done. The results of the literature study is presented in this chapter.

The calculation of forces on fish nets is one of the challenges with the Havfarm structure. There is no good way in doing so in the Bureau Veritas software yet. However elements that will be able to represents fish nets in the seakeeping software Hydrostar is in development. One way to calculate current forces on and flow through fish farms is there fore included in the literature review.

2.1 Current Forces on and Flow Through Fish Farms

Maybe the most challenging part of designing a structure like the HAVFARM concept is to calculate the forces acting on the nets correctly. Kristiansen et al. concludes in their paper that a direct CFD simulation of a fish farm is unrealistic. The reason for this is that the number of twines in a net is typically in the order of ten millions. It is also stated that although a Morison type of force model, which is widely used, is just as efficient as a screen model they will significantly overestimate the forces for highly deformed nets [18].

Geir Løland has developed a method for calculation of current forces on fish farming structures in his Doctor Thesis [21]. The derived method is compared to model test showing that the model gives drag forces ranging from 90 to 120 % of the measured drag forces from the model test. Lølands model is based upon the assumption that the net cage can be divided into several net panels. Further the drag

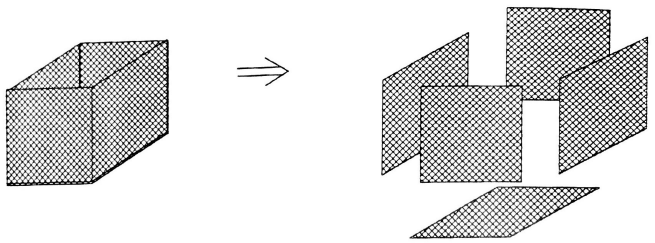

Figure 2.1: A net cage can be devided into a set of net panels (figure is taken form [21])

force of each net panel is calculated and the total drag force of the net is given as the sum on drag forces on the different net panels. The drag force on each net panel is calculated by demanding equilibrium between the drag force on the panel, the weight of the sinkers[1] and the deformation of the panel. The wake behind a screen is also investigated in the thesis, and a relationship between the velocity reduction factor[2] and the drag coefficient. When water is passing a net panel the velocity is then reduced in accordance with the velocity reduction factor. This is of importance both for the calculation on drag forces of nets in the "shadow" of the first net upstream as well as for the environment for the fish in the net. A brief review of Lølands model will be given in this section, all equation and figures are taken form the dr.ing thesis. For further readings on this topic the reader is referred to the thesis [21], a more concise article describing the method is also given in Aquaculture International [22].

2.1.1 Current force model

This section is more or less taken form the Lølands dr.ing thesis. The main assumption of the method is that the net can be divided into several net panels. The main steps in Lølands method to calculate the current forces on fish farming structures are:

1. The net cage is divided into a system of net panels. These panels may be parallel, normal or have an arbitrary angle relative to the flow. The number of net panels may depend on the shape of the cage. The number of panels depends on the shape of the net cage, E.g a square cage can be modelled as 4 side panels and one bottom, as illustrated in figure 2.1, or a hexagonal cage

[1] Sinkers are weights suspended underneath the nets to ensure that they don't deform but keep their intended geometry

[2] Defined as the ratio between the velocity in the wake behind a screen and the free flow

can be modelled as 6 side panels and one bottom panel. The total drag force on the cage system is given as the sum of the drag forces acting on each net panel. The structural compatibility between the net panels is neglected.

2. Establish lift and drag coefficient for the actual net type as a function of solidity and angle.

3. Determine the local current velocities at each net panel as function of position on the cage system. The local incident current velocity will be reduced when passing a net panel. This velocity reduction depends on number of net panel upstream.

4. Calculate the current forcve on each net panel as function of point weights, local current velocity and initial heading relative to the free flow.

5. Calculate the total drag force on the cage system as the sum of the forces acting on each net panel.

Further the method is based upon the assumption that the mean drag and lift forces on a net panel can be written as:

$$\begin{aligned} F_D &= \frac{1}{2}\rho C_D(\alpha) A U^2 \\ F_L &= \frac{1}{2}\rho C_L(\alpha) A U^2 \end{aligned} \tag{2.1}$$

The drag force is defined as the force in the direction of the flow and the lift force is normal to the flow direction. Generally in a global axis system the force components can be written as:

$$F = F_D \vec{n}(x,y) + F_L \vec{l}(x,y) \tag{2.2}$$

where $\vec{n}$ and $\vec{l}$ is defined as:

$$\begin{aligned} \vec{n}(x,y) &= \frac{\vec{U}}{|U|} = e_U \\ \vec{l} &= (e_T \times e_U) \times e_U \cdot (e_U \cdot e_T) \end{aligned} \tag{2.3}$$

and e_T is the unit tangential vector defined in the direction from the upper end to the lower end point of the net panel.

From equation 2.1 it is clear that the drag and lift coefficients are important to estimate the current forces on the net. The most reliable way to find these coefficients are through model tests. However they may also be estimated by sum up

the drag on each thread, which will be correct when the ratio between the area covered by the threads in the screen and the total area of the screen , the solidity ratio, approach zero, **Sn** $\rightarrow$ **0**. The solidity ratio is given i equation 2.4

$$Sn = \frac{2D}{\lambda} + \frac{1}{2}(\frac{D}{\lambda})^2 \tag{2.4}$$

Here λ is the mesh size and **D** is the twine diameter.

The drag and lift coefficients may then be found from:

$$\begin{aligned} C_D &= 0.04 + (-0.04 + 0.33S_n + 6.54S_n^2 - 4.88S_n^3)\cos(\alpha) \\ C_L &= (-0.05S_n + 2.3S_n^2 - 1.76S_n^3)\sin(2\alpha) \end{aligned} \tag{2.5}$$

Current Force on a Single Net Panel

Considering a single net panel. The drag force **dA**of a net panel is usually described by a pressure drop coefficient κ.

$$dF_D = \frac{1}{2}\rho\kappa u^2 dA \tag{2.6}$$

Here **u** represents the mean flow through the net. For convenience the drag force can be described with a drag coefficient C_D.

$$dF_D = \frac{1}{2}\rho C_D(\alpha)U^2 dA \tag{2.7}$$

Where **U** now represents the free flow velocity. The Total drag force is then found by integration of equation 2.7 over the net panel area.

$$F_D = \int_A \frac{1}{2}\rho C_D(\alpha)U^2 dA \tag{2.8}$$

Equation 2.8 gives the drag force directly if the net panel has a plane form, or if it is completely rigid. The angle α is then constant all over the panel for such cases. However, the net panel has very little or no structural bending stiffens, so in reality it is only able to withstand axial tension. This means that a net panel connected to a point, say point O, in the upper end and free to move in the liver end as it is exposed for current it will not be able to rotate about point O as a rigid plane, but instead as a curved plane. See figure 2.2 for illustration.

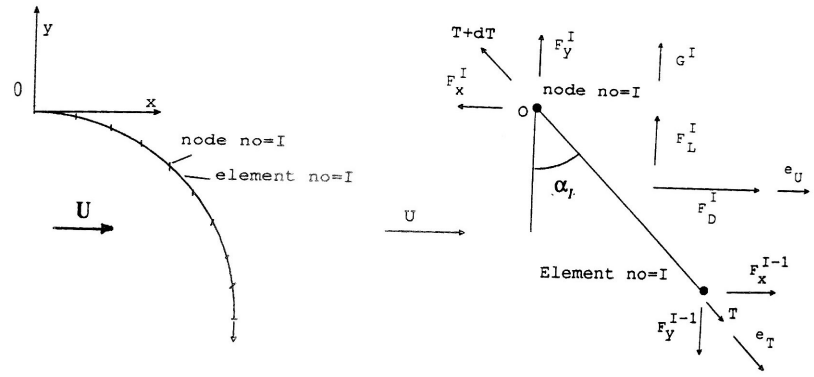

Figure 2.2: Deformation of a net panel in steady current, and element model of the analysis of the current force on a net panel. Figure taken form [21])

Based on assumption that the net panel has no bending stiffens the drag force and the form of the net may be found from a numerical analysis. As shown in figure 2.2 the net panel can be divided into a number of plane sub elements.

Since the net panel has no zero bending stiffness there cannot be transferred any bending moment between the nodes. Thus each sub element will have an equilibrium position when the moment in the element nodes vanishes. Each sub element will be exposed to a drag force, a lift force and the weight and buoyancy of the net it self as well as reaction forces from neighbouring elements. Figure 2.2 shows how the forces acts on a sub element.

Further the equilibrium position for sub element **no = I** is given by the angle α_I which gives zero moment in node **no = I**. In figure 2.2 this corresponds to the sum of moments about **O** is zero. We then have:

$$M_O^I = 0 \tag{2.9}$$

For figure 2.2 this becomes:

$$\frac{1}{2}\rho C_D(\alpha_I)U^2 dA\frac{dL}{2}\cos\alpha_I + \frac{1}{2}\rho C_L(\alpha)U^2 dA\frac{dL}{2}\sin\alpha_I + G^I\frac{dL}{2}\sin\alpha_I + F_X^{I-1}dL\cos\alpha_I - F_Y^{I-1}dL\sin\alpha_I = 0 \tag{2.10}$$

Equation 2.10 can be solved numerically with respect to α_I which leads to equation

2.11

$$\alpha_I = \arctan[\frac{\frac{1}{2}\rho C_D(\alpha_I)U^2 dA + 2F_x^{I-1}}{\frac{1}{2}\rho C_L(\alpha_I)U^2 dA + G^I - 2F_Y^{I-1}}] \tag{2.11}$$

From this we can obtain the equilibrium forces from the element model in figure 2.2:

$$\begin{aligned} F_X^I &= F_D^I + F_X^{I-1} \\ F_X^I &= F_L^I + G^I + F_Y^{I-1} \end{aligned} \tag{2.12}$$

The form of the net panel and the drag forces on the net panel can be found if we now start the calculation form the lower end of the net panel. In the lower end **I = 0**, $F_X^{I=0}$ and $F_Y^{I=0}$ and equal to the drag on and the weight of the sinkers. We can then find the equilibrium position of element **no=1**, and when this position is found we also have found the reaction forces on the next sub element. This way we can continue to the next sub element until we reach the top point, which in figure 2.2 corresponds to point **O**.

In some cases the net panel may have an initial angle β against the flow, shown in figure 2.3. To account for this initial angle the equilibrium position can then be given as:

$$\begin{aligned} \frac{1}{2}\rho C_D(\theta)U^2 A\frac{L}{2}\cos\theta + \frac{1}{2}\rho C_L(\theta)U^2 A\frac{L}{2}\sin\theta \\ + G\frac{L}{2}\sin\alpha + F_X^0 L\cos\theta - F_Y^0 L\sin\alpha = 0 \end{aligned} \tag{2.13}$$

where θ is given by

$$\theta = \arcsin\sqrt{\sin^2\alpha + \cos^2\alpha\sin^2\beta} \tag{2.14}$$

Velocity Reduction

At this point we are able to calculate the current forces on a single net panel. However, when a net is placed in a flow the flow will be altered in two ways. The flow will partly go through the net and around the net and there will be a pressure drop over the net. This is indicated in figure 2.4. The free flow velocity U_∞ and

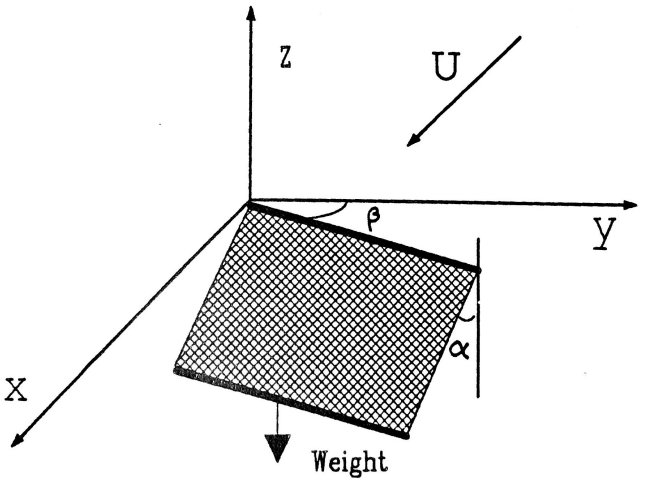

Figure 2.3: Figure taken form [21])

the velocity through the screen **u** is highly dependent on the solidity of the screen, i.e on the drag coefficient.

Since the drag force is a function of the square of the velocity, see equation 2.2, it is important to know the incident flow velocity. When we have several screens in a row, as we do in the HAVFARM structure, this becomes a problem since the flow velocity will be altered as it pass through the net. Thus we need to define how the velocity of the flow will behave as it passes through several nets.

In Lølands dr.ing. thesis a velocity reduction factor **r** is defined:

$$r = \frac{u_w}{U_\infty} \tag{2.15}$$

as the ratio between the velocity in the wake behind the screen u_w and the free flow U_∞. This factor is more or less constant over a large distance behind the scree. This is elaborated in Lølands dr.ing thesis [21]. Then the velocity in the wake behind the a series of equal screens placed in a row, with a distance between them large enough to neglect the upstream effect, will decay like:

$$U_i = U_\infty r^i \tag{2.16}$$

Here U_i is the velocity in the wake behind screen no=i.

In Lølands dr.ing thesis the measured ratio between velocity inside 3 cages placed behind each other and the free flow velocity is compared to the calculated one.

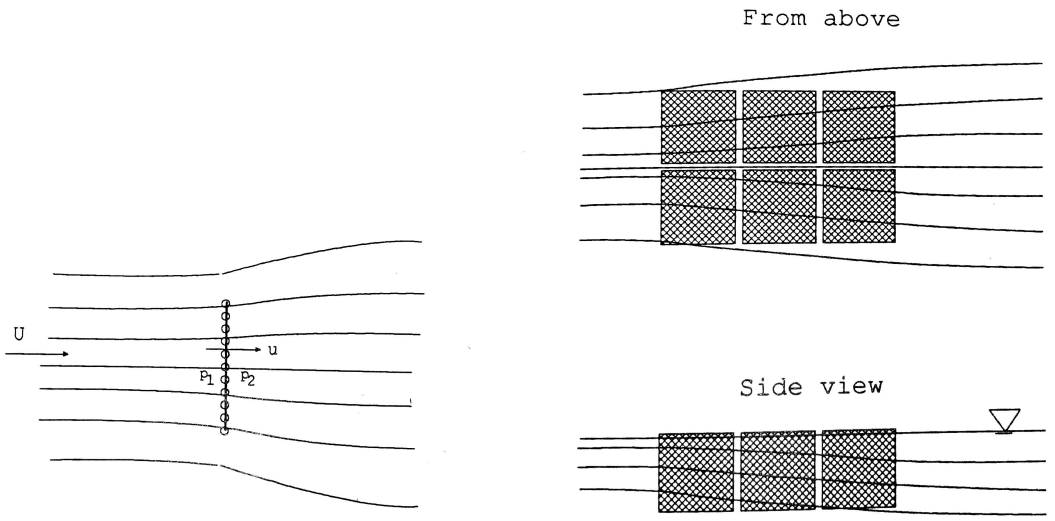

(a) $p_1 > p_2$ **(b)** $Re_c \approx 54000$

Figure 2.4: Figure **(a)** and **(b)** shows how the flow is altered with an incoming flow from the left and passing through/around six nets located next to each other. It is also indicated in figure **(a)** that we will have a pressure drop over the net. The figure is taken form [21]

The results indicate that the method of of estimation the local velocities inside the cages is good, the results are given in table 2.1

Table 2.1: Comparison between calculated and measured ratio between the velocity inside cages and the free flow

	Free flow	Cage 1	Cage 2	Cage 3	Wake
Measured	1.0	0.85	0.60	0.44	0.38
Calculated	1.0	0.85	0.61	0.44	0.38

In Lølands dr.ing thesis a relationship between the reduction factor and the drag coefficient is derived. The result is given in equation 2.17:

$$r = 1.0 - 0.46C_D \tag{2.17}$$

Current Force on a System of Cages

With the velocity reduction factor and a method of how to calculate the current forces for a single net established it is now possible to calculate the current force

on a system of cages. In Lølands dr.ing thesis it is given an example to describe the complete current force calculation on a fish farming structure. A brief summary of the example is given in the following.

In the example a cage system consisting of $2 \cdot 3 = 6$ cages is used, this is illustrated in figure 2.5. With a current direction with $\beta = 0$ the cage system can be divided into 12 panels normal to the current and 18 parallel to the flow. From figure 2.5 we can see that of the 12 panels normal to the flow we have; 2 panels without shielding, 2 with shielding from 1 panels, 2 with shielding form 2 panels and so on. It is assumed that the distance between each cage is large enough for the wake behind the screen to become uniform. It is elaborated in the Lølands dr.ing thesis that the wake behind a screen becomes uniform already in the near wake of the screen, and thus this assumption is reasonable. This means that the rear panel of one cage has a different local incident flow velocity than the front panel of the next cage.

For the current force on the parallel panels it is assumed that the side panels in one cage are exposed for the same velocity as the rear panel in the same cage. It is observed from model test in Lølands dr.ing thesis that this is a reasonable assumption.

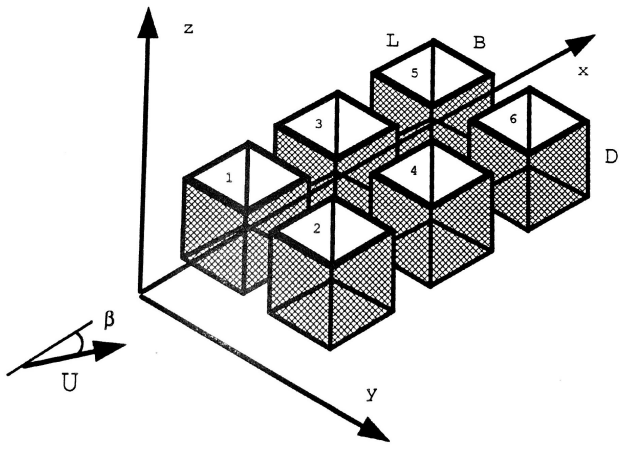

Figure 2.5: Cage system used as an example to explain the method of calculating the current forces on a fish farm structure. The dimentions of the cages are; **B=1.5m**, **L=1.5m** and **D=1.5m**. Distance between cages is **20 cm** in y-direction and **10 cm** in x-direction. Figure is taken from [21])

For a rigid net cage system (the cages can not be deflected) the drag force on the

net panels normal to the flow direction is given in Lølands dr.ing thesis as:

$$\begin{aligned} F_D^N &= 2\frac{1}{2}\rho C_D(\alpha=0)U_\infty^2 A_1^N \\ &+ 2\frac{1}{2}\rho C_D(\alpha=0)U_1^2 A_2^N \\ &+ ... \\ &+ 2\frac{1}{2}\rho C_D(\alpha=0)U_5^2 A_6^N \end{aligned} \tag{2.18}$$

In this case each net panel has equal area and drag coefficient, and the velocity decays as function of net panels upstream according to equation 2.16. Thus it can be shown that equation 2.18 becomes:

$$F_D^N = N_N \frac{1}{2}\rho C_D(\alpha=0)U_\infty^2 A^N \frac{1-r^{4N_C}}{1-r^2} \tag{2.19}$$

In the same way Løland shows how to calculate the drag force on the net panels parallel with the flow in equation 2.20 and drag force on the drag force on the tube frame used for spanning out the cage in equation 2.21.

$$F_D^P = N_N \frac{1}{2}\rho C_D(\alpha=90)U_\infty^2 A^P \frac{1-r^{4N_c}}{1-r^2}\frac{r^2}{1+r^2} \tag{2.20}$$

$$F_D^F = 2N_N \frac{1}{2}\rho C_D^F U_\infty^2 A^F \frac{1-r^{4N_c}}{1-r^2} \tag{2.21}$$

The total drag force can then be found by the sum of equation 2.19, 2.20 and 2.21

$$\begin{gathered} F_D^T = F_D^N + F_D^P + F_D^F \\ F_D^T = N_N \frac{1}{2}\rho U_\infty^2 \frac{1-r^{4N_c}}{1-r^2}[C_D(\alpha=0)A^N + 2C_D^F A^F + C_D(\alpha=90)A^P \frac{r^2}{1+r^2}] \end{gathered} \tag{2.22}$$

Løland have also derived an equation to calculate drag forces on a flexible net cage system. For a flexible net cage system, using sinkers instead of tubes for spanning out the net cages, the drag force can be calculated in a similar manner. This is

more relevant for the HAVFARM structure. As derived by Løland in the dr.ing thesis Equation 2.19 now becomes:

$$\begin{aligned} F_D^N &= 2\frac{1}{2}\rho C_D(\alpha_1)U_\infty^2 A_1^N \\ &+ 2\frac{1}{2}\rho C_D(\alpha_2)U_\infty^2 r^2 A_2^N \\ &+ ... \\ &+ 2\frac{1}{2}\rho C_D(\alpha_1 0)U_\infty^2 r^{10} A_1 0^N \end{aligned} \tag{2.23}$$

In equation 2.23 it is assumed that the shielding is independent of the net panel angle. The calculation behind this equation is also based on the initial position of the net panels in the cage system. There have also only one element in the drag force calculation on each net panel. This is elaborated in Lølands dr.ing thesis [21] The parallel drag forces is calculated according to equation 2.20 and there is no frame in this case so the total dragfoce is the sum of equation 2.23 and 2.20

2.2 Offshore Fish Farms

Some work one moving the fish farms further offshore have been done. In Sveälvs article, *Inshore Versus Offshore Farming*, Sveälv have done a comparing analysis of inshore versus offshore farmed rainbow trout. In his analysis he concludes that, first of all there exists a relationship between an offshore environment and high-quality fish, secondly the mortality among the offshore farmed rainbow trout was reduced by 50% and lastly the increased swimming activity, as a result of stronger and more stable currents, gives the rainbow trout a slimmer body. It is also indicated that Atlantic salmon during some extent of exercise get a slimmer body and utilize their feed more efficiently, indicating that also farmed salmon would benefit form being farmed offshore. In the same article it is also indicated that a large volume of the net and a circular shape will give the fish a more natural environment and increasing the thriving and welfare of the fish [34].

In a different article by Sveälv, *Strategies and technologies in offshore farming*, it is also indicated that offshore fish farms, in general, may turn out to be economically superior owing to lover production costs than inshore and land-based farms. In addition to lowered mortality, reduced self-pollution and faster growth are indicated as benefits of offshore farming [35].

Regarding the design of the offshore fish farm Shainee er al. writes in their paper "*the most prominent cage design concept would be a system placed in offshore waters with optimum biological conditions which provides both the best structural*

integrity to the system as well as welfare for the fish and the farmer" [30]. The authors of this article concludes that the most favourable fish farm concept to be applied to offshore locations is a single point moored submersible cage system. Further it is pointed out that a single pint mooring will require special attention as the anchor must be able to resist loading from any direction[30].

Other advantages by use of a single point mooring are pointed out by Goudey et al.: "*the use of a single point mooring (SPM) would allow the operation to maintain a "watch circle" where the position of the cage(s) depends on the sum of the environmental forces. By spreading out the accumulation of organic matter, one can prevent the local environment from being overwhelmed. Preliminary analyses of the benefits of SPM indicate a two-fold to 70-fold reduction in deposition of waste on the seabed, depending on mooring geometry and current type. Other advantages are related to reduced anchoring costs, improved accessibility, and the ability of having certain cages in the lead position with respect to currents and good oxygen conditions*" [13].

Chapter 3

ULS Loads and Load Effects Theory

Review and theory of various methods to calculate the ULS characteristic loads and load effects will be given in this section. This is theory relevant for further work. This theory section is primarily based on the NORSOK standard N-003 [25], Havers report on Prediction of Characteristic Response for Design Purposes [14], DNVGL-RP-C103 and NS-9415 [28].

The HAVFARM structure is characterised by submerged pontoons which gives buoyancy to the structure. As the columns, bow and stern are the only parts of the structure that break the water surface the HAVFARM will also be characterised by a small water plane area. These characteristics are not so unlike the characteristics of a semi submersible platform, with submerged pontoons giving buoyancy and only the columns breaking the water plane area. In order to be able to adapt the NORSOK standards for offshore petroleum structures to apply to the HAVFARM structure it is chosen to treat the HAVFARM structure as a semi submersible platform.

3.1 ULS Characteristic Loads and Load Effects

According to NORSOK standard N-003 a global wave motion analysis is necessary for structures with at least one free mode. And as the HAVFARM structure in the same way as a semi-submersible with catenary mooring have six degrees of freedom a global wave analysis is necessary. By doing a global motion analysis we are able to determine displacements, accelerations, velocities and hydrodynamic pressure relevant for the action on the super structure and the mooring system,

as well as relative motions needed to asses air gap and green water requirements. Wave, current and wind excitations should be considered for such an analysis [25].

Ultimate Limit State (ULS) characteristic loads and responses are to be determined in the Master Thesis. **ULS** values for environmental loads taken from NS-9415 are given in table 3.1. When wind and waves are governing the ULS value of the waves is suggested to be equal to the 50 year return wave [28]. However as the HAVFARM structure are to be placed in a less sheltered area than most aquaculture farms an adaption of the ULS values used in the NORSOK regulations could be a wiser choice. A excerpt of these values taken from N-003 are given in table 3.2, and when wind and waves are governing it is suggested that the ULS wave are to be of a 100 year return period.

Table 3.1: Combination of environmental loads, taken from NS-9415[28]

Combinations	Return period, environmental load year		
	Current	Wind	Wave
1	50	10	10
2	10	50	50

Table 3.2: Comination of environmental actions with annual probability of exceedance, excerpt of table taken from NORSOK standard N-003[25]

Limit State	Wind	Waves	Current
Ultimate Limit	10^{-2}	10^{-2}	10^{-1}
State	10^{-1}	10^{-1}	10^{-2}

Table 3.1 and 3.2 shows how the combined occurrence of wind, waves and currents is assumed to be in an ULS condition as a 100 year return value of all three values would be highly conservative. The profile of the HAVFARM structure is relatively low above the water line and thus an assumption to neglect the wind loading could be reasonable to ease the further calculations. It is further assumed that the wave forces will be governing the extreme responses. As the nets will be added to the main structure at a later stage, the current forces may need to be included. However, at this stage only the wave actions are considered.

3.1.1 Frequency domain vs Time Domain Analysis

A global motion analysis can be conducted in the frequency domain or in the time domain. The difference between the two domains will be explained in this section.

The equation of motion for a multi degree-of-freedom system is given by

$$M\ddot{r} + C\dot{r} + Kr = Q(t) \tag{3.1}$$

Here M is the mass matrix, C is the damping matrix, K is the stiffness matrix, Q is the loading and r is the nodal displacement vector. The solution to equation 3.1 can be given in the time domain or the frequency domain.

Frequency Domain

An arbitrary excitation (loading) can be written as an infinite sum of harmonic components. This can be expressed mathematically by the Fourier-transformation. The contribution to the sum from each single harmonic component will be a function of the frequency ω. This function, which is the Fourier-transform of the load history, expresses the excitation in the frequency domain. In the same way as for the excitation, the response(displacement) can be transformed into the frequency domain. To solve the equation of motion in the frequency domain hence amounts to the same as solving equation 3.1 for harmonic loading for various frequencies. This solution expresses directly the sensitivity of a structure to the load frequency, Langen [20]

Frequency domain solution techniques are commonly used and according to DNVGL-RP-C103[10] a frequency domain procedure is the most suitable for response analysis of column-stabilised units. This method requires linear equation of motions. For a short term period a frequency domain analysis may be carried out to determine wave frequency motions. For the actual condition a response spectrum obtained with the frequency domain analysis together with the assumption of Gaussioan process may be used to estimate the response statistics. However, when modelling velocity squared drag actions, time varying geometry, horizontal restoring actions and variable water surface elevations the linear equation of motion is inconvenient as these effects are nonlinear. Linearized solutions should be used with care when determining extreme values when nonlinear action or action affects could be important [25].

According to Havers report the equation of motion is given as:

$$m\ddot{x}(t) + c(x, \dot{x})\dot{x}(t) + k(x, \dot{x})x(t) = F(t) \tag{3.2}$$

In equation 3.2 the left hand side of the equation characterizes the mechanical properties of the system (how structure responds to the loading) and the right hand side represents the external loading. By considering the left hand side of the equation a convenient first classification level is obtained. Generally the damping and stiffness coefficient will be of a non-linear nature. However, results of sufficient accuracy may be achieved by modelling damping force as a linear function of $\dot{x}$ and the stiffness as a linear function of x. As a first distinction we therefore need

to consider a response problem to belong to either a non-linear mechanical system class (as in equation 3.2) or linear mechanical system class as in equation 3.3 where the damping and stiffness coefficient is independent of the magnitude of $\dot{x}(t)$ and $x(t)$ respectively.

$$m\ddot{x}(t) + c\dot{x}(t) + kx(t) = F(t) \tag{3.3}$$

If the right hand side of equation 3.3 also is a linear function of the free surface elevation process the response can be referred to as a linear response problem. Under these conditions the response quantity is characterized bye the transfer function, $h_{\Xi X}(f)$, which is the ratio between the complex response amplitude and the wave amplitude. The transfer function is a function of frequency, *f*, and it gives both the amplitude scaling and phase shift of response relative to a wave component. The absolute value of the transfer function, $\left|h_{\Xi X}(f)\right|$, the amplitude scaling, is often referred to as the response amplitude operator, ROA(f).

Provided the surface elevation process, $\Xi(t)$, for short term periods is modelled as a Gaussian process and therefore completely characterized by a wave spectrum, $s_{\Xi\Xi}(f)$, the response is conveniently analysed in the frequency domain. This means that the response process is also Gaussian and described by the response spectrum which is given by equation 3.4

$$s_{XX}(f) = \left|h_{\Xi X}(f)\right|^2 s_{\Xi\Xi}(f) \tag{3.4}$$

Further an example of practical response problem which typically belongs to this group is wave frequency response of a floating structure(i.e. the HAVFARM structure) provided that the load exposed members are sufficient large for viscous forces to be negligible.

Time Domain

For an analysis in the time domain *the solution of equation 3.1 is given directly as a function of time*, Langen [20].

According to Haver [14], this is done by solving the equation of motion in the time domain by some step by step procedure.

The idea is to solve the differential equation with the solutions for t = ti as initial conditions. If we shall be able to do so, we must introduce some additional assumptions. Most common is to assume how acceleration changes between ti and ti+1. Assuming acceleration to be constant and equal to the average value of accelerations at ti and ti+1, Haver [14].

The most common scheme for solving the equation of motion in the time domain is the Newmark - methods, these methods can be found in Langens "Dynamisk Analyse av Konstruksjoner" [20]. For practical analysis Haver suggests that the following steps are performed:

1. Simulate a possible realization of the surface elevation field of an adequate duration, often taken to be 3 hours. This could be a Gaussian random field or it could be a second order random field.
2. Calculate the corresponding kinematics in the fluid covering the load exposed structural members with sufficient accuracy. Generally, one needs to account for kinematics to the exact surface.
3. Calculate the load vector of the submerged part of the structure at each time step during the period covered by the simulated sea surface process.
4. Solve the equation motion for the given load vector history. This is typically very fast if the structural motions are small, i.e. the left hand side of the equation can be considered as a linear mechanical problem. If stiffness and/or damping need to be updated for each or each some few time steps, the time domain solution may become rather time consuming.
5. As a result of step no. 4 time histories of duration d hours for all nodal displacements are available. From these time histories one can estimate the distribution function for all “global” maxima (= the largest maximum between up-crossings of the mean level). If we rather focus on the d-hour maximum, one can identify an estimate for the d-hour maximum for each response per simulation. If we have simulated M time histories, we have M estimates of the d-hour extreme value. From these estimates we can establish a proper d-hour extreme value distribution.
6. In combination with using the environmental contour line method for selecting adequate short term sea state for design purposes, a proper estimate for the q-probability value is obtained by determining the α - percentile of the extreme value distribution. If the sea state considered is taken as the worst (in view of the problem under consideration) along the q-probability contour line, a proper estimate is often found using α = 90.

3.1.2 Design Wave, Regular Wave and Stochastic Analysis

Regarding the methods and models for global response analysis three methods is suggested by DNVGL-RP-C103 [10], these method are also described in NORSOK standard N-003[25] and by Haver [14]. The methoda are:

- Design wave Analysis
- Stochastic Analysis
- regular wave Analysis

A brief review of the design wave analysis and the stochastic analysis method will be given in the following.

Stochastic Analysis

The stochastic analysis method aims at the sea state which gives the worst response. The statistical distributions of the waves for calculation of short term and long term responses are applied in stochastic analysis. Further a stochastic long term response analysis is the most consistent method for predicting characteristic loads if the structural response is dependent on both sea severity , the period and the previous history of the wave process . To obtain a q-probability estimate for the load/response we need the long term distribution of the target response. According to Haver an approach which seams to work well for Norwegian Continental Shelf type of wave climates is the d-hour maximum of the target response process. Considering this approach with d = 3, which is usually adopted for Norwegian waters, the long term distribution of the 3-hour maximum response, X_{3h}, is given in equation 3.5[14]:

$$F_{X_{3h}}(x) = \int_h \int_t F_{X_{3h}|H_sT_p}(x|h,t) f_{H_sT_p}(h.t) dt dh \tag{3.5}$$

Here $f_{H_sT_p}(h.t)$ is the long term distribution of the sea state characteristics, significant wave height h_s and spectral peak period t_p. $F_{X_{3h}|H_sT_p}(x|h,t)$ is the short term distribution of X_{3h} given the sea state characteristics. This way of estimating the long term distribution may very well be used of the problem is close to linear and exposed to a Gaussian sea surface.

Design Wave Analysis

Extreme sea states may not cause maximum action effects, some times maximum action effects are rather sensitive to waves of a defined length and extreme steepness. This may be the case for structural action effects in floating installations with columns and pontoons [25]. Such a wave, giving the largest action effect/response is called the design wave. Thus in a design wave analysis we need to determine the properties of the design wave. According to NORSOK N-003 different combinations of wave periods, wave heights and directions at the same probability level, for a ULS analysis this probability level is 10^{-2}, shall be considered in order to

arrive at the most unfavourable values for the different action effects [25]. The contour line method may be used to establish a reasonable estimates of H_s and T_p values corresponding to a q-probability 10^{-2} sea state. Haver suggests that for early phase work it is recommended that the omni-directional wave climate is used for all harsh weather sectors. Experience suggests that there is considerable uncertainties in estimated directional extremes for the weather characteristics [14].

Choosing characteristic response parameters and corresponding wave headings to decide upon the properties of the design wave may be difficult. In DNVGL-RP-C103 it is suggested that characteristic response parameters and wave headings should be chosen according to experience with stochastic wave analysis. Some guidance on typically governing responses for the global strength of column based units are given in this RP [10]. In the same RP the method applied for a column stabilized unit is described. The properties of the design wave may be found from the transfer function established for the response parameter in question. With the design wave properties established a a design wave may be modelled by Stokes 2^{nd} or higher order theory for water depths (d) to wave length ratios greater than 0,15. The Stokes wave, or design wave, may now be used to calculate hydrodynamic forces for further input to the global structural model.

3.2 Mooring Analysis

Mooring lines are commonly termed slender marine structures. A finite element approach is normally applied using bar elements. When analysing slender structures an important future of the analysis is the treatment of nonlinearities. This can be induced by hydrodynamic (drag) actions, and wave elevation varying effects and contact problems in terms of contact between slender structure and seafloor as well as hull. The importance of these nonlinearities are strongly system and excitation dependent. however, hydrodynamic action and wave elevation effects will to some extent always be present. Analysis of catenary mooring system can be carried out according to the technical requirements in ISO 19901-7 or DNV-OS-E301, NORSOK-N-003 [25].

Chapter 4

Software

In this chapter the software which is used for modelling and analysis of the Havfarm structure is reviewed. Some of the theory behind the programs is also given, however the reader is referred to the user manuals and theory papers for Homer [4] and [23] and Hydrostar [7] for more thorough description. In the master thesis a significant amount of time have been spent to model the Havfarm structure. The modelling of the structure is done in FEMAP, which in the thesis is used for pre- and postprocessing. Homer and HydroStar will be used for hydrodynamic and structural analysis with NX Nastran as solver for the FEA. Figure 4.1 shows the overall flow between the software.

4.1 Femap

Femap is an advanced engineering simulation software that creates finite element analysis models of complex engineering products and systems, and displays solution results. In the thesis Femap is used for pre- and post processing. That is to establish a finite element model of the Havfarm structure and to visualize the results, such as the deformations and stresses due to the loading calculated by HydroStar and NX Nastran. The FE models are exported from Femap as .dat files which is then read by Homer to performe the hydrodynamic and structural analysis.

4.2 HydroSTAR

HydroSTAR is the state of the art hydrodynamic software developed by Bureau Veritas to evaluate 1^{st} & 2^{nd} order wave loads and induced motions of one or several ships or marine structures of any type in deep and finite water depth. It benefits from more than 20 years of development and it is continuously updated

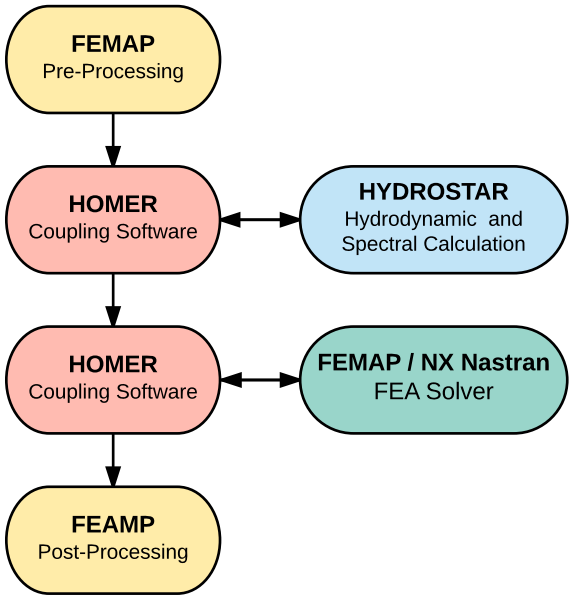

Figure 4.1: Overview of the flow between the different software used

and improved to rise to technological challenges.

HydroSTAR is used within HOMER to carry out seakeeping analysis. For the thesis the analysis will be performed in the frequency domain, and we thus have linearity. A Brief review of seakeeping model used in most seakeeping tools based on Boundary Integral Equation techniques, including Hydrostar. The rest of this section is adapted from the Hydro Strucutre Papers theory manuals for Hydrostar [7], written by Malencia [23]. All equations are taken directly from Malencia [23].

Seakeeping model

The problem is formulated in the frequency domain. Total velocity potential can be split into the three components. The incident, diffracted and radiated potential. This is given as:

$$\phi = \phi_I + \phi_D - i\omega\Sigma_{j=1}^{6}\xi_j\phi_{Rj} \tag{4.1}$$

Here ϕ_I denotes the incident potential, ϕ_D denotes the difraction potential, ϕ_{Rj} denotes the radiation potential and ξ_j denotes the rigid body motions.

The corresponding dynamic pressure can be found from the linear Bernouli equa-

tion and can written with a similar adoption as the total velocity potential:

$$p = i\omega p\phi = p_I + p_D + \Sigma_{j=1}^{6}\xi_j p_{Rj} \tag{4.2}$$

The dynamic variation of the hydrostatic pressure needs to be added to equation 4.2 to obtain the total hydrodynamic pressure. the dynamic variation of the hydrostatic pressure is given as:

$$p^{hs} = -\rho g\big[\xi_3 + \xi_4(Y - Y_G) - \xi_5(X - X_G)\big] \tag{4.3}$$

The motion equation is written in the earth fixed reference system. The subscript "G" in equation 4.3 denotes the position of the center of gravity. Since the motion equation is written in the earth fixed reference system the restoring matrix is not obtained directly by integration of the hydrostatic pressure, given in equation 4.3, but also the change of the normal vector should be taken into account. This gives:

$$\boldsymbol{F}^{hs} = \big[\boldsymbol{C}\big]\{\boldsymbol{\xi}\} = \iint_{S_B^H}\big[p^{hs}n - \rho g Z\boldsymbol{\Omega}\Lambda n dS\big] \tag{4.4}$$

Here $\boldsymbol{\Omega}$ denotes the rotational component of the motion vector $\boldsymbol{\Omega} = (\xi_4, \xi_5, \xi_6)$ and $\boldsymbol{S_B^H}$ denotes the hydrodynamic mesh of the wetted body surface. Also here a compact notation is used so that the normal vector $\boldsymbol{n}$ denotes (n_x, n_y, n_z) for i = 1,3 and $(R - R_G)\Lambda n$ for i = 4,6. Forces corresponding to the pressure acting on the wetted body surface is obtained after integrating the pressure over the wetted body surface. Then the rigid body motion equation, in the frequency domain, can be written as:

$$\big(-\omega^2([\boldsymbol{M}] + [\boldsymbol{A}]) - i\omega[\boldsymbol{B}] + [\boldsymbol{C}]\big)\boldsymbol{\xi} = \{\boldsymbol{F}^{DI}\} \tag{4.5}$$

Where:

- $[\boldsymbol{M}]$ - genuine mass matrix
- $[\boldsymbol{A}]$ - added mass matrix
- $[\boldsymbol{B}]$ - damping matrix
- $[\boldsymbol{C}]$ - hydrostatic restoring matrix
- $\{\boldsymbol{F}^{DI}\}$ - exitation force vector

Finally the exitation, added mass and damping can be expressed as:

$$F_i^{DI} = i\omega\rho \iint_{S_B} (\varphi_I + \varphi_D) n_i dS \tag{4.6}$$

$$\omega^2 A_{ij} + i\omega B_{ij} = \rho\omega^2 \iint_{S_B} \varphi_{Rj} n_i dS \tag{4.7}$$

Boundary Value Problem

This subsection about solving the Boundary Value Problem is taken directly from Malcencia [23] a part of Bureau Veritas selected hydro-structure publications[4]

In Hydrostar the Boundary Integral Equation (BIE) method based on the source formulation is used to solve the Boundary Value Problem (BVP) for different potentials. For a case of zero forward speed, the general form of the BVP is:

$$\left\{ \begin{array}{ll} \Delta\phi = 0, & \text{in the fluid} \\ -\nu\phi + \frac{\delta\phi}{\delta z} = 0, & z = 0 \\ \frac{\delta\phi}{\delta n} = V_n, & \text{on} S_b \\ lim[\sqrt{\nu R}\left(\frac{\delta\phi}{\delta R} - i\nu\phi\right)] = 0, & R \to \infty \end{array} \right\}. \tag{4.8}$$

where V_n denotes the body boundary condition which depends on the conciderd potential:

$$\frac{\delta\phi_D}{\delta n} = -\frac{\delta\phi_I}{\delta n}, \frac{\delta\phi_{Rj}}{\delta n} = n_j \tag{4.9}$$

Within the source formulation, the potential at any point in the fluid is expressed in the following form:

$$\phi = \iint_{S_B^H} \sigma G dS \tag{4.10}$$

where G stands for the Green function, and σ is the unknown source strength which is found after solving the following integral equation:

$$\frac{1}{2}\sigma + \iint_{S_B^H} \sigma \frac{\delta G}{\delta n} dS = V_n, on S_B^H \tag{4.11}$$

This equation is solved numerically, after discretizing the wetted part of the body into a number of flat panels over which the constant source distribution is assumed.

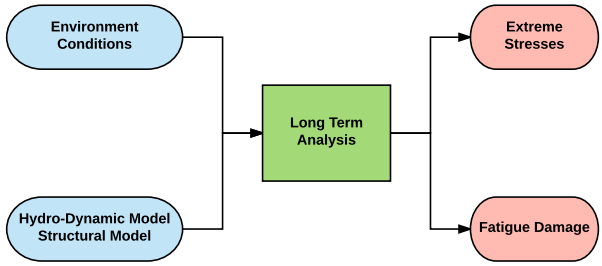

Figure 4.2: The principle of a direct calculation approach. A long term analysis of the structures response for a given environmental condition. Based on this extreme stresses can be established. The figure is adapted from Homer 2 Theory manual

4.3 Homer

Homer is Bureau Veritas' software for direct hydro-structure calculations. The software is based on an advanced coupling method developed in Bureau Veritas Research Department, and interfaces Bureau Veritas hydrodynamic solver, Hydrostar, with a structural solver, which for the analysis in the Master Thesis will be NX Nastran.

Homer is capable of checking the capacity of a design to withstand wave induced loads during its whole lifetime. It takes particulars of the floating unit and the environmental environment into account to consider both extreme loading and fatigue damage failure modes. For the thesis, only extreme lading will be assessed.

The objective for a direct calculation approach is to compute the behaviour (i.e. response and stresses of the structure) of the floating structure when facing certain environmental conditions. The principle is shown in 4.2

As Homer is a coupling software for hydrodynamic and structural calculations, there is mainly two calculations which is done. The first one is a hydrodynamic calculation to calculate the hydrodynamic pressure on the hull. This is usually done on a coarser mesh than the mesh for structural calculations. This to save computation time as this is a quite time consuming step. These calculations are done in Hydrostar, and in Homer this is seen as a black box. For the thesis the hydrodynamic calculations is performed in the frequency domain and is thus valid for the low and medium sea-states. The second calculation is the strucutral calculation. Before this calculation, Homer transfer the pressures from the hydrodynamic model used in the hydro calculations to the structural model. Then the structural calculation is done with a FEA solver, in this case NX Nastran.

Transfer of pressure from hydro to structural model

How the pressures is transferred form the hydro-model to the structural model is briefly described in the following. This section is largely based on Malencias [23] description of how the pressure is transferred form the hydro model to the structural model ... For a more through description this can be found in Bureau Veritas selected hydro structure publications [4]

The loading of the structural model is composed of two parts:

- Inertia loads
- External pressure loads

The issue of transferring loads between the hydro and structural FE model is that the models need to be in equilibrium between pressure and inertia loads. This is not a straight forward operation as the mesh of the structural model and the hydrodynamic model have different meshes.

Inertia loads can be included straightforwardly by associating the acceleration vector to each finite element. Concerning the pressure loading, most of the methods nowadays use the different interpolation schemes in order to transfer the total hydrodynamic pressure from hydro model (centroids of the hydro panels) to the structural model (centroids or nodes of the finite elements).

Besides the problems of interpolation, it is important to note that the motion amplitudes, which are present in the definition of the total pressure, are calculated after integration over the hydrodynamic mesh. For that reason it is impossible to obtain the completely equilibrated structural model. Indeed, the FEM model has its own integration procedure which is usually different. In order to obtain the perfect equilibrium of the structural model Homer is based on two main ideas:

- Instead of interpolation, the pressures is recalculated on the structural mesh
- Separate transfer of pressure components, and calculation of hydrodynamic coefficients (added mass, damping, hydrostatics and excitation) by integration over the structural mesh

Recalculation of the dynamic pressure is possible since Hydrostar, which is used to calculate the pressure on the hydro model, is based on the Boundary Integral Equation(BIE) method based on source formulation. A description of Hydrostar will be given in the following section. The BIE method gives the continuous representation of the potential through the whole fluid domain. This simplifies the

communication between the hydrodynamic and structural code. To get correct pressure on the structural model, the potential can now be evaluated by the hydrodynamic code at the structural coordinates of the points where the potential is required. The potential with structural coordinates can be expressed by:

$$\boldsymbol{\varphi(x_s)} = \iint_{\boldsymbol{S_B^H}} \boldsymbol{\sigma(x_h) G(x_h; x_s) dS} \tag{4.12}$$

Wher $\boldsymbol{x_s} = (x_s, y_s, z_s)$ denotes structural points, $\boldsymbol{x_h} = (x_h, y_h, z_h)$ the hydrodynamic points, φ is the potential, $\boldsymbol{S_B^H}$ denotes the hydrodynamic mesh of the wetted body surface, $\boldsymbol{\sigma}$ is the source strength and $\boldsymbol{G}$ denotes the Green function.

In the case of linear seakeeping without forward speed, the pressure is directly proportional to the velocity potential and, within the source formulation, the potential is continuous across the body wetted surface, thus this operation is sufficient.

Once each pressure component has been transferred onto the structural mesh, the hydrodynamic coefficients are calculated by integration over the structural mesh. This can be expressed by:

$$F_i^{DI^s} = i\omega\rho \iint_{S_B^S} (\varphi_I^S + \varphi_D^S) n_i dS \tag{4.13}$$

$$\omega^2 A_{ij}^S + i\omega B_{ij}^2 = \rho\omega^2 \iint_{S_B^S} \varphi_{Rj}^S n_i dS \tag{4.14}$$

here the superscript "^{S}" indicates that the quantities is taken on the structural mesh.

The total matrix can then be written as:

$$\big[\boldsymbol{C}\big]^S = \big[\boldsymbol{C}\big]^p + \big[\boldsymbol{C}\big]^g \tag{4.15}$$

Here the first term represent the hydrostatic restoring matrix and the second term account for the change of coordinate system in order to obtain the complete hydrostatic restoring matrix. The first term of the hydrostatic restoring matrix is obtained by integrating the hydrostatic pressure due to the body motions, over the hydrodynamic mesh of the wetted body surface. This can be written as:

$$C_{ij}^p = \iint_{S_B^S} p_j hs n_i dS \tag{4.16}$$

where p_jhs is the hydrostatic pressure due to the body motions and equals:

$$p_jhs = -\rho g\big[\xi_3 + \xi_4(Y - Y_G) - \xi_5(X_X G)\big] \tag{4.17}$$

$\xi_i =$ the rigid body motion and the subscript "G" denotes the position of the center of gravity, with respect to which the motion equation is written.

It can be shown that the second term is accounted for by the change of gravity action, and this is expressed as:

$$\boldsymbol{F^g} = -mg\boldsymbol{\Omega}\Lambda\boldsymbol{k} = \big[\boldsymbol{C}\big]^g\{\boldsymbol{\xi}\} \tag{4.18}$$

Here $\boldsymbol{\Omega}$ denotes the rotational component of the motion vector $\boldsymbol{\Omega} = (\xi_4, \xi_5, \xi_6)$.

Now the finale motion equation can be written as:

$$\big(-\omega^2([\boldsymbol{M}] + [\boldsymbol{A}]^s) - i\omega[\boldsymbol{B}]^s + [\boldsymbol{C}]^s\big)\boldsymbol{\xi}^s = \{\boldsymbol{F}^{DI}\}^s \tag{4.19}$$

The body motions $\{\boldsymbol{\xi}\}^s$ can now be obtained by solving equation 4.19. Finally the total linear pressure on the structural mesh can then be written as:

$$p^s = p_I^s + p_D^s + \Sigma_{j=1}^6 \xi_j^s(p_{Rj}^s + p_j^{hs}) \tag{4.20}$$

To sum up the final loading on the structural model can be summed up in three parts:

- p_i^s - Pressure loading applied to wetted finite elements only
- $-\omega^2 m_i \boldsymbol{\xi_i^s}$ - Inertia loading applied to every finite element
- $-m_i g\boldsymbol{\Omega}^s\Lambda\boldsymbol{k}$ - Gravity term to apply on every finite element

Now the structural loading described above will be in perfect equilibrium since this equilibrium is implicitly imposed by the solution of the motion equation 4.19. All the coefficients were calculated by using directly the information from the structural FE model. With the structural loads established the FE Analysis can now be carried out in NX Nastran to evaluate the deformations and stresses of the structure.

Solving the motion equation and establishment of RAOs

Now that all the different coefficients and the motion equation is established, Homer can solve the motion equation to determine the body motions $\boldsymbol{\xi}$. With the body motions established the Response Amplitude Operators (RAO) can be created. RAO is the transfer function of the body motions, i.e. the response amplitude per unit wave amplitude[11]. In the frequency domain the response can be written as [4]:

$$\boldsymbol{\xi} = \xi_a e^{i(\phi - kx)} \tag{4.21}$$

The wave elevation in the frequency domain is on the form[4]:

$$\boldsymbol{\eta} = \eta_a cos(\omega t - kx) + i\eta_a sin(\omega t - kx) = \eta_a e^{-ikx} \tag{4.22}$$

The RAO is determined by its amplitude and phase[4]:

$$RAO = \frac{Response}{Excitation} = \frac{\xi_a}{\eta_a} e^{i\phi} \tag{4.23}$$

Here ω defines the wave frequency, k the wave number, t time, λ the wave lenght and x location.

4.4 Starspec

This section gives a brief reviev of the Starspec module of Hydrostar. The following is largely based on the Strspec manual [8] where a more detailed description of the software may be found. All equations in this section is taken directly from the Starspec manual.

Starspec is a spectral analysis software that performs first order spectral analysis, short term and long term response analysis. In addition it can perform the fatigue damage calculation by using Miner's Rule if provided with a S-N curve for a structural detail. However for the thesis Starspec is used to make a long term response analysis of the internal loadings of the Havfarm. This resulting long term maximum will then be used to establish an equivalent design wave.

Spectral Analysis

The spectral density $S_\omega(\omega)$ represent the distribution in frequency (ω) of the wave energy and the $RAO(\omega)$ is considered as being the transfer function of any first order quantity, for example accelerations, motions or stresses.

The spectral density of response can now be written as:

$$S_R(\omega) = RAO^2(\omega) * S_\omega(\omega) \tag{4.24}$$

With the spectral density established the spectral moments can now be defined as:

$$m_n = \int_0^\infty \omega^n S_R(\omega) d\omega \tag{4.25}$$

If several spectra with different directions are used, the spectral momentum are sum :

$$m_n = \Sigma_i^m \int_0^\infty \omega^n S_\omega(\omega, \theta) * RAO^2(\omega, \theta) d\omega \tag{4.26}$$

Short Term Statistics

For the thesis the duration of one sea state corresponding to short term is chosen to be three hours, or 10800s. The sea sea state is then considered stationary. Furhter the ragne of response is considerd a random variable R. The process is assumed to be narrow banded and the probability density of response follows the Rayleig's distribution:

$$p(R) = \frac{R}{4m_0} exp(\frac{-R^2}{8m_0}) \tag{4.27}$$

The distribution function is given as:

$$P(R) = 1 - exp(\frac{-R^2}{8m_0} \tag{4.28}$$

JONSWAP Spectrum

The JONSWAP formulation is assumed to give a good representation of the sea states which the Havfarm is subjected to.

$$S_\omega(\omega) = A * \frac{5}{16} H_s^2 \omega_p^4 \omega^{-5} exp[-\frac{5}{4}(\frac{\omega}{\omega_p})^{-4}] \gamma^{\left[exp(\frac{-(\omega-\omega_p)^2}{2\sigma^2\omega_p^2})\right]} \tag{4.29}$$

Where A is:

$$A = \frac{1}{5 \cdot (0.065 \cdot \gamma^{0.803} + 0.135)} \tag{4.30}$$

γ is the peak-enchantment factor, and the only variable to adjust in the input to the Starspec. This factor is not determined in the metocean report provided by NSK Ship Design, however it is determined graphically by iterating it till it makes

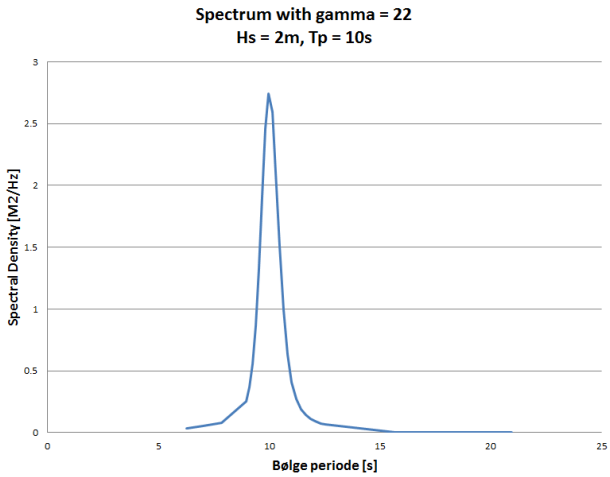

Figure 4.3: Fitted Wave Spectrum. This wave spectrum is obtained by adjusting the peak-enchantment factor in equation 4.29 til the spectrum is the same as in the metocean report recived from NSK Ship Design which can be found in appendix A

a good fit to a spectrum suggested for a sea state in the metocean report [3] in appendix A. The resulting spectrum is shown in figure 4.3 It is then assumed that this value us valid for all sea states.

The error of the spectrum is is less than 1.5%, up to $\gamma = 30$.

Long Term Statistics

Considering that a short term analysis, as above described, is performed for a list of sea states observed during a reference period DREF . The long term distribution can then be obtained by cumulating the results from the short term analysis. the method implemented in Starspec is described down in the following paragraph.

The method consists in counting, over all sea-states, of all maxima of the response (i. e. each response cycle). This method, identical to the Battjes wave counting, is commonly used for the evaluation of structural response of ships and offshore structures under cyclic (wave) actions, for both fatigue and extremes.It can be written as:

$$n_{ex}(X) = \Sigma_{SS}^{SS=N_{SS}} n_{SS}(1 - P(X)) \tag{4.31}$$

where,

- N_{SS} is the total number of sea states

- $n_{ex}(X)$ is the expected number of exceedance of a response level X, over a reference duration D_{REF}
- P(X) is the Rayleigh distribution of the sea state SS accodring to equation 4.28
- n_{ss} is nuber of response cycles for a sea state SS, defined as (DREFx365.25x24x3600)/RT_Zxpro prob(SS) being probability of occurrence of the sea state.

Further if the long-term is long enough, all the waves can be considered independent, and the long term cumulative distribution can then be written as :

$$P(R) = \Pi_{SS}^{N_{SS}}(1 - e^{R^2/8m_0})^{n_{SS}} \tag{4.32}$$

This equation can then be solved to get the range exceeded with a risk α in a given duration $(\alpha = 1 - P(R))$

4.5 NX Nastran

NX Nastran is a FE solver. It can be used for a numerous types of analysis, including stress, vibration, buckling, structural failure, heat transfer, acoustics and aeroelasticity analyses. For the thesis NX Nastran is used to run the FEA of the Havfarm with the load cases established by Homer.

Chapter 5

Modelling of the Havfarm Structure

In this Chapter the modelling process and justification of the modelling will be presented.

Several models have been made of the Havfarm as the structure have been subjected to changes continuously during the work of this master thesis. There are mainly two models established. One for the early design, and one for the design at this stage. For the latter model an attempt was made to include the lice skirt in the hydrodynamic model. Due to numerical problems within the seakeeping analysis software, Hydrostar, it turned out to be impossible to obtain good results when an attempt to include the lice skirt was made. Thus a model of the current design of the structure without the lice skirt was established which the rest of the analysis is based upon. However, development of an element which can correctly model both the lice skirt and nets are in development whit in the research department of Bureau Veritas. At a later time these parts of the structure may be included. A thorough description of all the models analyzed will be presented in the following.

5.1 Limitations, Assumptions and Simplifications

Homer and Hydrostar are both software designed to performer analysis on ships and other seagoing structures such as semi-submersibles. Although the Havfarm structure can be regarded as a semi-submersible in many ways, there are some new challenges occurring when the seakeeping analysis are going to be performed in Hydrostar. First of all there are the nets which at this stage are impossible to model in a good way in Hydrostar, and thus they are completely neglected. Secondly there

is the lice skirt.

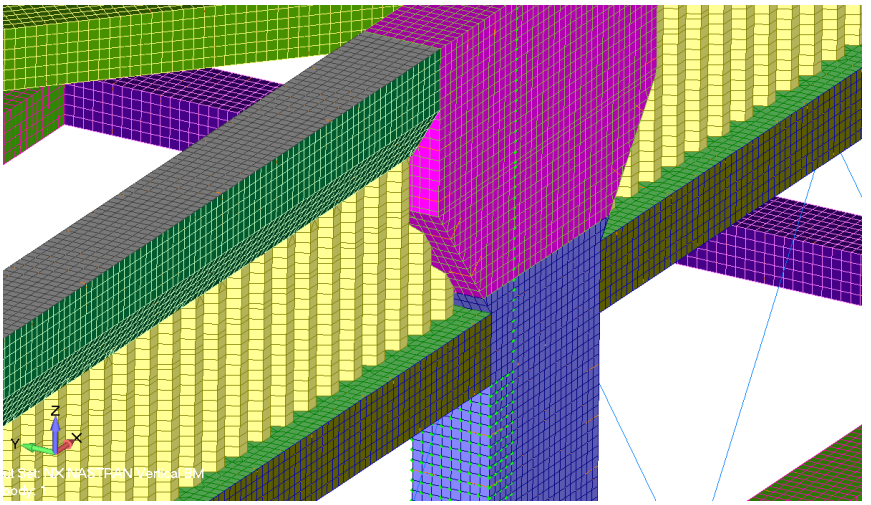

Figure 5.1: Finite element model of lice skirt

Normally in Hydrostar, when a ship or a semi-submersible is analyzed, the hull is modelled with panels, in the same way as done with the Havfarm. However, for a ship hull the panels will only see pressure from one side, the wetted side, of the panel. This is the case for the pontoons and columns of the Havfarm as well. However, the lice skirt will see pressure from both sides, and this is where the problem occur. The panels in Hydrostar can only see pressure on one side. Thus there is not a straight forward way of modelling the lice skirts for the seakeeping analysis in Hydrostar. In addition to this, there are also another limitation. Due to numerical problems in Hydrostar, panels cannot be placed too close to each other. In order to be able to model the lice skirt at all they then have to be modelled with panels on both side of the lice skirt, and in addition the distance between them cannot be to short. Thus the only way to model them at this stage is to model panels as indicated in figure 5.2. Here the lice skirts are modelled with panels on both side, with a distance between them corresponding to the breath of the pontoons. Figure 5.1 shows the lice skirt in the FE model, which represents the true physical case. By comparing these two figures, figure 5.2 and 5.1, it is easy to see that a the hydro-model doesn't represent the physical case in a good way. The consequence of this is that the water plane area is increased significantly compared to what it really is. Also the mass needed to obtain the draft of 30m is significantly increased. This will affect the response properties of the Havfarm structure. Some seakeeping analysis are performed on the latest design with lice skirts modelled as in figure 5.2 and will be presented to show the effect. For the main analysis the the

lice skirts are thus assumed to have little influence of the response of the Havfarm, and completely neglected.

In short thees assumptions are made for the main analysis:

- Mooring loads are assumed to have negligible effect on the global analysis of the Havfarm
- The effect of the lice skirts are assumed to be negligible
- The effect of the weight of and the loads on the fish nets are assumed to be negligible

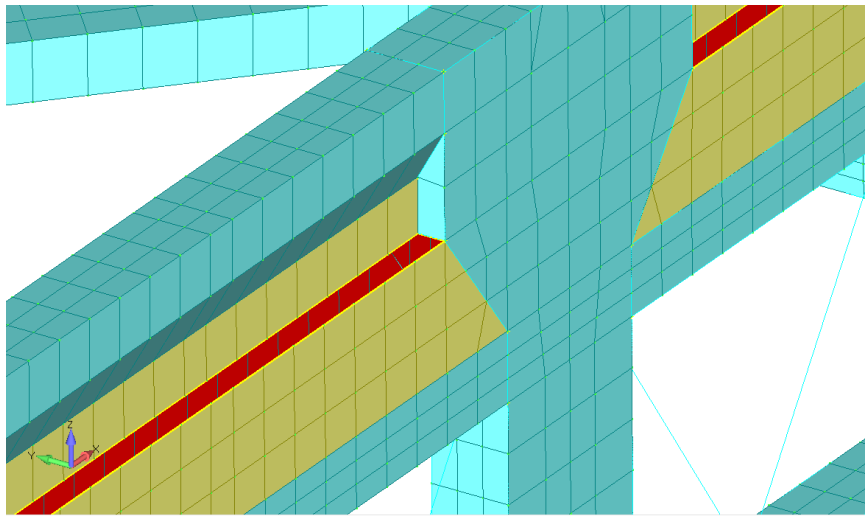

Figure 5.2: Hydro model of lice skirt

5.2 Coordinate System

Table 5.1: Coordinate system

Coordinate system origin			
	X = 0	Y = 0	Z = 0
Structural Model	AP	Center Line	Base Line
Hydro Model	AP	Center Line	Mean Free Water Surface

5.3 Early Havfarm Model

The hydro-model of the early Havfarm model is shown in figure 5.3. The mesh is created in FEMAP and imported to Hydrostar for sea keeping analysis. The the mesh consist of rigid panels representing the hull of the Havfarm.

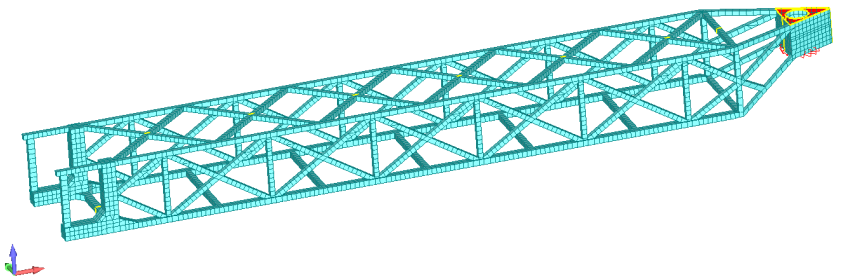

Figure 5.3: Early Havfarm Design

No structural model was established for this design thus only the seakeeping analysis in Hydrostar was preformed. This because the concept was subjected to a major change in the design at this stage, and it was decided to update the model and focus on the new design. Main dimensions and hydro properties calculated by Hydrostar are given in table 5.2.

Table 5.2: Hydrodstatic properties

Hydrostatoc Properties		Main Dimensions	
Mass	30 467 [tonnes]	Loa	423 [m]
Displaced Volume	29 724 $[m^3]$	Breath	60 [m]
Vertical Center of Gravity	-1,7 [m]	draft	30 [m]
Vertical Center of Buoyancy	-19,6 [m]	Number of panels	2 811
Water Plane	738.7 $[m^2]$		
GM_L	630.1 [m]		
GM_T	-4.8 [m]		

This seakeeping analysis of the early Havfarm design was quite simplified. This due to lac of detailed information about the structure. The mass is evenly distributed along the length of the structure. The longitudinal center of gravity is placed at the same location as the longitudinal center of buoyancy calculated by Hydrostar in order to obtain zero trim. Worth noticing is the negative GM_T for this model calculated by Hydrostar. In general this is not a good value with stability properties in mind. The reason for this negative value is probably a badly placed

vertical center of gravity. This should have been corrected/updated based on more detailed weight distribution, however as stated in the beginning of this section it was decided to focus on the updated design instead. The seakeeping analysis of this model didn't give any good results due to the way it was modelled. For this reason the results are not presented in the report.

5.4 Finale Hydro-Model

Based on the latest drawings received form NSK Ship Design, two Hydro-models was established. The main differences between them are the weight distribution and the lice skirts. A thourough description of the two models is given below. Both models are modelled as a three dimensional panel model.

5.4.1 Hydro-Model with Lice Skirt

The hydro-model of the finale Havfarm with lice skirts is shown in figure 5.4. Much like the early Havafarm model, the weight distribution on this model is also simplified. The hull is modelled by panels according to drawings provided by NSK Ship Design. The liceskirts are modelled as shown in figure 5.2.

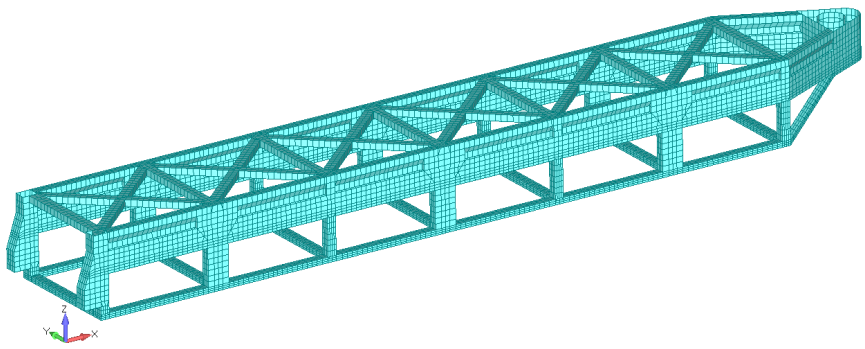

Figure 5.4: Final Havfarm Design with Lice Skirt

This model consist of a total of 7353 panels. The pressure calculation over the panels is the most time consuming step in the analysis, thus the number of panels have to be kept as low as possible. The size of the panels are in general $2.5[m]x2.5[m]$. The exceptions are at the pontoons where Hydrostar requires a minimum of 3 panels in the with of the pontoon in order to give accurate results.

Table 5.3: Hydrostatic properties and main dimensions of the hydro-model of the Havfarm with lice skirts

Hydrostatoc Properties		Main Dimensions	
Mass	54 122 $[tonnes]$	Loa	401 $[m]$
Displaced Volume	52 802 $[m^3]$	Breath	59,5 $[m]$
VCoG	-1,7 $[m]$	draft	30 $[m]$
VCoB	-11,9 $[m]$	Number of panels	7353
Water Plane	3 320 $[m^2]$		
GM_L	875,8 $[m]$		
GM_T	32,6 $[m]$		

When comparing the properties of this model, with the one without lice skirts, it is clear that there is a huge difference in the water plane area and GM_L. Evaluating the natural period equation for heave and pitch given in equation 6.1 and 6.2, it is clear that this will lower the natural period in heave and pitch. This was also observed form analysis performed, however the results was preliminary and since it was decided to neglect the lice skits, good results for this model was not established.

5.4.2 Hydro-Model without Lice Skirt

This model is the finale model. This model is used to calculate the pressures which is later transferred to the structural FE model. As the models described above, it is modelled as a 3D panel model. The elements have a size of $2.5x2.5$ in general. The exceptions are at the pontoons where Hydrostar requires a minimum of 3 panels in the with of the pontoon in order to give accurate results. The hydrodynamic properties and main dimensions of the model can be found in table 5.4. For this model the weight have been accurately applied. This is done by Homer which import the weight form the structural model and applies it to the hydrodo-model. The water ballast tanks have been modelled as concentrated masses. This is done also done for the fore and aft ship. The weight of each water ballast tank corresponds to the volume of the tank times the water density. The steel weight is calculated with the density assigned for the steel in the FE model and automatically applied by Homer. A more detailed description of how the weight is applied to the structure is given later in section 5.5.1

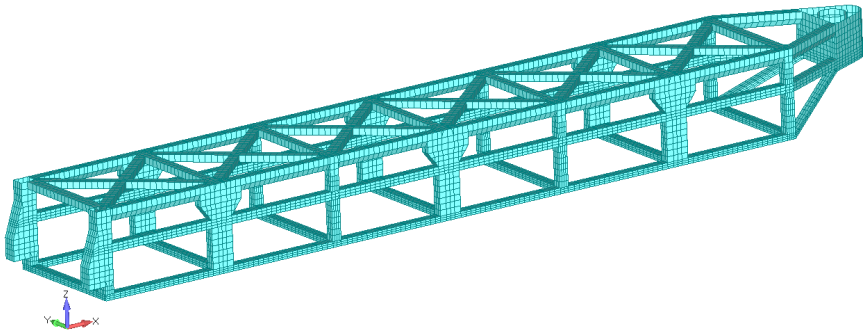

Figure 5.5: Final Havfarm Design without lice skirt

Table 5.4: Hydrodstatic properties and main dimentions, Reference system from hydro model, AP CL Free Surface. Values calculated by Homer

Hydrostatoc Properties		Main Dimensions	
Mass	37 252 [tonnes]	Loa	401 [m]
Displaced Volume	36 067 $[m^3]$	Breath	59,5 [m]
VCoG	-17,9 [m]	draft	30 [m]
VCoB	-15,8 [m]	Number of panels	5926
Water Plane	909,4 $[m^2]$		
A_{33}	36 160 [tonnes]		
Roll Radius of Gyration	26,9 [m]		
Pitch Radius of Gyration	108,1 [m]		
Yaw Radius of Gyration	110 [m]		
GM_L	487,2 [m]		
GM_T	16,1 [m]		

5.5 FE Model

The build of the finite element(FE) model have been the most time consuming part of the thesis. As new information and drawings have been received from NSK Ship Design continuously during the work of the thesis the model have been updated continuously as well. A detailed FE model is established to evaluate the global strength of the Havfarm structure.

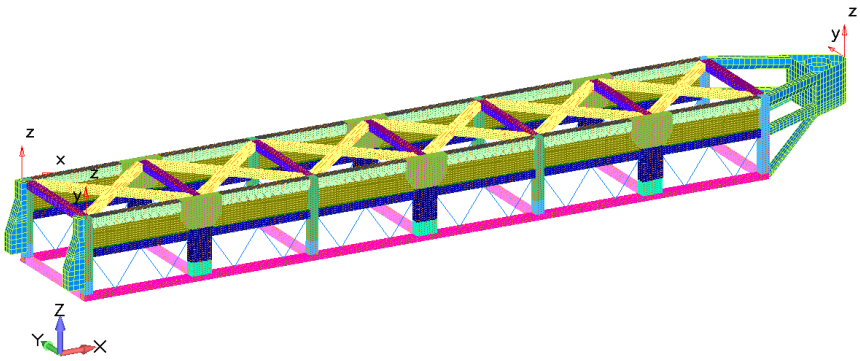

Figure 5.6: An overview of the FE model. The constraints are marked wiht red arrows and restricted degree of freedom.

For the global analysis the bow and stern of the structure are not of interest, and thus these parts of the structure are simplified. The bow and the stern are modelled with panels as in the hydro-model. These panels are rigidly connected to the rest of the model as well as a mass element to simulate the steel weight. The bow and stern are modelled like this to ensure a proper transfer of the load from the seakeeping analysis and into the rest of the model.

Between the bow and the stern the whole model are fully modelled with all stiffeners and web frames. The hull of the pontoons and the lice skirts are modelled with isoparametric quadrilateral shell elements. The size of the shell elements are in general $0,5[m]x0,5[m]$.

Stiffeners and web frames are modelled with beam elements with a general length of $0,5[m]$.

The water ballast tanks have been modelled with mass elements representing the mass of the ballast tank. The mass element is connected to the elements making up the ballast tank with a rigid element.

A thoughrough description of the elements used in the modell is given in section 5.5.2

Details of the FE model are shown in figure through

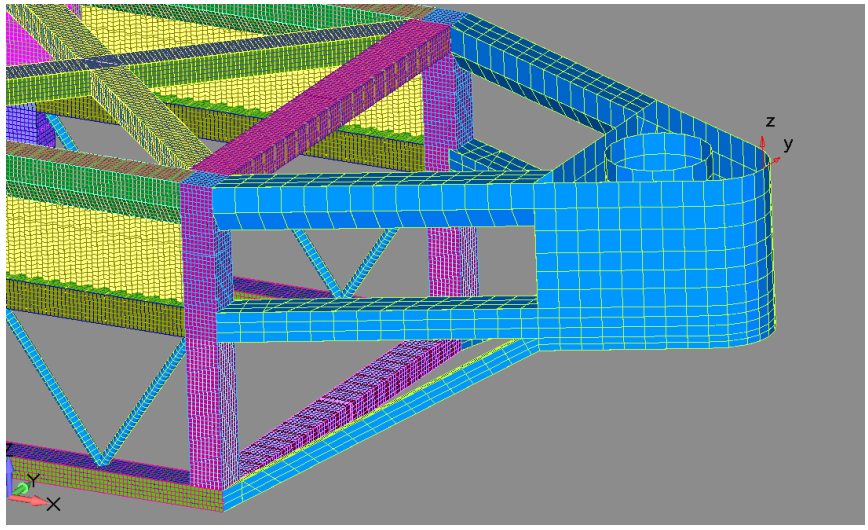

Figure 5.7: Here the coarse panels and the much finer structural mesh is shown

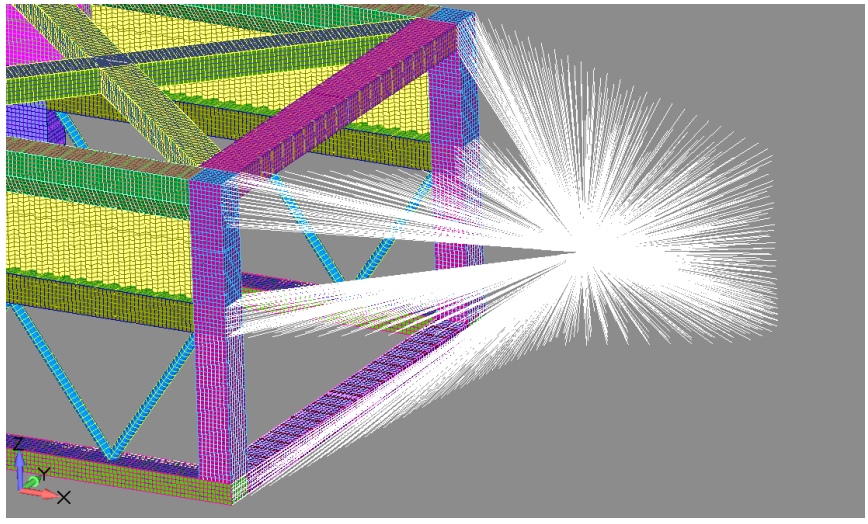

Figure 5.8: The rigid element connecting the coarse panels to the much finer structural mesh is shown. A mass element is connected in the "center" of the rigid element. The same way of modelling is performed for the aft ship

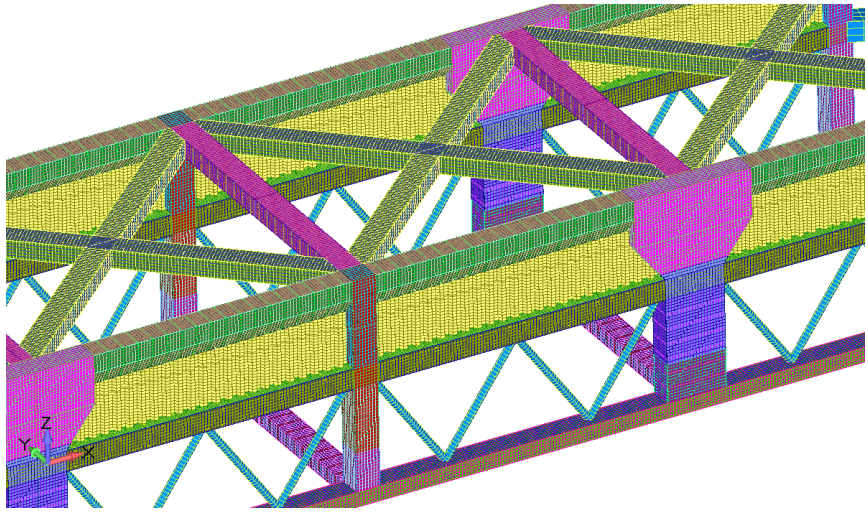

Figure 5.9: Closer overview of the mid-section

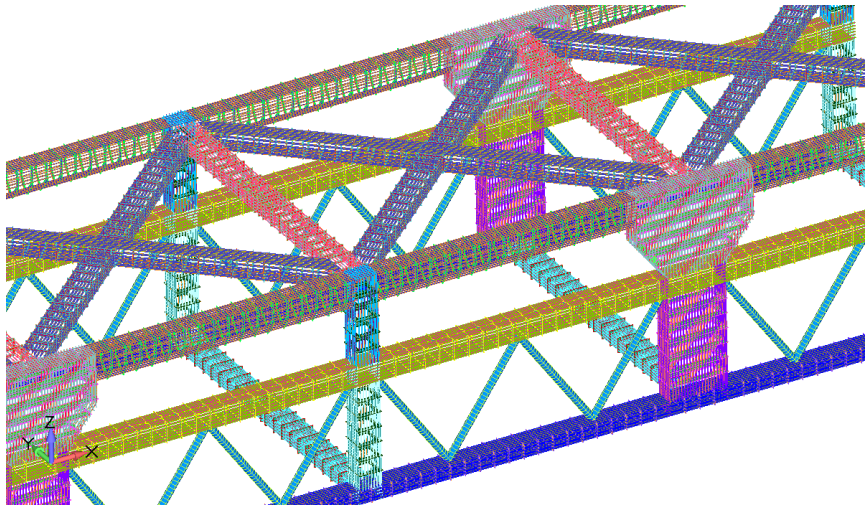

Figure 5.10: Close overview of the mid section without plate to show stiffeners and webframes

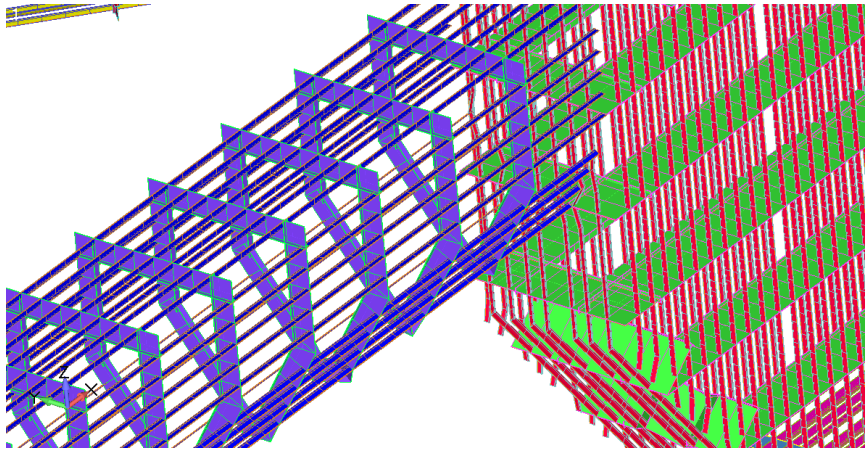

Figure 5.11: Closeup of the connection between top pontoon and one of the big columns

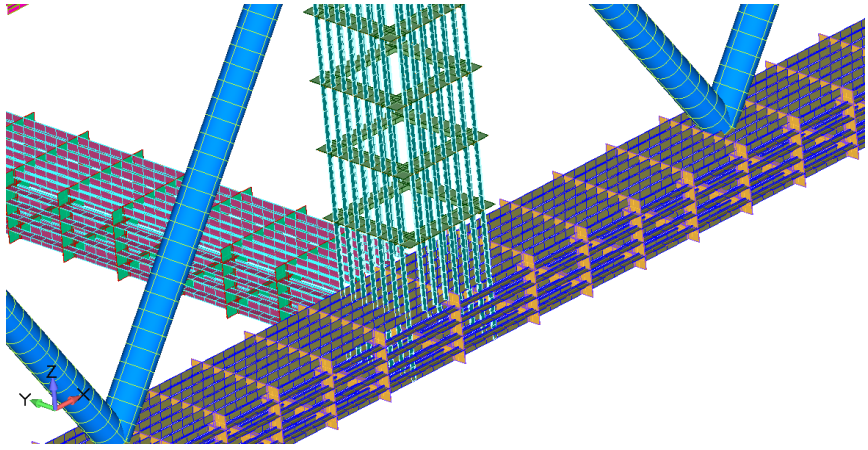

Figure 5.12: Stiffeners and web frames in connection between bottom pontoons and one of the small columns

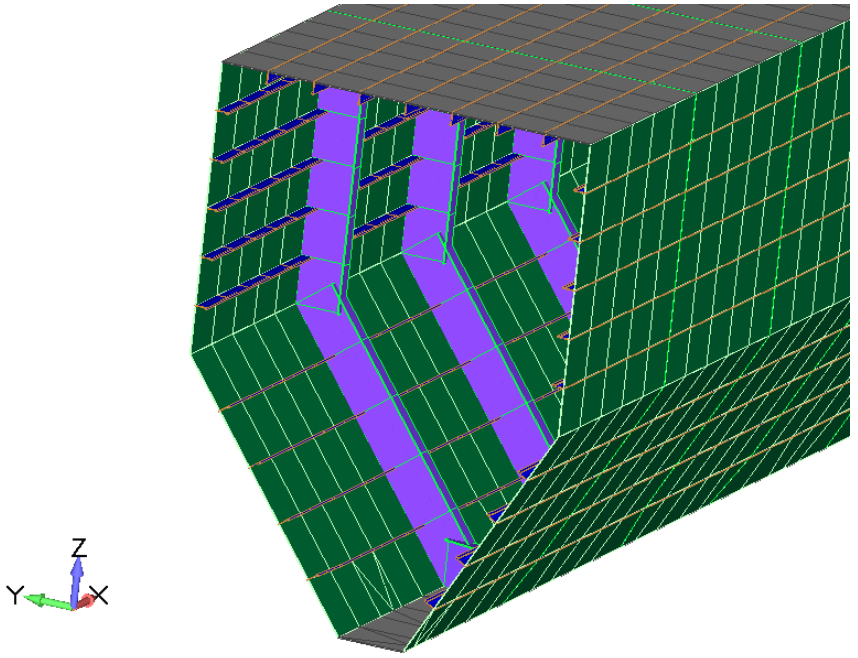

Figure 5.13: Detailed view of top pontoon showing webframes and stiffeners

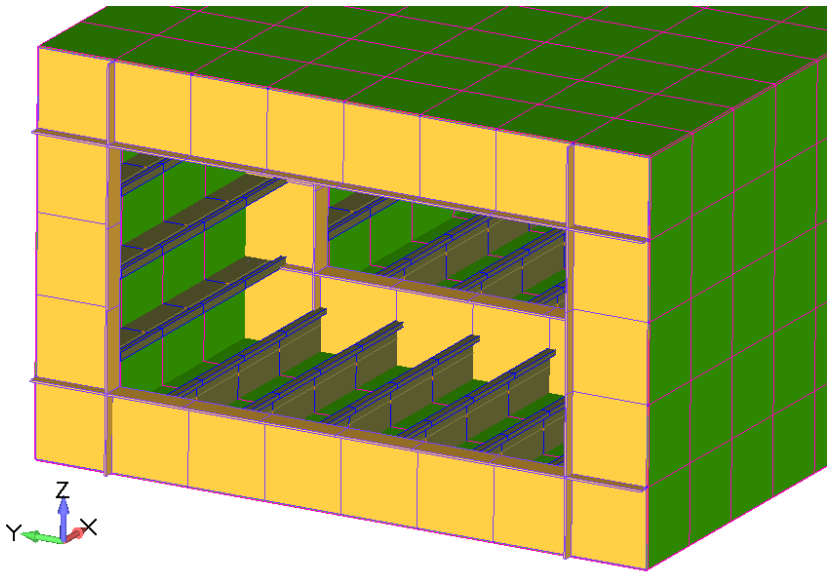

Figure 5.14: Detailed view of bottom pontoon showing web frames and stiffeners

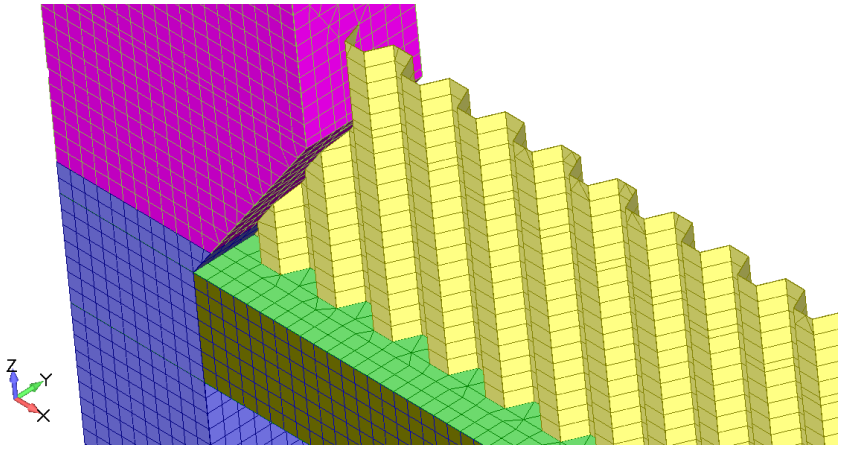

Figure 5.15: Lice Skirt

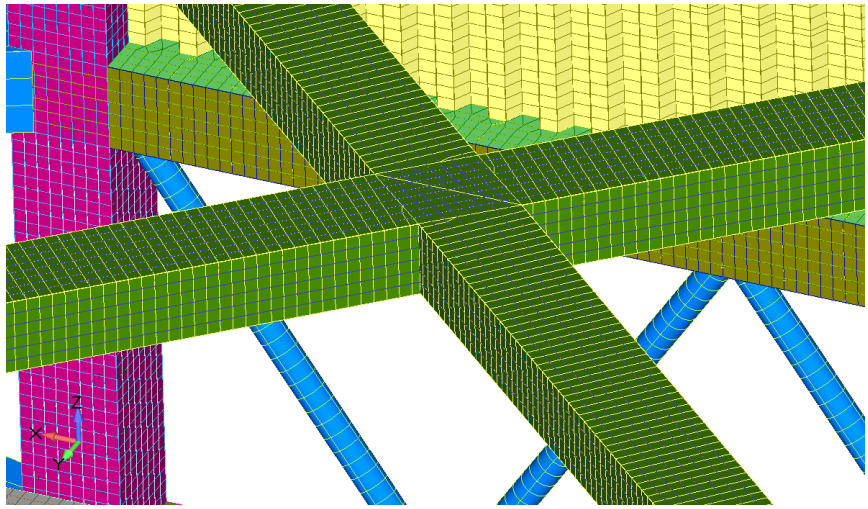

Figure 5.16: Diagonal top pontoons

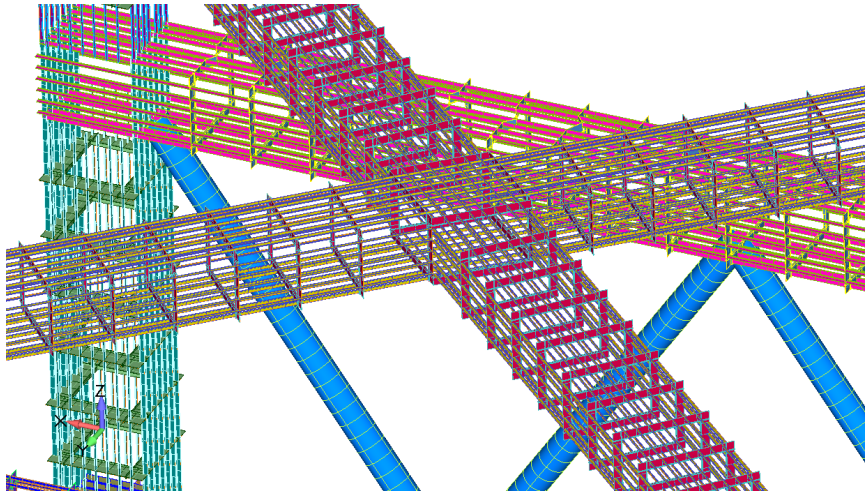

Figure 5.17: Stiffeners and web frames in diagonal top pontoons

Constraints

Boundary conditions are applied to the FE model in order tho prevent rigid body motions. According to BV rules [6] the model is constrained in six degrees of freedom:

- On node on the fore end of the structure: Displacement fixed in $\boldsymbol{Y}$ and $\boldsymbol{Z}$ directions
- One node on the port side shell at aft of the structure: Displacement fixed in $\boldsymbol{X}$ and $\boldsymbol{Z}$ directions.
- One node on the port side shell at aft of the structure: Displacement fixed in $\boldsymbol{Y}$ and $\boldsymbol{Z}$ directions.

These constrains can be seen in figure 5.6

5.5.1 Weight Distribution

This section gives an overview of how the weight of the structure is applied to the FE model. This will also be how the weight is represented in the hydro-model as Homer automatically the weight distribution form the FE model to the hydro-model used for seakeeping analysis in Hydrostar.

The steel weight for the net area is calculated by Femap based on the steel density entered. For the bow and aft of the structure this is modelled with rigid elements

connected to a mass element, representing the mass of the bow/aft, and connected to the panels representing the geometry of the bow/aft. The ballast tanks are modelled in a similar way as the bow and aft. Mass elements are connected to the elements making up the ballast tank with rigid elements. Both the modelling of the bow, aft and the ballast tanks are illustrated in figure 5.18. A detailed list of the mass applied to the modelled is given in table 5.5. However, this table represent the actual weights applied to the model. The information about the mass received form NSK Ship Design have been modified slightly in order to get the correct trim of the structure. This is done by decreasing the weight of the aft structure and aft ballast tanks and increase the weight correspondingly in the front structure and ballast tanks. Also a slight increase in the steel density is applied in order to get the correct draft.

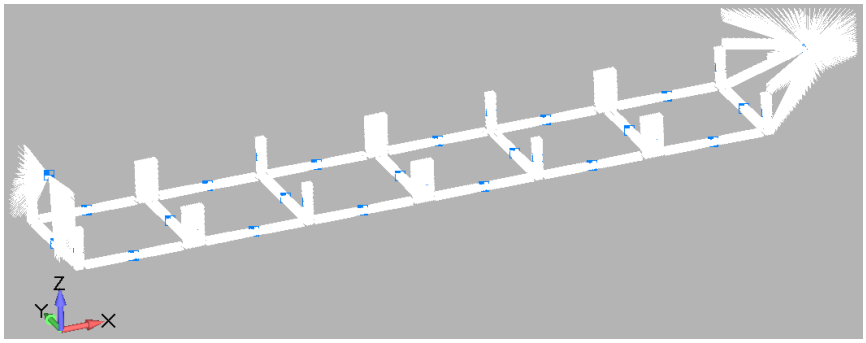

Figure 5.18: Rigid elements represented by white and mass elements as blue dots representing the water ballast tanks and the bow and aft part of the strucure

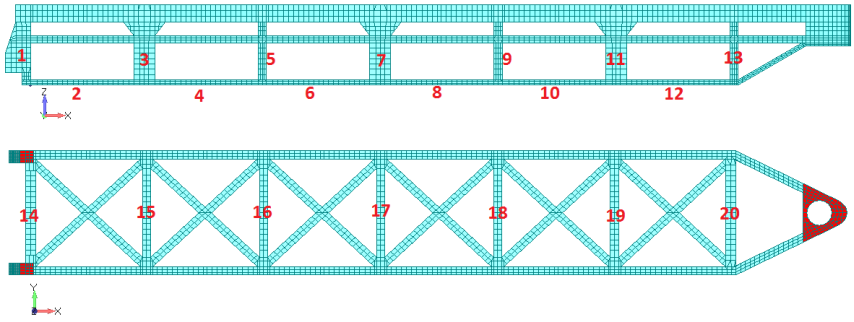

Figure 5.19: Numbering of water ballast tanks. Ballast tanks in columns and longitudinal pontons are shown in the top figure. Ballast tanks in transverse pontons are shown in the bottom figure

Table 5.5: Weight of structure. This table describes the mass aplied to the FE model. Ballast tanks 1 through 13 are placed on both port and starboard side of the strucutre, and thus the mass for thees tanks are multiplied with by a factor 2 when total ballast is calculated. Center of Gravity(GoG) is given in structural cordinate system, with origo in AP, at center line(CL) and base lien(BL)

Ballast Tanks [nr]	CoG (x,y,z) [m]	Density [tonnes/mm3]	Mass [tonnes]
1	-		203,2
3	-		632
5,9,13	-		406,4
7	-		1016
11	-		1500
2	-		311
4,6,8,10	-		622
12	-		933,5
14	-		513
15,16,17,18	-		654
19	-		754
20	-		899
Total ballast	(190, 0, 5.8)		21 390
Net area	(166.6, 0, 20)	9,99e-09	13 745
Bow	(365.6, 0, 24.4)		1 200
Aft	(-4.2, 0, 35.5)		917
Total	(182.3, 0, 12.1)		37 253

5.5.2 Choice of elements

This section gives a short description of all the elements used in the FE model. The information about the elements is taken form Siemens "Element Library Reference" [31]. For a more detailed description of the elements the reader is referred to this document. An overview of the elements used and what area they are used to model is shown in table 5.6.

Table 5.6: Elements used in the FE Model

Element	Type	Area
CQUAD4	4 noded Shell Element	Hull
CTRIA3	3 noded Shell Element	Hull
CBEAM	Beam Element	Stiffeners/Web Frames/Braces
CONM2	Mass Element	Mass of ballast tanks, fore and aft ship
RBE2	Rigid Element	Connecting fore aft panels to structure
RBE3	Rigid Element	Connecting WB tanks and mass

CQUAD4

The CQUAD4 elements are used to model the hull. It is NX Nastran's most commonly used element for modeling plates, shells, and membranes. The element is a quadrilateral flat plate connecting four grid points. It can represent in-plane, bending, and transverse shear behavior. The CQUAD4 element should be used when the surfaces you are meshing are reasonably flat and the geometry is nearly rectangular. The formulation of the CQUAD4 and also CTRIA3 elements are based on the Mindlin-Reissner shell theory [31].

CTRIA3

This element is a triangular plate connecting three grid points. It is most commonly used for mesh transitions and filling in irregular boundaries, which it is used for in the FE model. It is mainly used in the connections with the liceskirt and the pontoons where a it is problematic to keep the CQUAD4 elements rectangular. The element may exhibit excessive stiffness, particularly for membrane strain. Thus, as a matter of good modeling practice, the CITRA3 element should be located elements away from areas of interest whenever possible. In other respects, the CTRIA3 is analogous to the CQUAD4. Triangular elements should be kept as nearly equilateral as possible to ensure accuracy of the element.

CBEAM

The CBEAM element is a beam element. It is used to model stiffeners, webframes and the braces between the bottom and midle pontoon. The beam element includes extension, torsion, bending in two perpendicular planes, and the associated shear.

CONM2

CONM2 is a concentrated mass element. It allows to specify a concentrated mass about its center of gravity.

RBE2

The RBE2 provides a very convenient tool for rigidly connecting the same components of several grid points together. In the FE model the RBE2 element is used to connect the mass elements of the bow and the aft to the panels representing the bow or aft as well as the connection to the rest of the model. The RBE2 (Rigid Body Element, type 2) element defines a rigid body whose independent degrees of freedom are specified at a single point(center of gravity of bow or stern) and whose dependent degrees of freedom are specified at an arbitrary number of points(dof of panels representing the hull of the bow or stern and connection dof to the rest of the structure). The RBE2 element uses constraint equations to couple the motion of the dependent degrees of freedom to the motion of the independent degrees of freedom. Consequently, RBE2 elements do not contribute directly to the stiffness matrix of the structure and ill-conditioning is avoided.

RBE3

The Rigid Body Element type 3 element is used to connect the mass elements of the ballast tanks to the elements making up the tank. The RBE3 element is a powerful tool for distributing applied loads and mass in a model. The RBE3 doesn't add additional stiffness to your structure. Forces and moments applied to reference points (located in the center of gravity of the ballast tank) are distributed to a set of independent degrees of freedom (the dof making up the ballast tanks) based on the RBE3 geometry and local weight factors.

5.5.3 Main Dimensions, Scantlings and Material

Table 5.7: Main Dimensions

Loa	401 [m]
Breath moulded	59.5 [m]
Dept moulded	38.25 [m]
Draft	30 [m]
Web frame spaceing	2.5 [m]
Stiffener spaceing	0.5 [m]
Length of each fish pen compartment	56 [m]
Number of panels	521 634

Table 5.8: Scantlings are listed in this table. The plate thickness of the columns are different dependent on the height above base line. In the table three thicknesses are listed, where the largest thickens is used for 0-10 [m] above baseline, the second largest for 10-20 [m] above base line and the smallest above 20 [m] above base line

Structure	B [m]	H [m]	Plate Thic.[mm]	Stiffener Dim.[mm]	Web Frame Dim.[mm]
Bottom Pontoon	4	2.5	18	HP 280x12	T-shape 500x11x150x12
Transverse Bottom Pontoon	4	2.5	18	HP 280x12	T-shape 500x11x150x12
Middle Pontoon	4	3.5	10-15	HP 200x9	T-shape 400x10x100x12
Top Pontoon	4	5.5	8-12	HP 140x7	T-shape 500x8x150x12
Transverse Top Pontoon	4	3	8-15	HP 140x7	T-shape 350x7x100x12
Diagonal Top Pontoon	4	3	15	HP 140x7	T-shape 350x7x100x12
Large Column	4	10-20	10 12 14	 HP 140x7 HP 200x9	T-shape 1200x12x150x12
Small Column	4	4	10 12 14	 HP 140x7 HP 200x9	T-shape 700x11x150x15

Material

Steel with yield stress 355 [MPa] have been used in the model. The properties of the material is specified down below. The density of the material is increased compared to regular steel to achieve the correct draft

- Young's modulus: 210,00 [MPa]
- Density: 9990 [kg/m3]
- Poison's ratio: 0.3
- Yield stress: 355 [MPa]

Chapter 6

Analysis and Results

A global analysis of the final Havfarm model is performed with BV software. Transfer functions for motions, accelerations and internal loads are established. Vertical, horizontal and torsional moments are selected key response quantities for the main dimension parameters. Three equivalent design waves(EDW) are established to target the characteristic ultimate limit state (ULS) response of the selected key response quantities.

The seakeeping and FE analysis procedure and results will be presented in the following sections. The complete, hydrodynamic and FEA, analysis of the final Havfarm will be presented. All plots of stresses from the FEA shows the von Mises stresses.

6.1 Analysis Procedure

The analysis procedure is summed up in the following:

- Hydro FE model and Structural FE model established
- Model imported and Still water loads calculated
- Hydrostatic pressures computation in Hydrostar
- Mechanical problem solved and responses established
- RAOs established for motions and internal loading, vertical, horizontal and torsional bendingmoment etc. Internal loading RAOs established at indicated sections.

- For vertical, horizontal and torsional bendingmoment worst heading and wave frequency is determined based on the RAOs.
- critical RAOs for internal loading is used as input into Starspec to create a long term distribution of the internal loading.
- this extreme value is used to determine wave height of and three Equvivlaent Design Vaves is established.
- The three EDW is then subjected to the Havfarm hydro model
- Loads recalculated on structural model by Homer and a FEA is done performed. The result is then evaluated.

6.2 Finale Havfarm Model

In this section the hydrodynamic and FE analysis of the finale Havfarm is presented and evaluated. The hydro and FE model are described in chapter 5 and can be seen in figure 5.5 and figure 5.6 respectively.

As the Havfarm consist of six fish pen compartments each compartment have been numbered from 1 to 6, where 1 is assigned the aft compartment and 6 for the front compartment, in order to clearly indicate what area the figures in this chapter shows. The numbering of the fish pen compartments is shown in figure 6.1

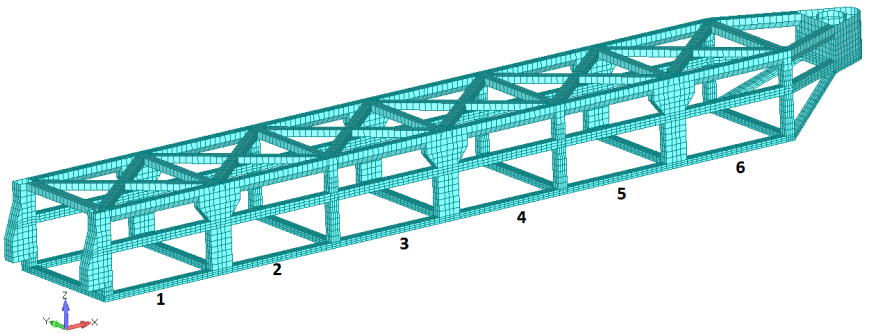

Figure 6.1: Numbering of the fish pen compartments

6.3 Hydrodynamic Analysis

Homer and Hydrostar have been used to perform a hydrodynamic analysis of the Havfarm to determine the response of the Havfarm and to calculate loads for input in the structural analysis. The software and theory behind is described in chapter 4.

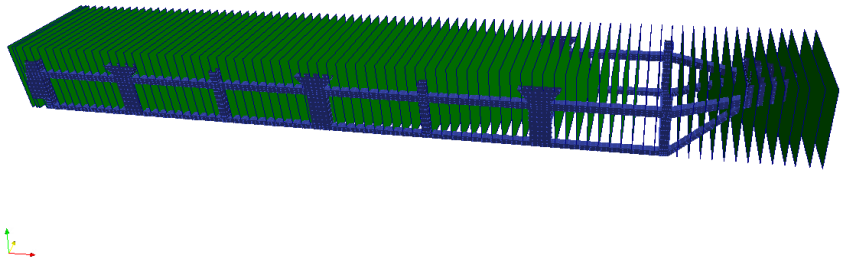

Figure 6.2: Cross sections for which internal load RAOs are calculated

6.3.1 Wave Headings

The responses of the Havfarm are calculated for incomeing wave headings ragneing from 0^o - 180^o with 15^o increment. 180^o corresponds to head sea, 90^o starboard beam sea and 0^o follow sea.

6.3.2 Wave Periods

The hydrodynamic analysis have been carried out with wave periods rangeing form 3 - 30 second. Before the analysis the natural periods of the Havfarm was predicted. To be sure to capture peak values in the RAOs the interval between periods was refined close to the natural periods.

6.3.3 Cross-Sections

Several sections are defined along the length of the Havfarm, as shown in figure 6.2. RAOs for internal loads, bending and torsional moments, have been established at each section in order to determine the location, heading and wave period which causes maximum forces to occur.

6.3.4 Weight distribution

Homer is used in order to prepare the hydro model for the seakeeping analysis in Hydrostar. This is done by transferring the weight distribution of the FE model to the hydro model. A detailed overview of the weight distribution is given in section 5.5.1.

6.3.5 Still Water Loads

First the still water load case is calculated in Hydrostar. The resulting loads are prepared for FE analysis with the structural FE model. Still water bending and torsional moments are also calculated for the hydro model. The still water bending

moments are shown in figure 6.3. A FE analysis with the still water load case is also run. The results will be presented in section 6.4, however the deformations from the FE analysis is shown in figure 6.4.

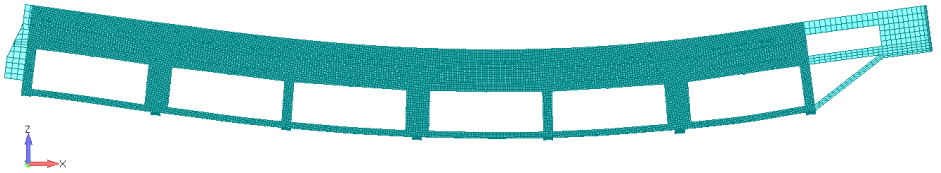

Figure 6.3: Still water deformations. The deformations are scaled to give a clear view of the deformations

The Havfarm structure have large volumes in the bow and the stern compared to the rest of the structure. This and the fact that most of the weights of the structure is distributed between the bow and stern, one would expect the structure to be in sagging condition. This is clearly the case as can be seen from the scaled deformations in figure 6.4

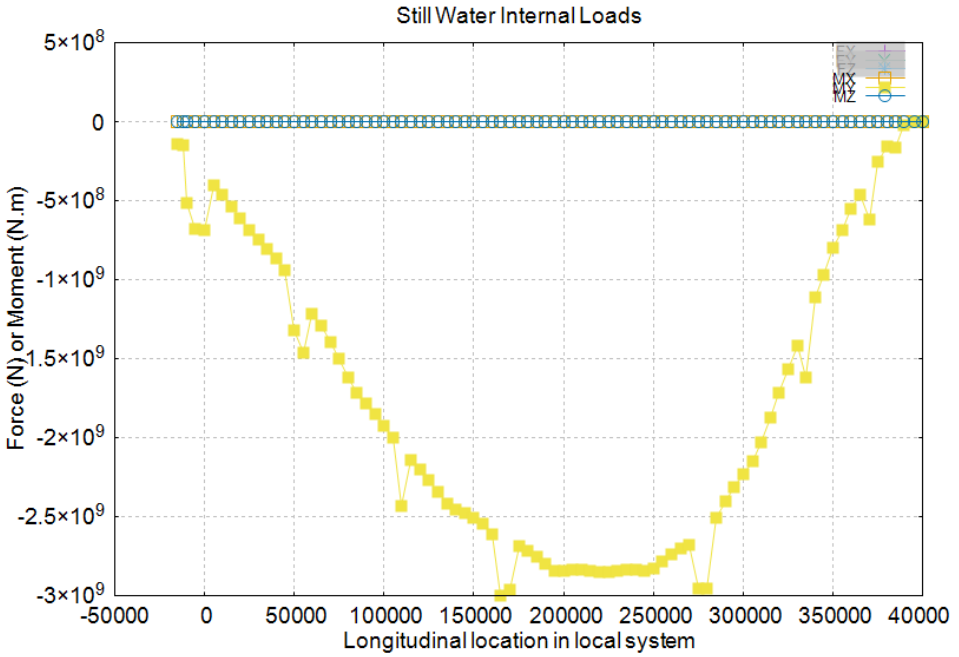

Figure 6.4: Still Water Bending Moment, the vertical bending moment in with yellow legend

The still water bending moment in figure 6.3 seems to be reasonable. The moment is zero in the ends of the structure as expected. seven peaks can also be observed. These peaks occur at the locations of the columns, and this is also expected. The columns will work as a support for the pontoons and may be regarded as some degree of clamped (since the pontoon is continues on both side whit weight and loads) and thus a moment increase would be expected in the columns(supports). As a first evaluation of the analysis this indicates that the model and BV software gives reasonable results.

6.3.6 Pressure calculation and solving the mechanical problem

Hydrostar is used to perform the seakeeping analysis as described in chapter 4. Pressure and response of the Havfarm is calculated for all headings and wave periods given above.

6.3.7 Response Amplitude Operators

Homer is used to establish RAOs for the motions, accelerations and selected key response quantities of the Havfarm. The RAOs are calculated for headings and wave periods as stated earlier in this section. The motion RAOs for heave and pitch motions are presented in figures 6.5 and 6.6 respectively. These RAOs will be used to evaluate the RAOs by a simple calculation of the natural periods in heave and pitch. The rest of the motion and acceleration RAOs will be given in appendix B.

Before the RAOs are presented a comment regarding the large amplitudes for for example heave motion should be noted. In Homer and Hydrostar it is possible to assign damping values for the different motions. For a typical ship structure these damping values can be assigned based on experience. As for the Havfarm structure I it is hard to estimate or make a best guess on these values, and thus they were not assigned. However the motion RAOs will still give good information about the behaviour, such as critical resonance periods.

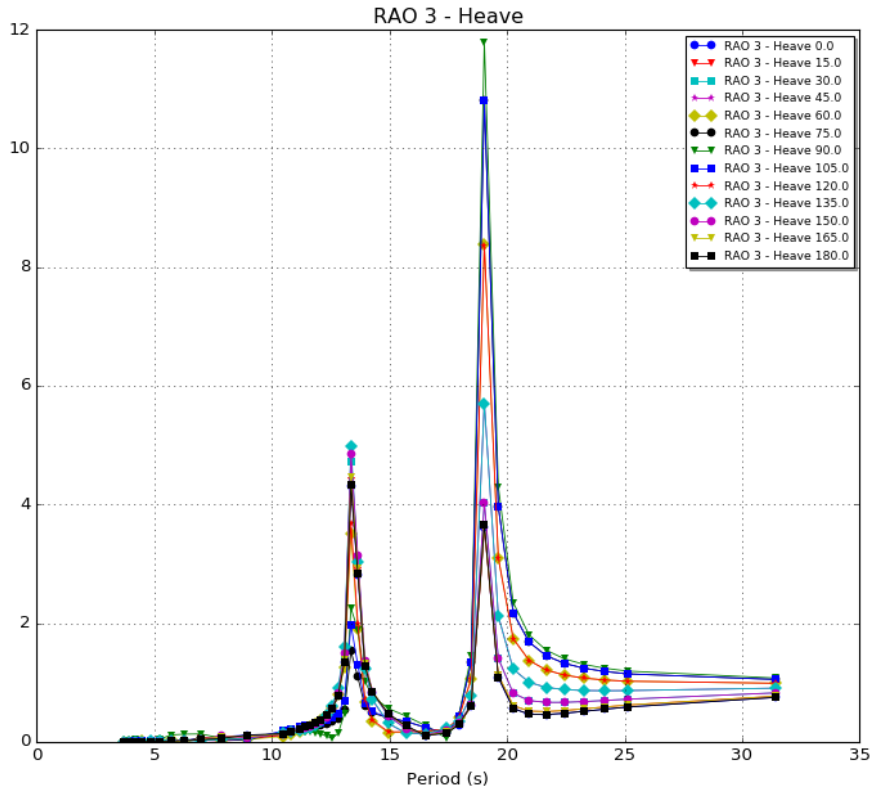

Figure 6.5: Response Amplitude Operator for heave motion, the y-axis unit is [m/m]. The large amplitudes should be noted. This is due to lac of proper modeling of the damping. This would not change the shape of the RAO nor the positioning of the peaks, only the amplitude.

In figure 6.5 it can be seen that the RAO for the heave motion have two peaks. These the first peak around 13.4 seconds is caused by pitch motion and the second peak around 19 seconds by the heave motion. For large periods it can be seen that the RAO for heave motion is approaching unity, which also is expected. For large waves the Havfarm the heave motion will follow the heave amplitude.

The uncoupled and undamped natural period for in heave for a semi-submersible or any type of freely floating body given as [11]:

$$T_{n3} = 2\pi\sqrt{\frac{M + A_{33}}{\rho g A_W}} \tag{6.1}$$

With properties taken from table 5.4 equation 6.1 gives a uncoupled and undamped

natural period in heave of approximately $T_{n3} = 17.9$ seconds. This is reasonably close to the resonance period of the second peak as Hydrostar also take coupling effects into account.

The uncoupled and undamped natural period in pitch for a semi-submersible or any type of freely floating body is given as:

$$T_{n5} = 2\pi\sqrt{\frac{Mr_{55}^2 + A_{55}}{\rho g V \overline{GM}_L}} \tag{6.2}$$

Where A_{55} according to Faltinsen [11] can be found as (assumed $A_{11} = 0$ for simplicity):

$$A_{55} \approx 2\int_{-L/2}^{L/2} A_{33}^{2D} x^2 dx \tag{6.3}$$

Here A_{33}^{2D} can be expressed from strip theory as [11]:

$$A_{33}^{2D} = \frac{A_{33}}{2L} \tag{6.4}$$

With properties taken form table 5.4 equation 6.2 gives a natural period in pitch of $T_{n5} = 14.1$ seconds. This is also reasonably close to the resonance period, of about 13.4 seconds, for the first peak in both figure 6.5 and 6.6 as Hydrostar account for coupling effects. The motion RAOs are also compared to results calculated by Multiconsult and provided by NSK Ship Design which can be found in the appendix D. From the comparison of the RAOs obtained with Homer and the RAOs provided by NSK Ship it is clear that they give the same peaks and seems to be very much a like. Thus it is further assumed that the other RAOs established in the thesis are accurate and can be used as a good basis to estimate characteristic extreme response levels for chosen quantities.

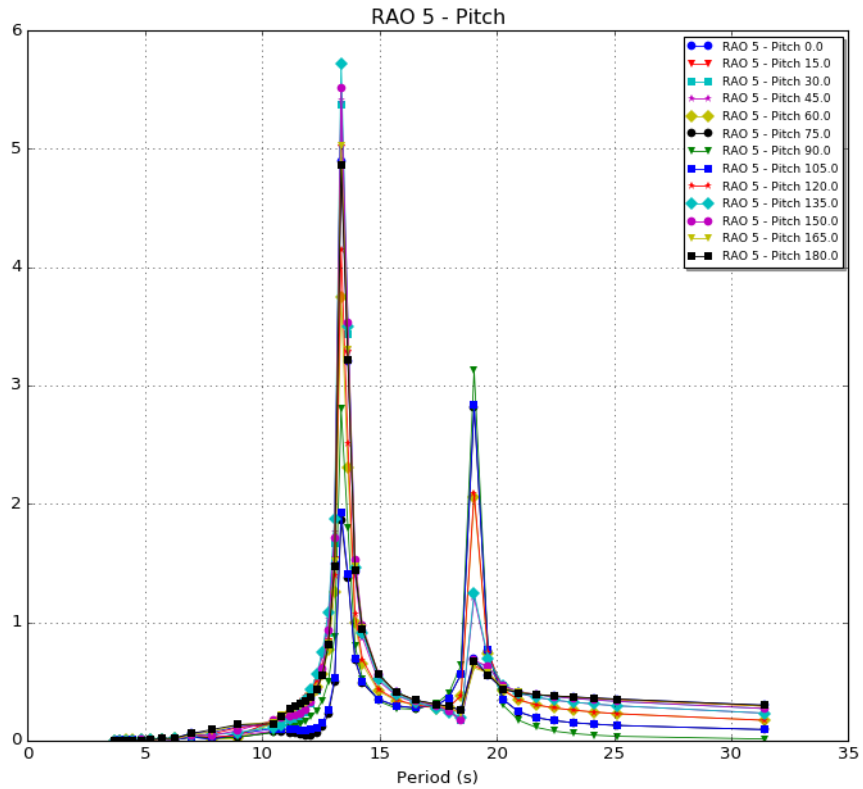

Figure 6.6: Response Amplitude Operatior for pitch motion, the y-axis unit is [deg/m]

Motion RAOs established with Homer seems to very similar to the motion RAOs established by Multiconsult given in appendix D. The peaks occurs at the same periods and the RAOs in general have the same shapes.

RAOs for internal loading such as vertical bending moment, horizontal bending moment and torisonal moment are establishes for all cross-sections shown in figure 6.2. All RAOs are evaluated to find the sections where the maximum RAO of vertical, horizontal and torsional moment occur. The results are given in table 6.1 and indicated in figure 6.7. The RAOs for maximum vertical bending moment, maximum horizontal bending moment and maximum torsional moment at critical headings are given in figure 6.8, 6.9 and 6.10 respectively. RAOs for all headings at these sections are given in appendix C

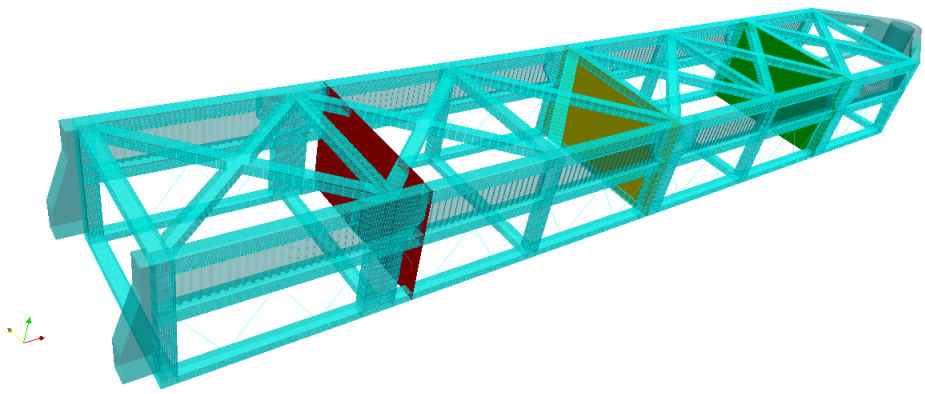

Figure 6.7: Sections indicateing where maximum torsional moment (red section), horizontal bending moment(yellow section) and vertical bending moment(green section) occur

In table 6.1 two peak values are given for maximum torsional moment. This is because the maximum torsional moment is indicated to occur for wave heading 90^o as seems a bit strange. When this peak is evaluated in the FE analysis it turns out to be wrong. The second largest maximum peak at a different heading and wave frequency was chosen in addition, which turns out to be the true maximum when the FEA results are evaluated later on. Both torsion moment peaks can be seen in figure 6.10.

Table 6.1: Peak RAO values for internal loads

Load	Longitudinal Location (X) [m]	Peak Value [MN.m]	Heading	Wave Frequency[rad/s]
Vertical Bending Moment	275	3 636	135^o	0.47
Horizontal Bending Moment	165	652	105^o	1
Torsional Moment	65	148	105^o	1
Torsional Moment	65	185	90^o	0.34

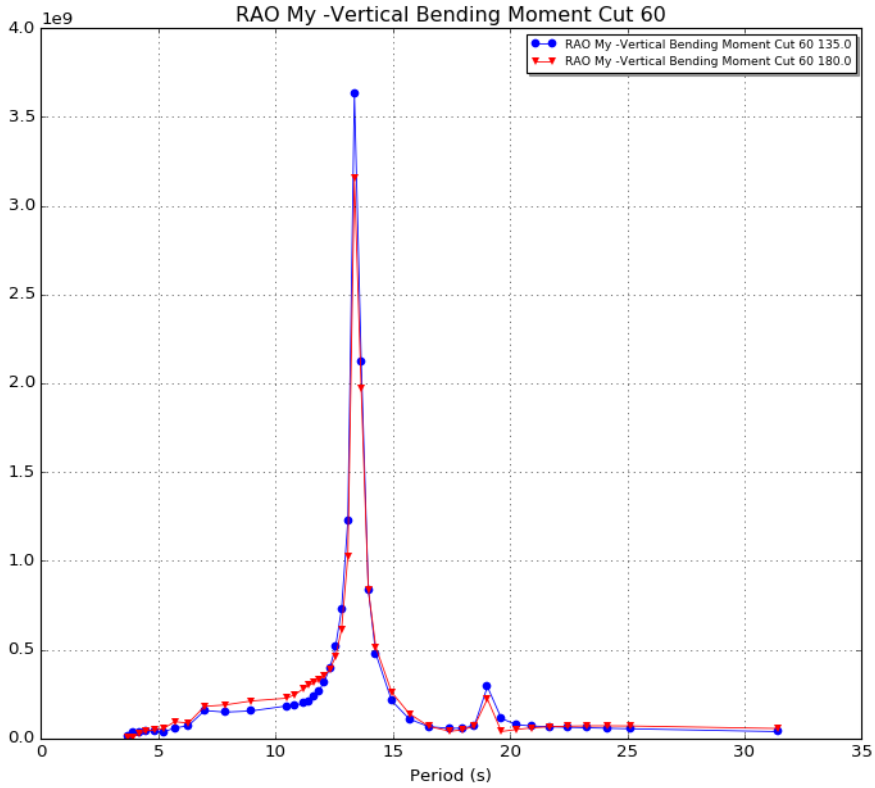

Figure 6.8: RAO for vertical bending moment at longitudinal coordinate 275m, where the maximum torsional moment occur. Normally one would expect the maximum vertical bending moment to occur when subjected to head sea, 180^o. However for the Havfarm structure this is not the case.

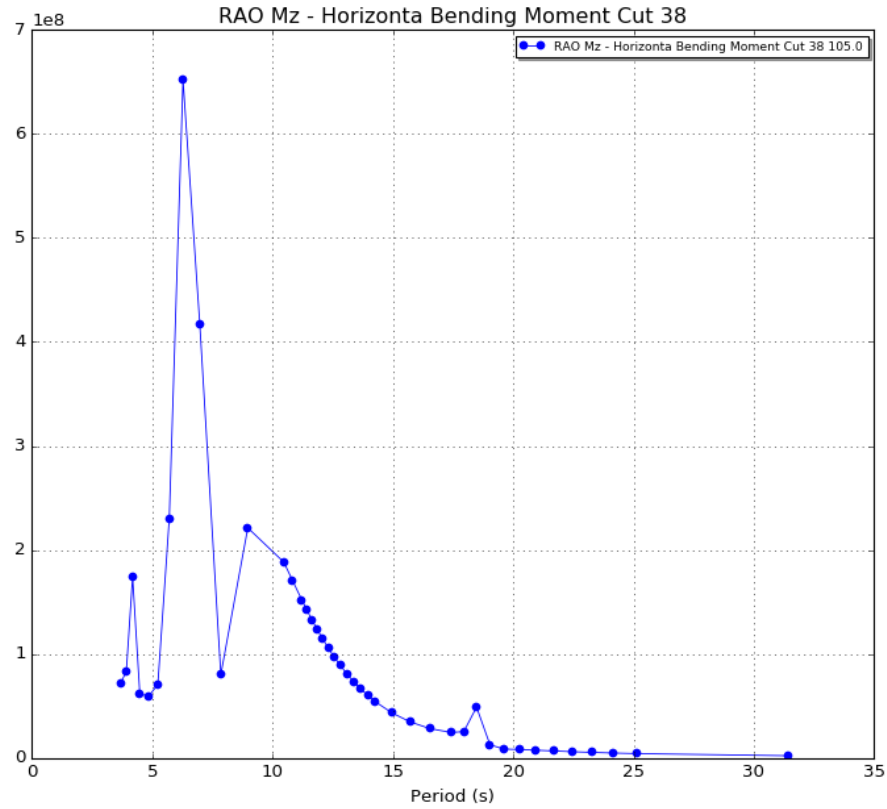

Figure 6.9: RAO for horizontal moment at longitudinal coordinate 165m, where the maximum torsional moment occur.

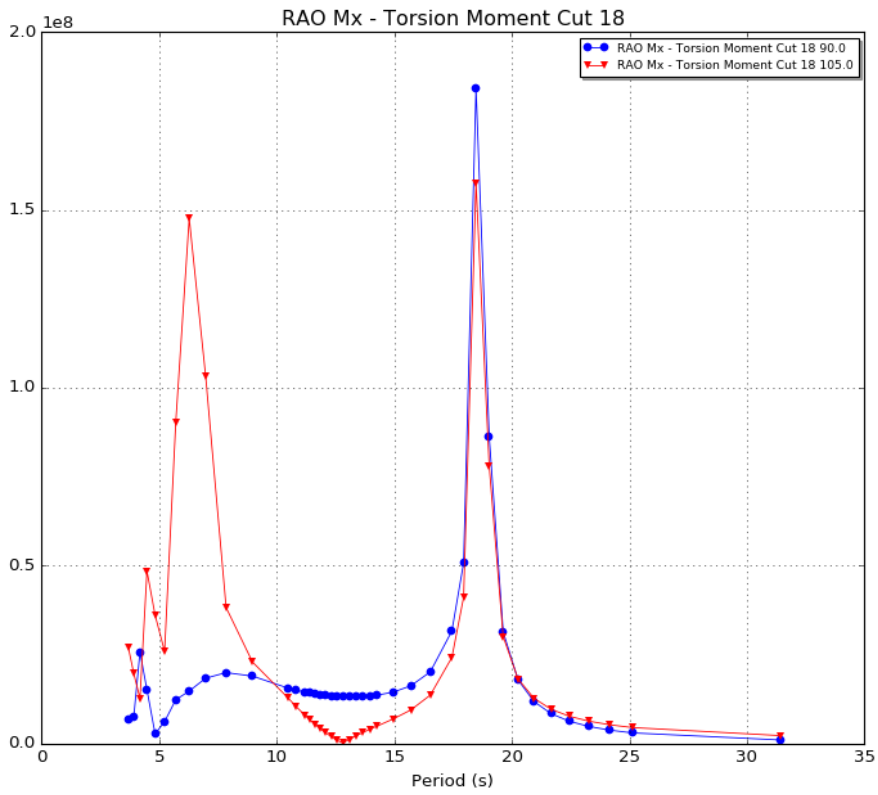

Figure 6.10: RAO for torsional moment at longitudinal coordinate 65m, where the maximum torsional moment occur.

6.3.8 Characteristic extreme response of internal loads

Based on the RAOs established for maximum vertical bending, horizontal bending and torsional moment, Starspec, a module in Hydrostar, is used to predict an Ultimate Limit State response level. This is done by a long term analysis based on metocean data provided by NSK Ship Design for the location where the Havfarm will be located. The long term analysis procedure is briefly described in chapter 4. A more thorough description of the theory is also given in the Starspec User manual [8].

Metocean data is provided by NSK Ship Design, gives a scatter diagram for swell- and wind sea. In the thesis only swell sea have been considered. The reason for this is because the metocean data provided is based on simulated data, and the wind sea and the swell sea have been provided in separate scatter diagrams. In addition there have also been provided a joint distribution of the combined seastates. However, it

is not a straight forward process to combine these scatter diagrams in the Starspec module. An effort to combine the scatter diagrams was made, however, since the probability of a sever swell sea and sever wind sea to occur at the same time is low it was decided to focus on the swell sea, which represents the worst sea states of the two. This will ned to be updated in further work in order to get a correct long term extreme estimate. The metocean data is from NSK Ship Design is provided in the appendix A

Further, since no information about the azimuth of the Havfarm was provided it was assumed that all azimuths of the Havfarm ranging from 0^o to 345^o with an increment of 15^o have the same probability.

Further the JONSWAP wave spectrum is applied as described in chapter 4.

In short the extreme response of internal loads are predicted based on the following:

- JONSWAP wave spectrum
- Scatter diagram for the swell sea based on a constructed time series for the period 1955-2007
- Azimut of the Havfarm assumed to be 0^o to 345^o with an increment of 15^o and with equal probability
- extreme value corresponding to a 100-year return period, Ultimate Limit State
- The internal load RAOs for section 18, 38 and 60, where the maximum torsional moment, horizontal bending moment and the vertical bending moment occur respectively. These RAOs can be found in the appendix C

The results from the long term analysis of vertical bending moment is shown in figure 6.11. The results for the horizontal and torsional moments are given in table 6.2

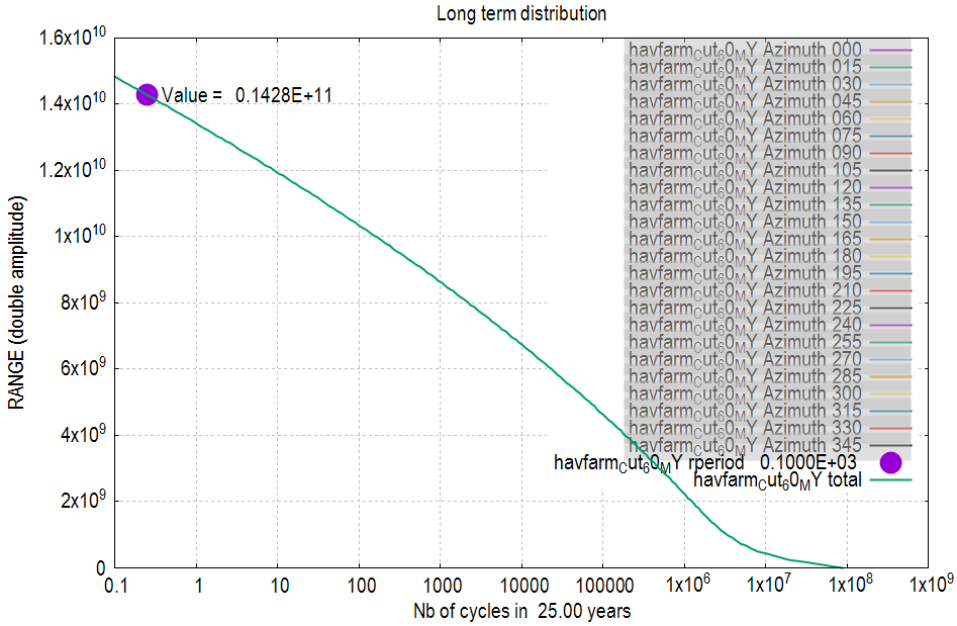

Figure 6.11: ULS range of vertical bending moment. The range of the vertical bending moment corresponding to a 100 year return period is marked in the figue, the value is 14 280 [MN.m], which is the double amplitude

Table 6.2: Extreme response values for selected key response quantities

Load	Longitudinal Location (X) [m]	Extreme Respnse Value (Double Amplitude) [MN.m]	RAO Value [MN.m]
Vertical Bending Moment	275	14 280	3 636
Horizontal Bending Moment	165	3 751	652
Torsional Moment	65	916	148

6.3.9 Establishment of Equivalent Design Waves

To compel the extreme response values obtained from the long term analysis three Equivalent Design Waves (EDW) are established. The wave heading is defined by the heading where the maximum occur for the desired response quantity. The wave period is found where the peak in the RAO for the desired quantity occur. The wave height of the EDW is determined by devideing the long term value by

Table 6.3: Equvivalent Design Waves

Design Wave	Targeted Load	Extreme Response Value [MNm]	RAO Value [MNm/m]	Wave Height [m]	Wave Heading [^{o}]	Wave Period [s]
1	Vertival Bending Moment	14 280	3 630	3.93	135	13.4
2	Horizontal Bending Moment	3 751	652	5.76	105	6.3
3	Torsional Moment	916	148	6.19	105	6.3
4	Torsional Moment	916	184	4.97	90	18.5

the RAO peak value. This gives the three EDWs described in table 6.3

6.4 Finite Element Analysis

Still Water FE Analysis

The FEA results are shown in figures 6.12 trough 6.14. The von Mises stresses are plotted in thses figures, and no stresses exceeding 300 [MPa] are observed.

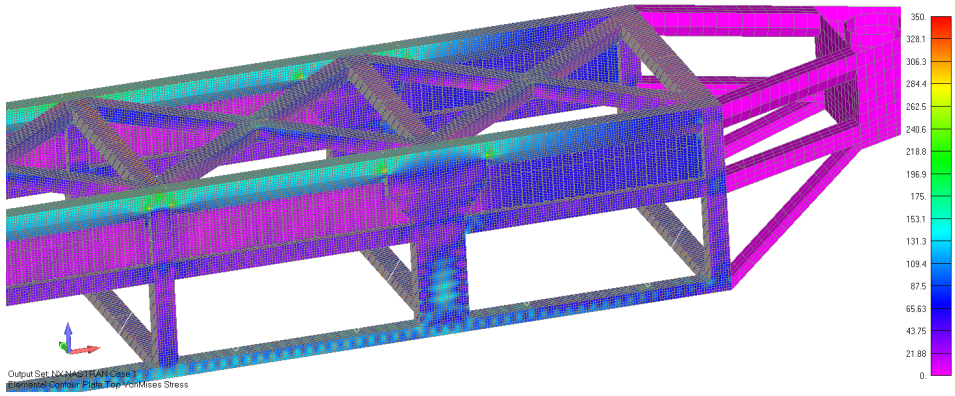

Figure 6.12: Von Mises stresses in fish pen **compartment 5 and 6**

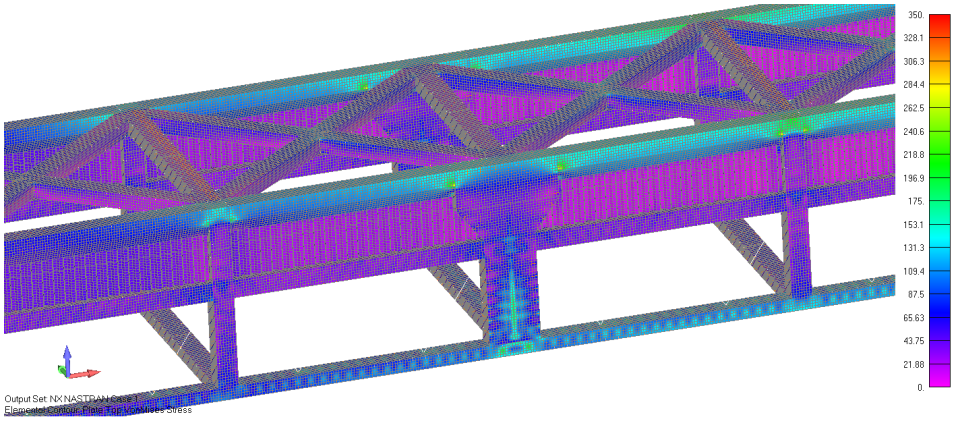

Figure 6.13: Von Mises stresses in fish pen **compartment 3 and 4**

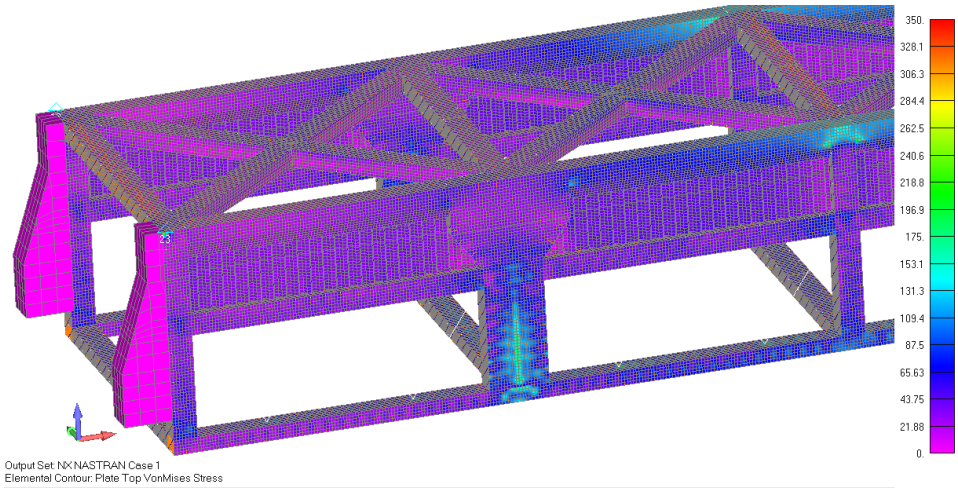

Figure 6.14: Von Mises stresses in fish pen **compartment 1 and 2**

6.4.1 Equivalent Design Wave FE Analysis

The equivalent design waves established in section 6.3 are applied to the hydro model. The waves are positioned so that the extreme response values are obtained. This is done by plotting the targeted response quantity at the sections they are expected to occur as the wave is passing by. From these plots the time step of the hydro analysis where the targeted response quantity is maximized is determined. Then the loads for this load case is transferred from the hydro model to the structural FE model by Homer.

As a control to ensure that the EDWs actually produce the targeted extreme response desired, the targeted moments are checked at the locations where they are expected to occur in FEMAP (post-processing tool of the FEA). The extreme responses calculated by Starspec, the expected responses and actual responses in the FE analysis are shown in table 6.4. The moments obtained in the FE analysis is also shown in figure 6.15, 6.16, 6.17

The moment expected to be found in the FE analysis is based on the extreme prediction and still water moments. It is calculated by adding the extreme response(double amplitude) with the absolute value of the still water moment(to correct for the neutral bending moment) and divide it by two. or as:
(Extreme Response(double amplitude) + | Still Water Moment |)/2.

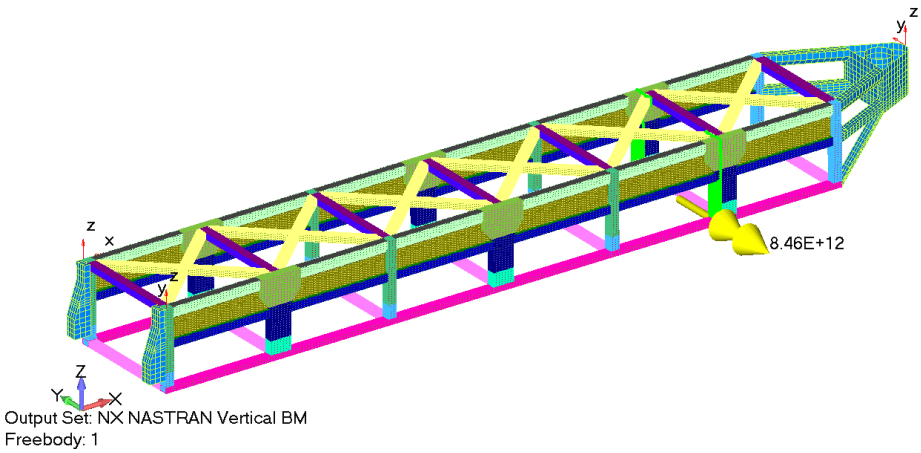

Figure 6.15: Vertical bending moment in Nmm at cut 60 (x=275m) when subjected to EDW 1

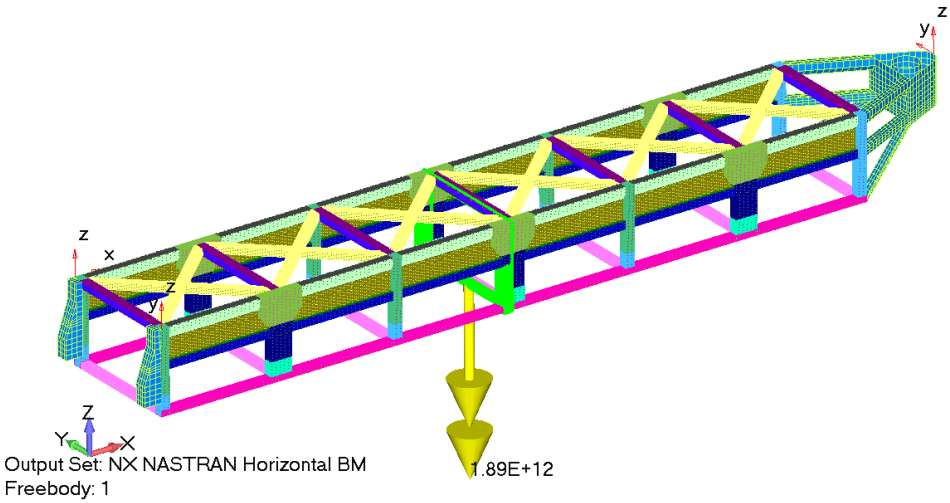

Figure 6.16: Horizontal bending moment in Nmm at cut 38 (x=165m) when subjected to EDW 2

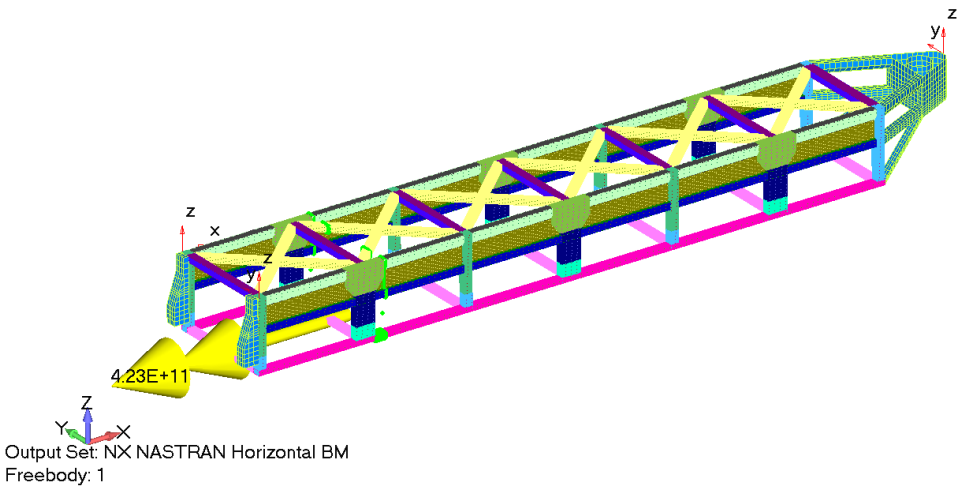

Figure 6.17: Torsional bending moment in Nmm at cut 18 (x=65m) when subjected to EDW 2.

Table 6.4: Control of FE analysis. The expected response in the FE analysis is calculated as: (Extreme response moment (double amplitude) + abs(still water moment))/2. Note that the obtained moment for torsional moment induced by EDW 3 is given for EDW 2 as shown in figure 6.17 and the scaled value which will be the value for EDW 3

Targeted Load /EDW	Extreme Response [MNm] (double amp.)	Still Water [MNm]	Expected FEA [MNm] (single amp.)	Obtained FEA [MNm] (single amp.)	Location X [m]
Vertival Bending Moment / 1	14 280	-2 639	8 460	8 460	275
Horizontal Bending Moment / 2	3 751	0	1 875	1 890	165
Torsional Moment / 3	916	0	458	423 / 454	65
Torsional Moment / 4	916	0	458	1.5	65

From table 6.4 we can see that the targeted vertical and horizontal bending moment in fact are obtained with EDW 1 and 2. That is the ultimate limit state vertical and horizontal bending moment are obtained with the design waves described in table 6.3. It is further assumed that these two design waves gives a good representation of the ULS state with respect to vertical and horisontal bending moment. Regarding the torsional moment induced by EDW 4, no torsional moment is obtained in the FE analysis at the critical section. This design wave was chosen based on the torsional moment RAO for section 18 shown in figure 6.10. From the same figure, figure 6.10, the RAO for heading 105^o is used to establish a different EDW to compel the extreme torsional moment. As there are two peaks for this heading, one at the same period as for the EDW nr 4, it is chosen to try the other period of 6.3 seconds. These parameters makes up the EDW nr. 3 as described in table 6.3. However the only difference between The EDW nr 2 and 3 is the wave height. And since the analysis is performed in the frequency domain we have linearity. Thus the torsional moment are checked at section 18 with EDW nr 2, and it can be seen from figure 6.17 that the obtained torsional moment equals 423[MNm]. Since the

only difference between EDW 2 and 3 is the wave height and we are operating in the frequency domain, this value can be scaled by $\frac{6.19[m]}{5.76[m]}$ in order to find the moment which will be obtained with EDW 3. In a clearer way, the torsional moment for EDW nr 3 is obtained as follows:

$$M_{T_{EDW3}}^{section_18} = M_{T_{EDW2}}^{section18} * \frac{6.19[m]}{5.76[m]} \tag{6.5}$$

Now it is clear that the targeted moments are obtained in the FEA analysis and it is assumed that all the three design waves yields good results for a global structural analysis. The FEA result will be presented and evaluated in the following sections.

6.4.2 FEA Vertical Bending Moment

Here the FE analysis results of EDW 1 targeting the extreme vertical bending moment will be presented and evaluated.

The position of the EDW relative to the Havfarm is shown in figure 6.18. The deformations of the Havfarm are indicated in figure 6.19.

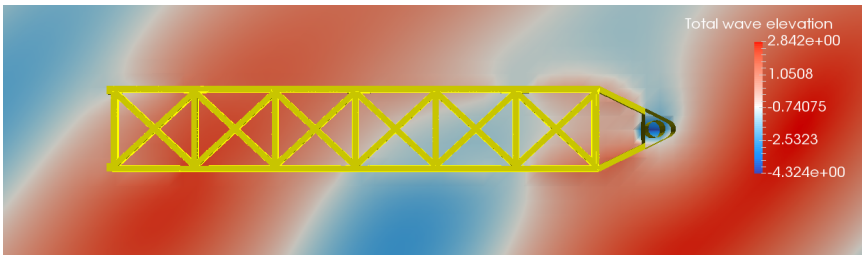

Figure 6.18: The equivalent design wave 1, targeting extreme vertical bending moment

From figure 6.18 it is clearly seen that the 5th fish pen, counted from the aft of the structure, will be "hanging" in a through between two crests. It is also in this section the maximum vertical bending moment is obtained. Figure 6.20 through 6.22 shows the stresses in the shell elements in all fish pen areas. In these figures the stress levels have been cut at 400 [MPa] in order to easily see the ares subjected to large stresses. In other words all elements colored red have stresses exceeding 400 [MPa] in these figures.

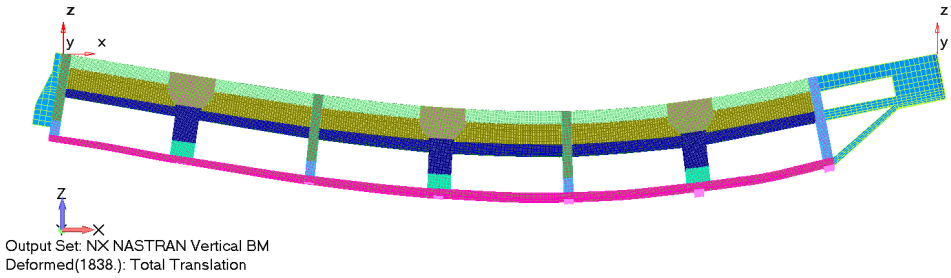

Figure 6.19: Scaled deformation of the Havfarm when subjected to EDW 1

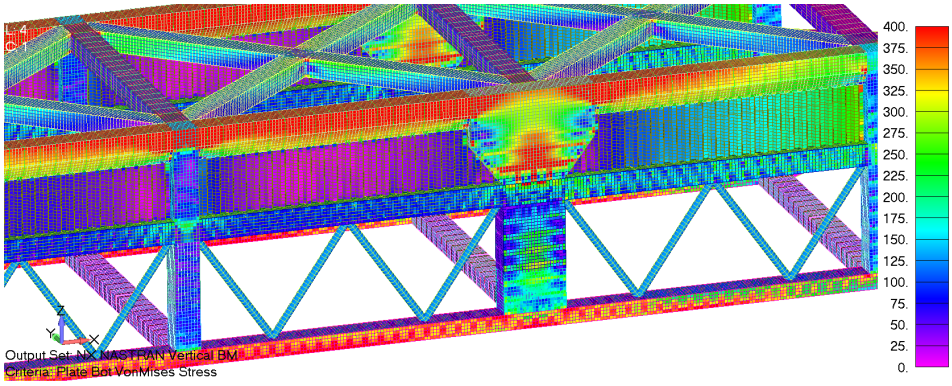

Figure 6.20: FEA stresses for EDW 1 in fish pen **compartment 5 and 6**. The stress levels have been limited to 400 [MPa] to easily show all elements exceeding this stress level. It is seen that the top and bottom pontoons in fish pen compartment 5 have stresses exceeding 400[MPa] over the length of the compartment

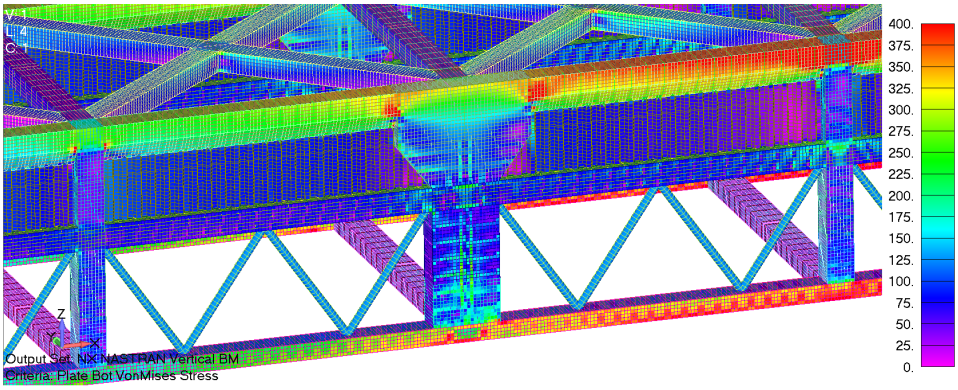

Figure 6.21: FEA stresses for EDW 1 in fish pen **compartment 3 and 4**. The stress levels have been limited to 400 [MPa] to easily show all elements exceeding this stress level. It is seen that the top and bottom pontoons in fish pen compartment 4 have stresses exceeding 400[MPa]. The top and bottom pontoons in compartment nr 3 have stresses in the range od 250[MPa] - 325[MPa]. Some stress concentrations exceeding 400 [MPa] is seen in the connections between the columns and the top pontoons

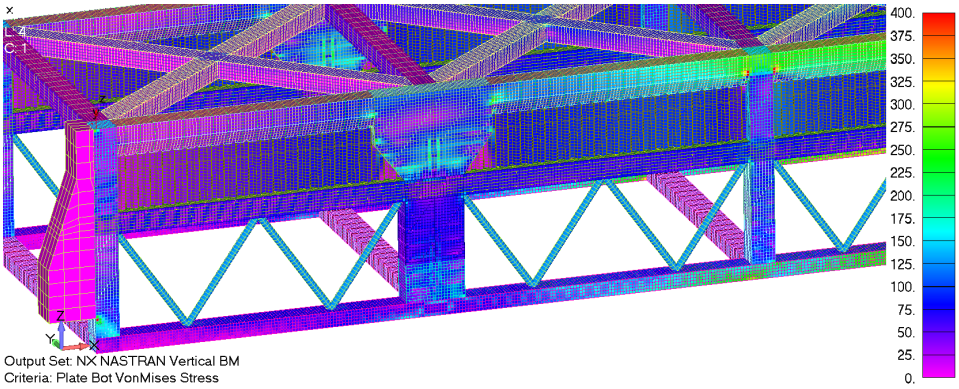

Figure 6.22: FEA stresses for EDW 1 in fish pen **compartment 1 and 2**. The stress levels have been limited to 400 [MPa] to easily show all elements exceeding this stress level. It is seen that all elements in general are subjected to low stresses. However, also here the stress concentrations in the connections between the columns and the top pontoons are seen

From figures 6.20 and 6.21 is seen that the top and bottom pontoons in compartment 4, 5 and 6 are experiencing stresses exceeding 400 [MPa]. With a yield stress of 355 [MPa] the pontoons will be over stressed and without sufficient capacity.

In the following figures, figure through ste stresses are plotted with a higher stress

level fangeing from 0-600 [MPa] in order to show the "hot spots" or stress concentrations better. All these figures are taken form the area around fish pen compartment 5, but the tendencies of stress concentrations are the same for the rest of the compartments, in sharp connections between the pontoons and columns. Hot-spots is also observed in the connections of the top diagonal pontoons and in the connections between the braces and the middle and bottom pontoons.

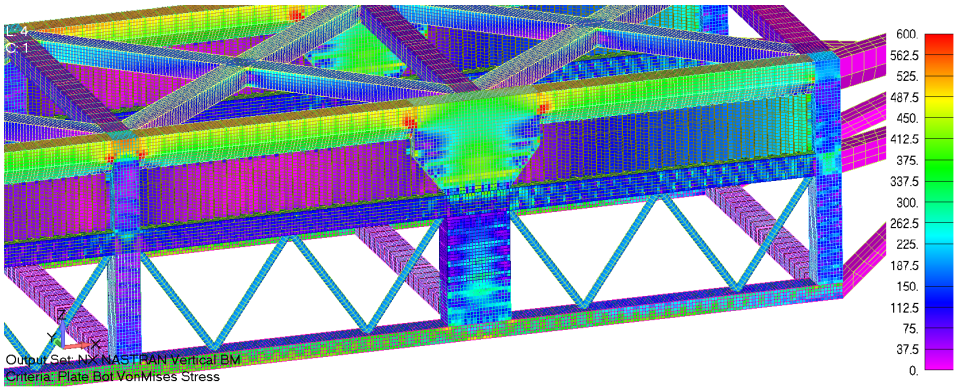

Figure 6.23: Overview of hot-spot stresses in fish pen compartment 5 and 6. Hot-spots with stresses exceeding 600 [MPa] is clearly seen in the connections between the top longitudinal pontoons and the columns.

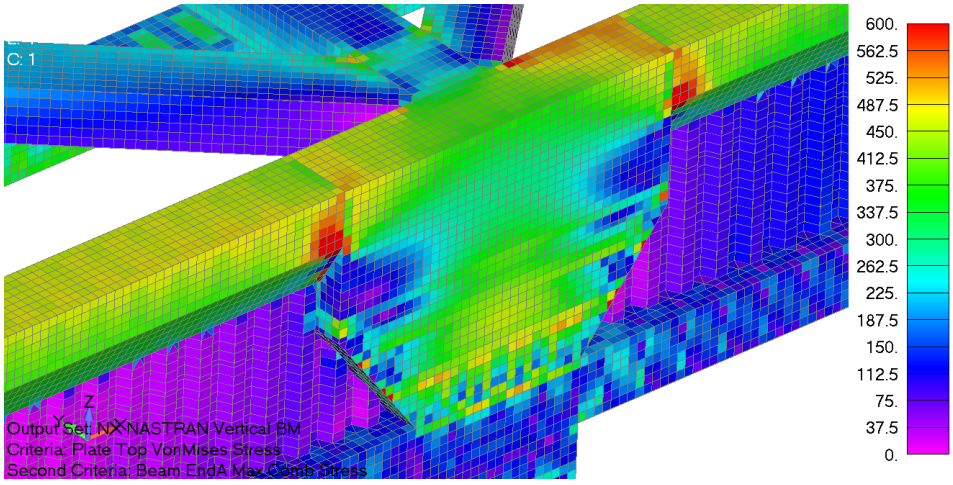

Figure 6.24: Overview of hot-spot stresses in fish pen **compartment 5 and 6**. Hot-spots with stresses exceeding 600 [MPa] is clearly seen in the connections between the top longitudinal pontoons and the columns.

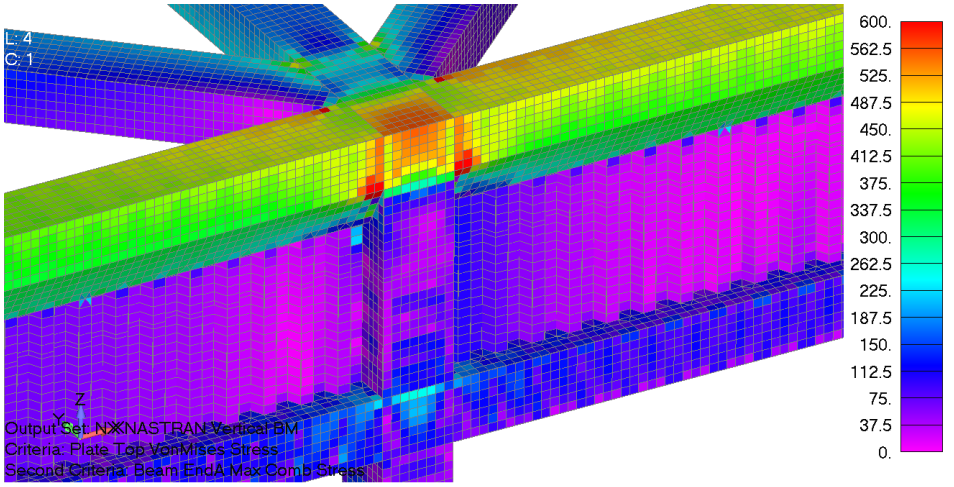

Figure 6.25: Overview of hot-spot stresses in fish pen **compartment 4 and 5**. Hot-spots with stresses exceeding 600 [MPa] is clearly seen in the connections between the top longitudinal pontoons and the columns.

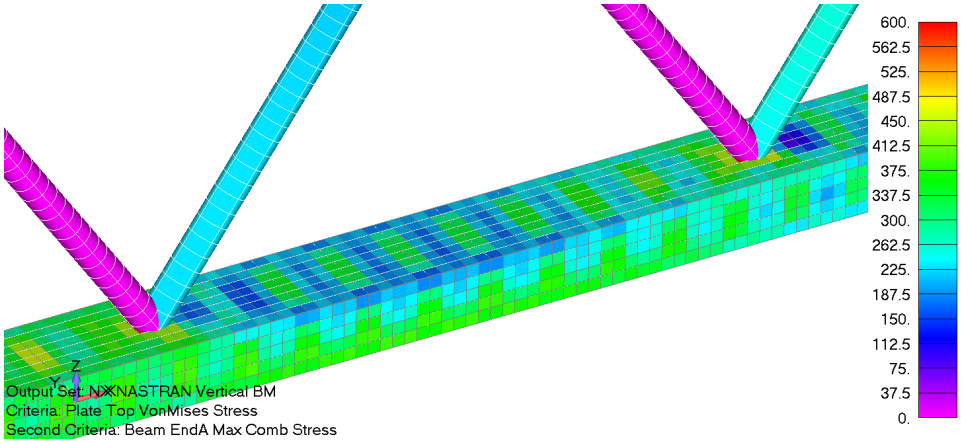

Figure 6.26: Overview of hot-spot stresses in fish pen **compartment 5**

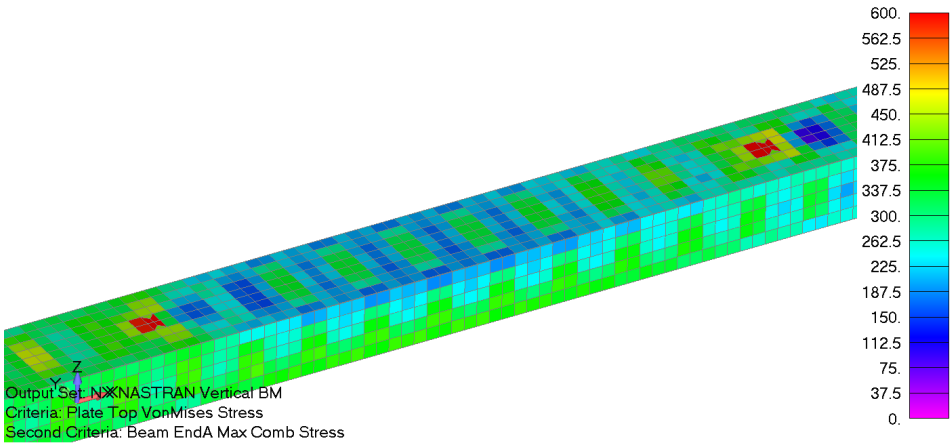

Figure 6.27: Overview of hot-spot stresses in fish pen **compartment 5**. Hot-spots with stresses exceeding 600 [MPa] is clearly seen in the connections between the bottom longitudinal pontoons and the braces.

In Femap there no convenient way to plot Von-Mises stresses in all beam elements at once. The only way is to check for the cross section of a selected beam element or a few selected beam elements at a time. However, the stiffeners have also been checked at critical locations. such as in the connections between the longitudinal top pontoon and the big column in. If the columns are regarded as (clamped)supports of the longitudinal pontoons, it is is expected that the maximum bending stresses will occur in the connection. Figure 6.28 shows a stiffener in the connection between the longitudinal pontoon and the big column between fish pen number 5 and 6. Figure 6.29 shows the Von-Mises stresses in the selected beam elements (stiffener) shown in figure 6.28.

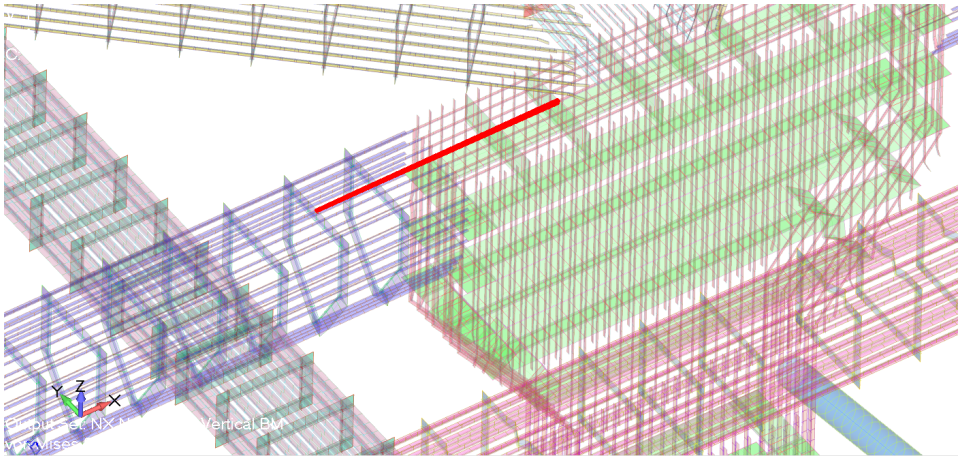

Figure 6.28: The selected beam elements representing the stiffener in the connection between the top longitudinal pontoon are indicated with red

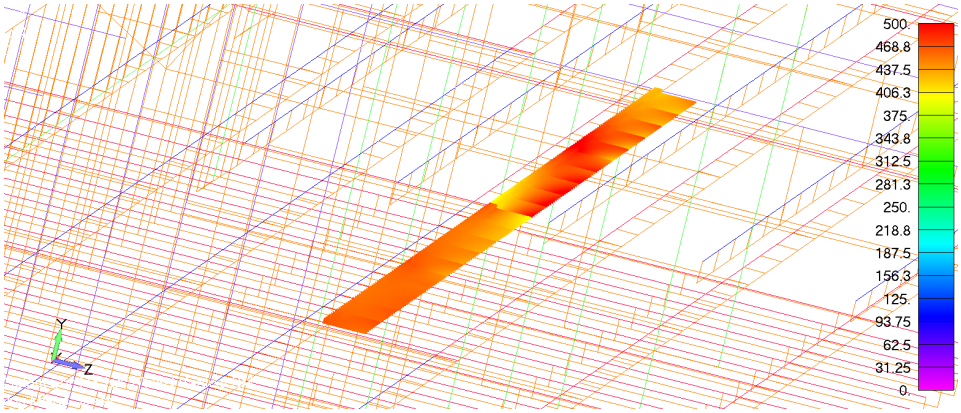

Figure 6.29: Von-Mises stresses in longitudinal stiffener located in the connection with the big column between fish pen **compartment 5 and 6**. Stresses exceed the stress levels which are limited to 500[MPa] at some places

It is clear that the stiffeners in this area are over stressed. Although not all stiffeners have been checked it is safe to say that a lot of the stiffeners do not have sufficient capacity for the ULS vertical bending moment.

6.4.3 FEA Horizontal Bending/ Torsional Moment

The FE analysis of the EDW 2/3 is presented here. Since EDW nr 2 and nr 3 is the same wave except the of the wave height only the results of EDW nr 3 will be presented here. This because if the Havfarm have sufficient strength to survive EDW nr 3 it will also EDW 2 will be ok as this is the same wave with a lower wave height.

To give an idea of the deformations the Havfarm experiences when subjected to EDW 2/3 the deformations are scaled and shown from above in figure 6.31 and from the bow in figure 6.32. From figure 6.18 it is easy to see where the wave crest of the EDW make an impact on the big columns between the fish pen compartments 3 and 4. It is this impacts that causes the extreme horizontal bending and torsion moment.

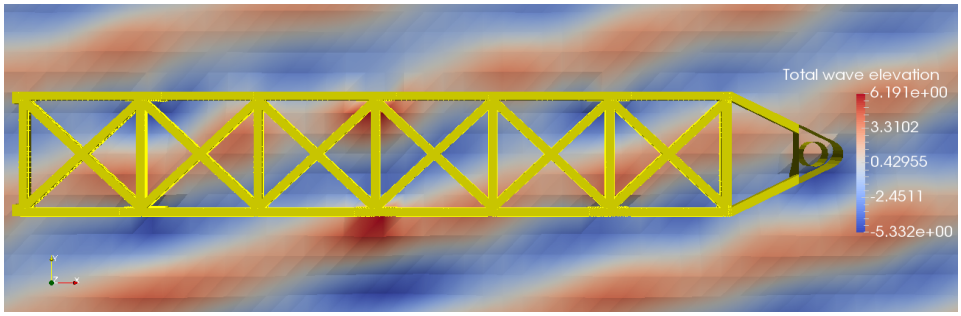

Figure 6.30: The equvivalent design wave 2/3, targeting extreme horizontal bending moment and torsinal moment. The wave is propagating towards the "north west direction"

From figure 6.31 it is clearly seen how the Havfarm deflects in the horizontal direction when subjected to the EDW 2/3. In figure 6.32 it is possible to see how the lower pontoons are subjected to a larger deflection than the top pontoons. This is due to the stiffening effect in the top part of the structure provided by the diagonal top pontoons. The lac of similar stiffening in the bottom part of the structure allows the bottom part to deflect more and thus subject the structure to torsion.

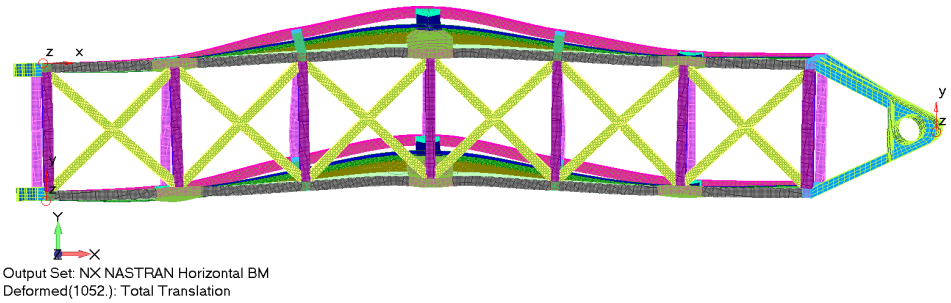

Figure 6.31: Top view of deformation due to EDW 2/3 targeting horizontal/torsional moment

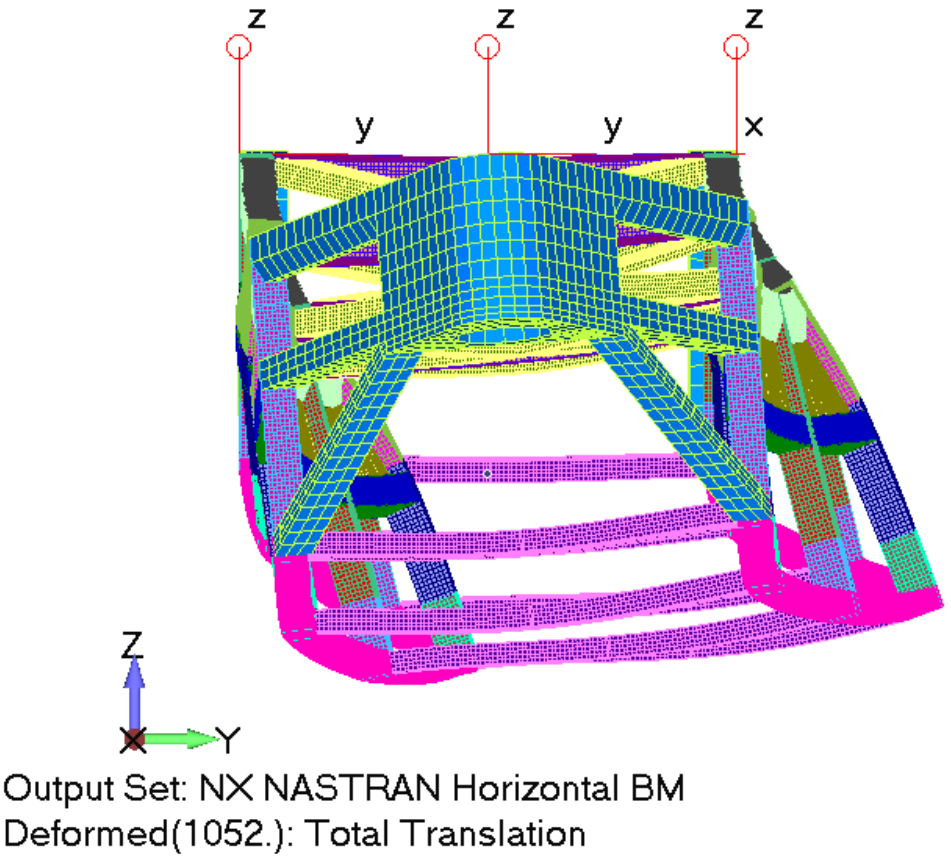

Figure 6.32: Side view of the deformation due to the equivalent design wave 2/3, targeting extreme horizontal bending moment and torsional moment

Figure 6.33 trough 6.35 gives an overview of the stresses in the Havfarm when subjected to EDW 3, targeting extreme torsion moment. In these figures the stress levels have been limited to 350 [MPa] in order to easily show critical areas where yielding will occur. In general it is clear that the structure will have sufficient capacity. However there are some areas where stresses exceeds 350 [MPa]. This is in the connections with the small columns and the top pontoons between fish pen compartment 2 and 3, as well as 4 and 5. This is seen in figure 6.34 and a more detailed view in figure 6.39 and 6.39 . Also in the connections between the big column between fish pen compartment 3 and 4 on the starboard side, there are severe stresses exceeding 350 [MPa] as seen in figure 6.34, with a more detailed view and evaluation of this column in the following figures 6.36 and 6.37.

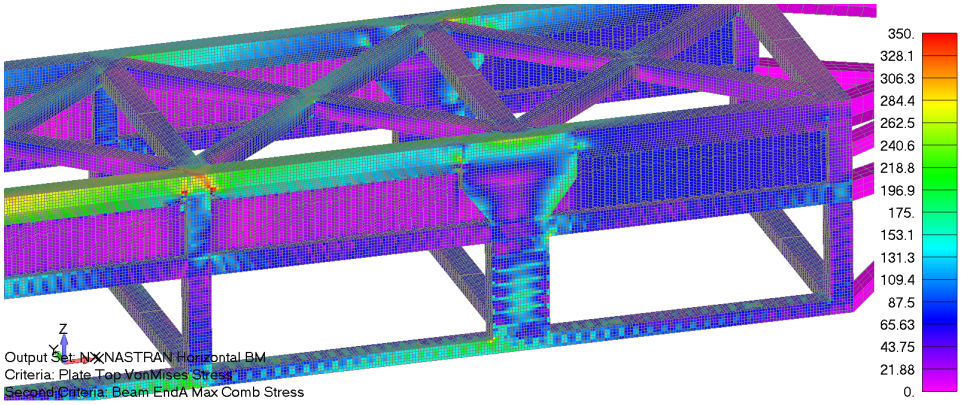

Figure 6.33: Stresses in fish pen **compartments 5 and 6** when subjected to the equvivalent design wave 3, targeting extreme horizontal torsinal moment

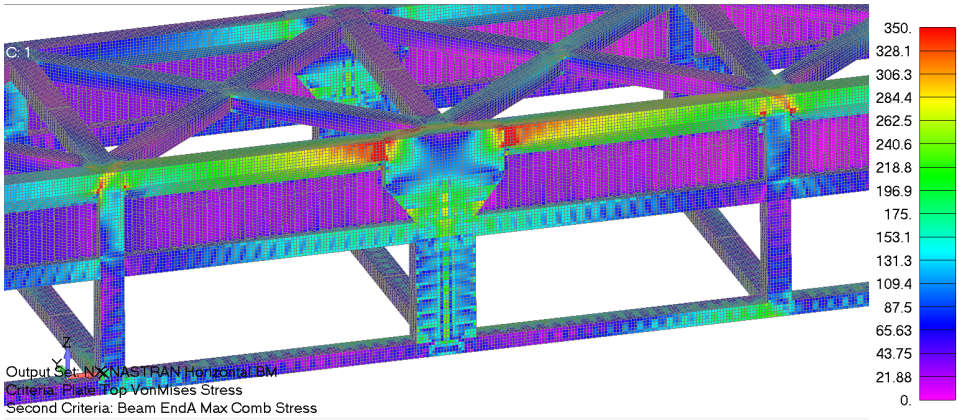

Figure 6.34: Stresses in fish pen **compartments 3 and 4** when subjected to the equvivalent design wave 3, targeting extreme horizontal torsinal moment

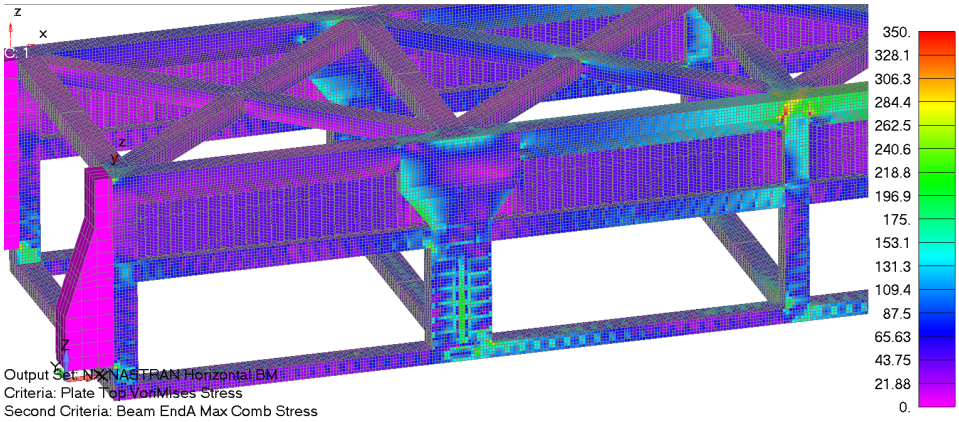

Figure 6.35: Stresses in fish pen **compartments 1 and 2** when subjected to the equvivalent design wave 3, targeting extreme horizontal torsinal moment

Figure 6.36 and 6.37 shows a closeup of the big column on starboard side between fish pen 3 and 4. In this figure the stress levels have been limited to 400 [MPa] in order to easily show stress concentrations. Elements that exceeds 400 [MPa] and thus critical for yielding is easily spotted. High stress concentrations in these connections between the column and the pontoons are as expected, due to sharp corners. As the column also acts as a support for the pontoons

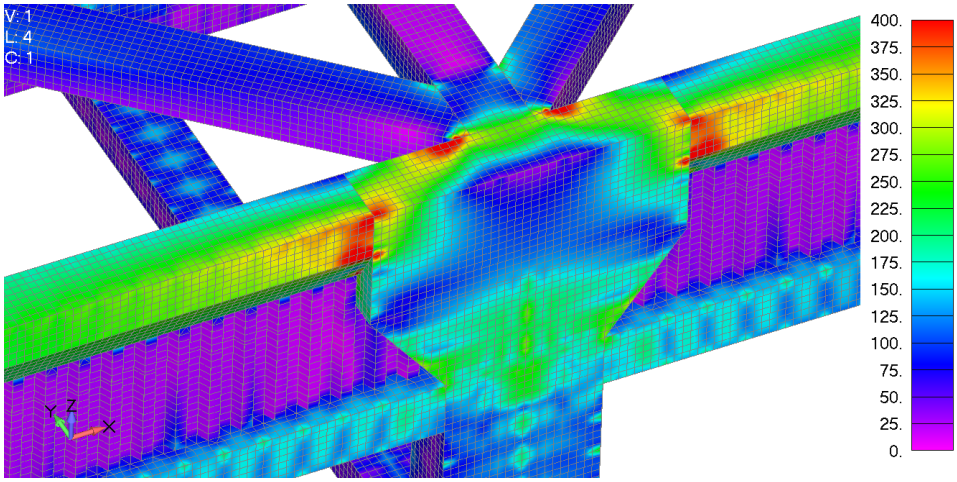

Figure 6.36: Stresses in the starboard side big column between fish pen **compartment 3 and 4** seen from starboard side. Stress concentrations can clearly be seen in the connections between the column and the pontoons.

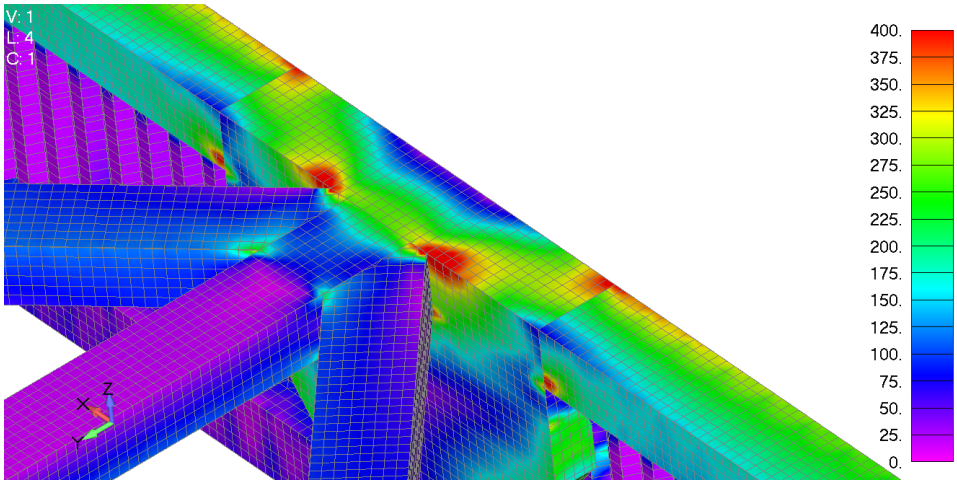

Figure 6.37: Stresses in the starboard side big column between fish pen **compartment 3 and 4** seen from port side. Stress concentrations can clearly be seen in the connections between the column and the pontoons.

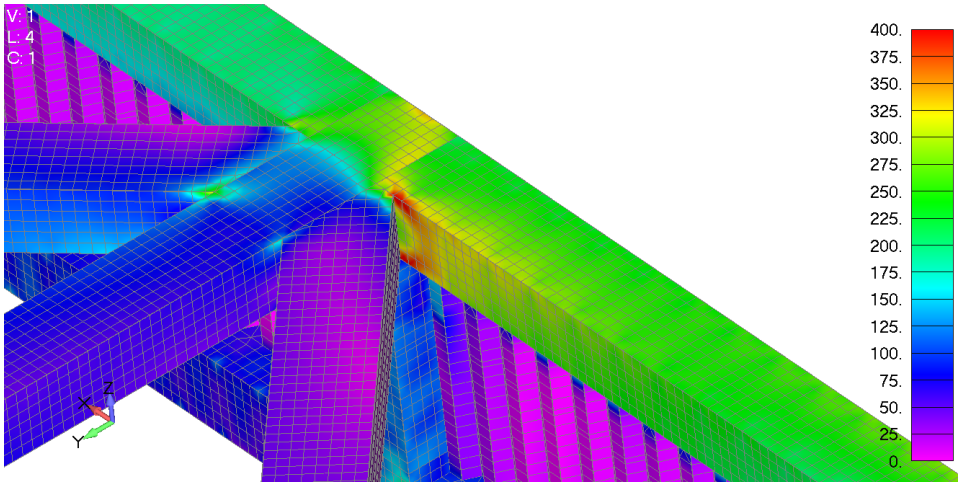

Figure 6.38: Stresses in the starboard side small column between fish pen **compartment 2 and 3** seen from port side. Stress concentrations can clearly be seen in the connections between the column and the pontoons.

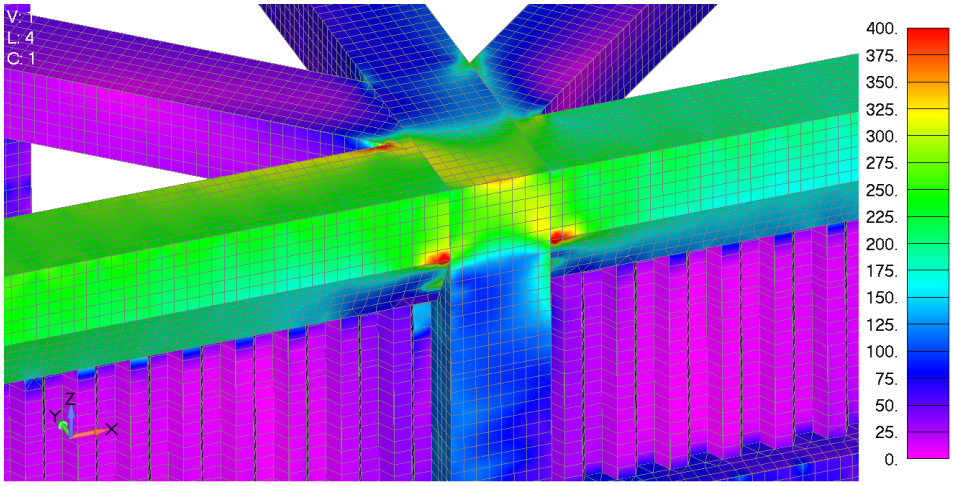

Figure 6.39: Stresses in the starboard side small column between fish pen **compartment 2 and 3** seen from starboard side. Stress concentrations can clearly be seen in the connections between the column and the pontoons.

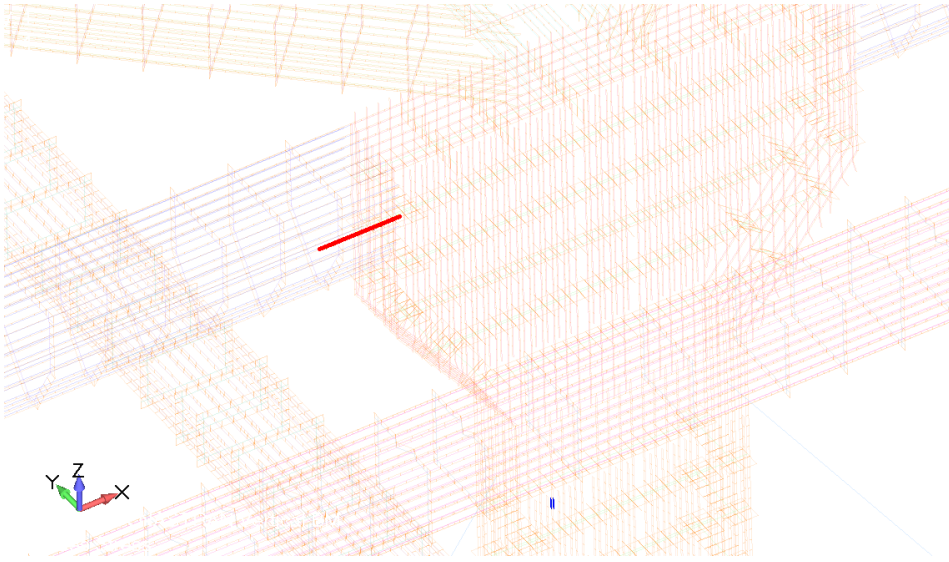

Figure 6.40: Evaluated stiffener in connection with longitudinal top pontoon and column between fish pen **compartment 3 and 4** when subjected to EDW 3

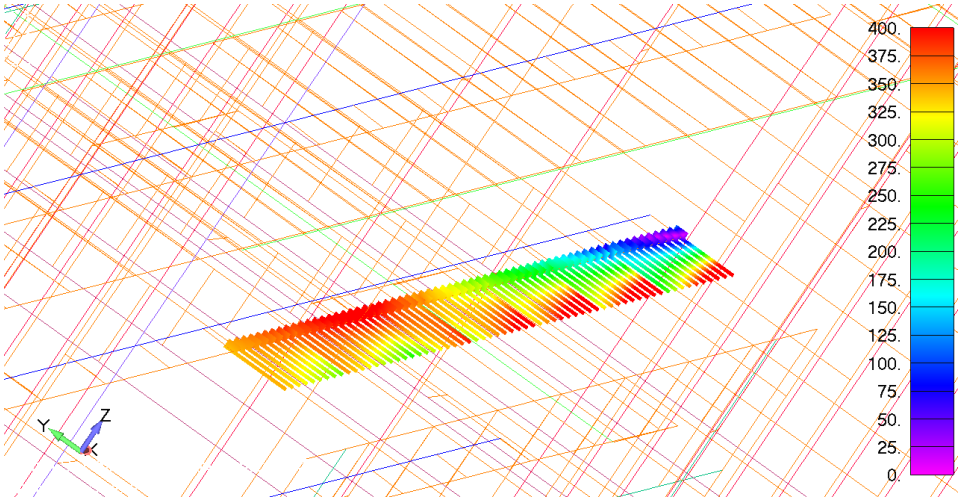

Figure 6.41: Von mises stresses in evaluated stiffener indicated in figure 6.40

6.5 Conclusion and Proposals

Based on the results presented in the previous sections it is clear that the Havfarm structure, with dimensions as described in chapter 5 and table 5.8, do not have

sufficient capacity to avoid yielding when subjected to neither the ULS vertical bending moment, horizontal bending moment or torsional moment.

For the load case where the extreme vertical bending moment is targeted it is clear that the top and bottom longitudinal pontoons, both plating and stiffeners, are severely over-stressed in compartment 5 with stresses exceeding 400 [MPa] as indicated in figure 6.20. To lower the stresses in the pontoons and to avoid yield it is proposed to increase the plating thickens as well as the stiffener dimensions in the top and bottom pontoons.

Further it is also seen that the connections between the top longitudinal pontoons and the different columns will experience high stress concentrations. It is suggested that a refined mesh for these areas are established for a detailed analysis. However the current model is quite detailed and thus it is expected that a refined mesh will yield the same results more or less. To avoid these stress concentrations it is suggested to add large brackets to the connections between the top longitudinal pontoons and the columns. This will help to transfer the loads in the pontoons and into the columns ensuring a smooth stress pattern without large stress concentrations. Alternatively a redesign of the connections removing sharp connections could be a good option to avoid the high stress concentrations.

Also the sharp connections with the diagonal top pontoons should be reinforced with brackets or re designed to avoid high stress concentrations.

A refined mesh of the connections with the braces between the middle and bottom pontoon, indicated in figure 6.26 and 6.27, should be established in order to properly evaluated the stresses in this areas.

Chapter 7

End Remarks

The goal for this thesis was to perform a global analysis on the Havfarm fishfarm concept for exposed waters. This involved boulding both a hydromodel for seakeeping analysis and a structural model for FE analysis. This proved to be very time consuming, mainly due to several reasons. One was the use of new software and the other the fact that the design have been subjected to updates continousely and the models were rebuilt/updated in order to represent the current/latest design. However I am very satisfied with the finale models. Evaluations of the seakeeping analysis with simple calculations for the natural periods of the Havfarm seems to be in good agreement. Also when the motion RAOs are compared with results obtained by NSK Ship Design they are in good agreement.

As described in the thesis some simplifications had to be made. This include neglecting the lice skirts as well as the fish nets. Further it was assumed in the long term estimation of ULS value of the internal loads that each heading of the incoming sea had equally large possibility. For a long time it was made an attempt to include the swell and wind sea in the long term analysis of the vertical bening moment. In the end i didn't manage to do so and it was decided to only evaluate the swell sea to simplify the analysis in the thesis. All these assumptions introduces uncertanties to the analysis to some degree. For example if one heading can be ruled out, say the incoming waves from the 135^o, this will probably lower the ULS vertical bending moment value and thus change the results of the FEA. This will have to be investigated further in order to make a more precise evaluation of the Havfarms capacity.

However, the results described in chapter 6.4 indicates that the Havfarm will experience severe stresses exceeding yield stresses for normal steel in large part of

the top and bottom pontoons when the EDW targeting ULS vertical bending moment is applied. Also high stress concentrations are detected in the connections with the top longidudinal pontoons and the colomns in particular. These stresses concentrations exceeds 600 [MPa]. This shows that the Havfarm structure do not have sufficient capacity to survive the ULS loads. In order to reduce the stresses in general and it avoid the high stress concentrations it is proposed to increase the scantlings in the structure and evaluate how to improve the sharp cornered connections in order to avoid high stress concentrations.

7.1 Further Work

A hydrodynamic and a structural model have been established and a global analysis targeting extreme internal loads corresponding to ultimate limit state have been performed in this thesis. Hopefully this should help to point out areas which needs to be strengthened in order to survive an ULS sea state. In order to fully to validate the Havfarm structure there remains a lot of work. A list of suggestions to further work on this project is given below.

- **Model**
  - An updated model should be established based on updated drawings and scantlings form NSK Ship Design to in order to validate the capacity of the latest design.
  - Point masses of deck loads and fish pelets (fish food) should also be added to the model in order to get a better weight distribution.
  - Validation of the model should be performed. For example the structures motion RAOs calculated by Homer should be compared with results from model test when/if such results is made available.
  - When elements for modelling of lice skirts and fish nets in the hydromodel are made available in Homer/Hydrostar the Hydro-model should be updated.
  - A model of a typical transverse section of the Havfarm should be established in Mars and the strength of the transverse section verified. This will also be a god way to controll the ULS stresses obtained in the FE analysis.
- **Ultimate limit state**
  - The estimation of the extreme internal loads was based on the metocean data for swell sea only. In addition it was assumed that the azimut of the Havfarm was ranging from 0^o to 345^o with an increment of 15^o

and to have equal probability. To further validate the structures response and ULS internal loads the wind sea should be included in the analysis.

  - A directional heading analysis of the Havfarm in the area where it will be located, should be performed in order to obtain the correct azimuths(with corresponding probability) of the Havfarm relative to the incoming waves. This will probably affect the prediction of ULS of internal loads.

- **Fatigue calculations**

  - With the complete model of the Havfarm structure established it is also possible to perform fatigue and life time calculations with Homer.

- **Miscellaneous**

  - Bureau Veritas already have a set rules for classification and certification of fishfarms [5], even for exposed waters. It is suggested that the structure i validated according to these rules.

Bibliography

[1] al., L. G. P. e., 2010. An overview of aquaculture in the nordic contries. Journal of the World Aquaculture Society 41 (1).

[2] Aqua, H., 2016. Technology for sustainable growth in aquaculture. URL http://www.haugeaqua.com

[3] Borge, J., 2017. Metoceanstudie for lokaliteten hadseløya. Report 10675, Multiconsult.

[4] Bureau-Veritas, -. Selected hydro-structure publications.

[5] Bureau-Veritas, 1994. Rules for the classification and certification of fish-farms.

[6] Bureau-Veritas, 2011. Rules for the classification of steel ships - part b hull and stability.

[7] Bureau-Veritas-Research-Department, 2014. Hydrostar for experts user manual.

[8] de Hauteclocque, B.-V.-M.-D. G., 2013. Starspec user guide.

[9] Design, N. S., 2016. Nsk - 3417 offshore fish farm. URL http://www.nskshipdesign.com/designs/aquaculture/fish-farm/

[10] DNVGL-RP-C103, 2015. Column-stabilised units.

[11] Faltinsen, O., 1993. Sea loads on ships and offshore structures. Vol. 1. Cambridge university press.

[12] fiskeridepartementet, N.-o., 2011. Forskrift om krav til teknisk standard for flytende akvakulturanlegg (nytek-forskriften).
URL https://lovdata.no/dokument/SF/forskrift/2011-08-16-849

[13] Goudey, C., 2001. Mitigating the environmental effects of mariculture through single-point moorings (spms) and drifting cages. ICES Journal of Marine Science 58 (2), 497–503.

[14] Haver, S. K., 2013. Prediction of characteristic response for design purposes rev 5, preliminary version, Statiol document.

[15] Hersoug, B., Andreassen, O., Johnsen, J. P., Robertsen, R., 2014. Hva begrenser tilgangen på sjøareal til havbruksnæringen? Report 10675, Nofima.
URL http://hdl.handle.net/10037/8003

[16] Jensen, O., Dempster, T., Thorstad, E. B., Uglem, I., Fredheim, A., 2010. Escapes of fishes from norwegian sea-cage aquaculture: causes, consequences and prevention. Aquaculture Environment Interactions 1 (1), 71–83.
URL <GotoISI>://WOS:000292392600008

[17] Korsøen, O. J., Dempster, T., Fjelldal, P. G., Oppedal, F., Kristiansen, T. S., 2009. Long-term culture of atlantic salmon (salmo salar l.) in submerged cages during winter affects behaviour, growth and condition. Aquaculture 296 (3-4), 373–381.

[18] Kristiansen, T., Faltinsen, O. M., 2012. Modelling of current loads on aquaculture net cages. Journal of Fluids and Structures 34, 218–235.

[19] Lader, P., Dempster, T., Fredheim, A., Jensen, O., 2008. Current induced net deformations in full-scale sea-cages for atlantic salmon (salmo salar). Aquacultural Engineering 38 (1), 52–65.

[20] Langen, I., 1979. Dynamisk analyse av konstruksjoner. Tapir, Trondheim.

[21] Løland, G., 1991. Current forces on and flow through fish farms. Dkotor, Norges Tekniske Høgskole.

[22] Løland, G., 1993. Current forces on, and water flow through and around, floating fish farms. Aquacultural International 1, 72–89.

[23] Malenica, S., 2007. Hydro structure interactions in seakeeping. In: International Workshop on Coupled Methods in Numerical Dynamics.

[24] NORSOK-N-001, 2012. Integrity of offshore structures.

[25] NORSOK-N-003, 2007. Actions and action effects.

[26] NORSOK-N-004, 2013. Design of steel structures.

[27] Norway, S., 2015. Akvakultur, 2015, foreløpige tall.
URL https://www.ssb.no/jord-skog-jakt-og-fiskeri/statistikker/fiskeoppdrett

[28] NS-9415, 2009. Marine fish farms requirements for site survey, risk analyses, design, dimensioning, production, installation and operation.

[29] SalMar, 2016. Offshore fish farming – a new era!
URL http://www.salmar.no/en/offshore-fish-farming-a-new-era

[30] Shainee, M., Leira, B. J., Ellingsen, H., Fredheim, A., 2013. An optimum design concept for offshore cage culture. Proceedings of the Asme 31st International Conference on Ocean, Offshore and Artic Engineering, Vol 7, 85–93.
URL <GotoISI>://WOS:000324507000011

[31] Siemens, -. Element library reference.
URL https://docs.plm.automation.siemens.com/data_services/resources/nxnastran/10/help/en_US/tdocExt/pdf/element.pdf

[32] Standard.no, 2016. Petroleum.
URL http://www.standard.no/en/sectors/energi-og-klima/petroleum/

[33] Stensvold, T., 2016. Riggeksperter i aker solutions lanserer nytt merdkonsept.
URL http://www.tu.no/artikler/riggeksperter-i-aker-solutions-lans346030

[34] Sveälv, T., 1988. Inshore versus offshore farming. Aquacultural Engineering 7 (4).
URL http://ac.els-cdn.com/0144860988900271/1-s2.0-0144860988900271-main.pdf?_tid=4ba99cba-7f3d-11e6-886a-00000aab0f6c&acdnat=1474381372_e90e7cac4239a10199d9f42b61e2a66f

[35] Sveälv, T., 1991. Strategies and technologies in offshore farming. Fisheries Research 10, 329–349.

Appendix A

Metocean Data

5.4.2 Operasjonelle forhold - Dønning

Bølgerosen for dønning ved Hadseløya basert på den konstruerte tidsserien for perioden 1955 - 2007 er vist i Figur 24. Bølgeretningen av opptredende dønning er fra vest. Bølgeklimaet varierer med årstiden (Tabell 22).

Tabell 22 viser kumulativ sannsynlighetsfordeling av signifikant bølgehøyde av dønning for de tre relevante sektorene (240°, 270°, 300°) for hele året og de fire årstidene. Omtrent 30 % av tiden er det ikke dønning ved lokaliteten. Analysene viser at den signifikante bølgehøyden av dønning er mindre enn 2 m 91.7 % av tiden. Om vinteren er andelen av tiden med Hs mindre enn 2 m 83.34% mens den om sommeren er hele 98.73 %. Varigheten av perioder med Hs over visse grenser er gitt i Tabell 23. Perioder med signifikant bølgehøyde over 2 m kan vare lengre enn 48 timer omtrent to ganger i året tilsvarende 1.85 % av tiden.

Simultanfordelingen av signifikant bølgehøyde og topperioden av dønning er gitt i Tabell 24. Topperioden av dønning er under 12 s 91.6 % av tiden (inkludert tiden det ikke er dønning). De høyeste dønningene forventes å ha topperioder på mellom 12 og 16 s. Det vil kunne opptre dønning med lengre perioder på 16 s omtrent 0.2 % av tiden. Det foreligger bølgespektra for alle 140 tilfeller som er kjørt med bølgemodellen (se avsnitt 4.3.1). Det er gitt et eksempel av et dønningspektrum ved lokaliteten Hadseløya i Figur 25. Det er ikke gjort tilpasninger til idealiserte spektra som JONSWAP.

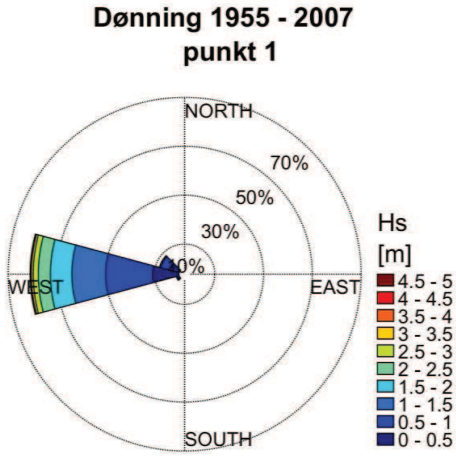

Figur 24 Dønning ved Hadseløya (1955-2007)

Tabell 22 Dønning: Kumulativ sannsynlighetsfordeling [%] for signifikant bølgehøyde for 3 retningssektorer, dønning opptrer ikke fra andre sektorer enn 240°, 270° og 300°, angitt for data fra hele året, og fire årstider, 1955-2007

Hele året					**Vinter (Des-Feb)**				**Vår (Mar-Mai)**			
Hs [m]	Alle ret.	240°	270°	300°	Alle ret.	240°	270°	300°	Alle ret.	240°	270°	300°
0	29.47	-	-	-	24.18	-	-	-	31.44	-	-	-
<0.50	45.73	1.20	10.78	4.28	38.93	0.95	11.29	2.51	48.32	1.54	10.02	5.31
<1.00	68.5		30.06	7.77	58.62		27.7	5.79	69.91		27.61	9.32
<1.50	82.86		43.85	8.34	72.51		41	6.39	84.32		41.33	10
<2.00	91.70		52.67	8.36	83.34		51.8	6.42	93.21		50.19	10.03
<2.50	96.65		57.62		92.16		60.61		97.56		54.55	
<3.00	98.73		59.70		96.92		65.38		99.13		56.11	
<3.50	99.58		60.55		98.89		67.35		99.77		56.76	
<4.00	99.91		60.88		99.75		68.2		99.93		56.92	
<4.50	100		60.97		99.99		68.45		100		56.99	
<5.00	100		60.97		100		68.45					

Sommer (Jun-Aug)					**Høst (Sep-Nov)**			
Hs [m]	Alle ret.	240°	270°	300°	Alle ret.	240°	270°	300°
0	35.27	-	-	-	26.89	-	-	-
<0.50	52.71	0.93	10.92	5.59	42.84	1.37	10.9	3.68
<1.00	79.8		35.48	8.12	65.5		29.41	7.83
<1.50	93.78		49.25	8.34	80.66		43.79	8.6
<2.00	98.73		54.2		91.4		54.51	8.62
<2.50	99.83		55.29		96.99		60.11	
<3.00	99.97		55.44		98.87		61.99	
<3.50	100		55.46		99.64		62.75	
<4.00					99.94		63.06	
<4.50					99.99		63.11	
<5.00					100		63.12	

Tabell 23 Dønning: Varighet av perioder med signifikant bølgehøyde kontinuerlig over enn viss høyde

Antall hendelser per år								Maksimal varighet [h], 1955-2007
Hs [m]	Varighet							
	>6 h	>12 h	>18 h	>24 h	>36 h	>48 h	>72 h	
>0.0	49.49	43.77	39.62	36.87	32.28	28.32	22.81	1464
>0.5	64.34	54.57	47.72	42.66	34.38	28.06	20.19	792
>1.0	58.74	47.85	39.42	32.96	23.06	16.32	9.11	420
>1.5	40.08	30.45	23.98	18.94	11.94	7.77	3.34	294
>2.0	24.11	16.6	12.23	8.45	4.32	2.3	0.72	168
>2.5	11.6	7.11	4.13	2.55	0.85	0.4	0.09	102
>3.0	4.75	2.53	1.11	0.55	0.13	0.06	0	60
>3.5	1.66	0.55	0.21	0.04	0	0	0	30
>4.0	0.23	0.06	0	0	0	0	0	18
>4.5	0	0	0	0	0	0	0	6
>5.0	0	0	0	0	0	0	0	0
Prosent av tiden								
Hs [m]	Varighet							
	>6 h	>12 h	>18 h	>24 h	>36 h	>48 h	>72 h	
>0.0	69.92	69.13	68.28	67.52	65.81	63.77	59.84	1464
>0.5	52.95	51.61	50.2	48.81	45.7	42.47	36.84	792
>1.0	29.92	28.43	26.69	24.92	21.2	17.75	12.61	420
>1.5	15.93	14.61	13.28	11.89	9.27	7.14	4.06	294
>2.0	7.36	6.33	5.43	4.4	2.88	1.85	0.78	168
>2.5	2.82	2.2	1.59	1.15	0.53	0.3	0.09	102
>3.0	0.97	0.67	0.38	0.22	0.08	0.04	0	60
>3.5	0.28	0.13	0.06	0.01	0	0	0	30
>4.0	0.03	0.01	0	0	0	0	0	18
>4.5	0	0	0	0	0	0	0	6
>5.0	0	0	0	0	0	0	0	0

Tabell 24 Dønning: Simultanfordeling [%] av signifikant bølgehøyde Hs og topperiode Tp, 29.47 % av tiden er det ikke dønning ved Hadseløya

Hs [m]	Tp [s]								Sum
	<6	6-8	8 -10	10-12	12-14	14-16	16-18	>18	
0.0-0.5	1.77	6.04	4.28	2.57	1.13	0.35	0.10	0.03	16.26
0.5-1.0	1.28	7.26	7.65	4.58	1.63	0.32	0.04	0.01	22.77
1.0-1.5	0.16	3.64	5.49	3.83	1.06	0.18	0.01	0.00	14.36
1.5-2.0	0.00	1.08	4.01	2.74	0.88	0.14	0.00	0.00	8.84
2.0-2.5	0.00	0.16	1.74	2.01	0.94	0.10	0.00	0.00	4.95
2.5-3.0	0.00	0.06	0.28	0.97	0.63	0.14	0.00	0.00	2.08
3.0-3.5	0.00	0.03	0.03	0.37	0.36	0.07	0.00	0.00	0.85
3.5-4.0	0.00	0.01	0.00	0.05	0.22	0.04	0.00	0.00	0.33
4.0-4.5	0.00	0.01	0.00	0.00	0.04	0.04	0.00	0.00	0.09
4.5-5.0	0.00	0.00	0.00	0.00	0.00	0.00	0.00	0.00	0.00
Sum	3.21	18.28	23.48	17.12	6.88	1.37	0.15	0.04	70.53
Maksimal Hs [m], 1955-2007	1.4	4.5	4.1	4.5	4.6	4.4	2.5	0.7	

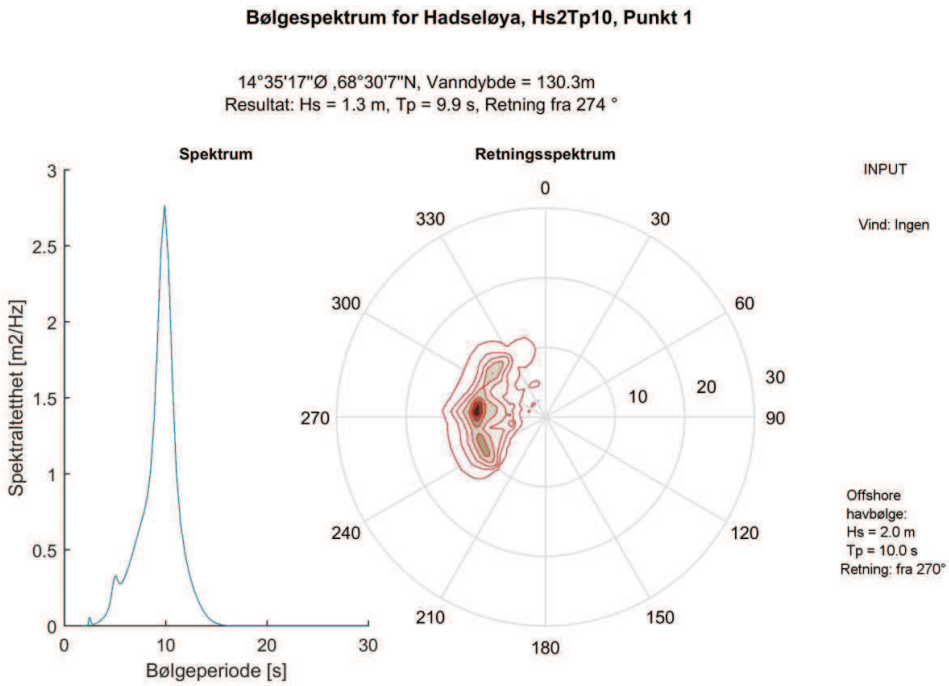

Figur 25 Eksempel dønningspektrum for offshore dønning med signifikant bølgehøyde på 2 m, med topperiode på 10 s

Appendix B

Motion and Acceleration RAOs

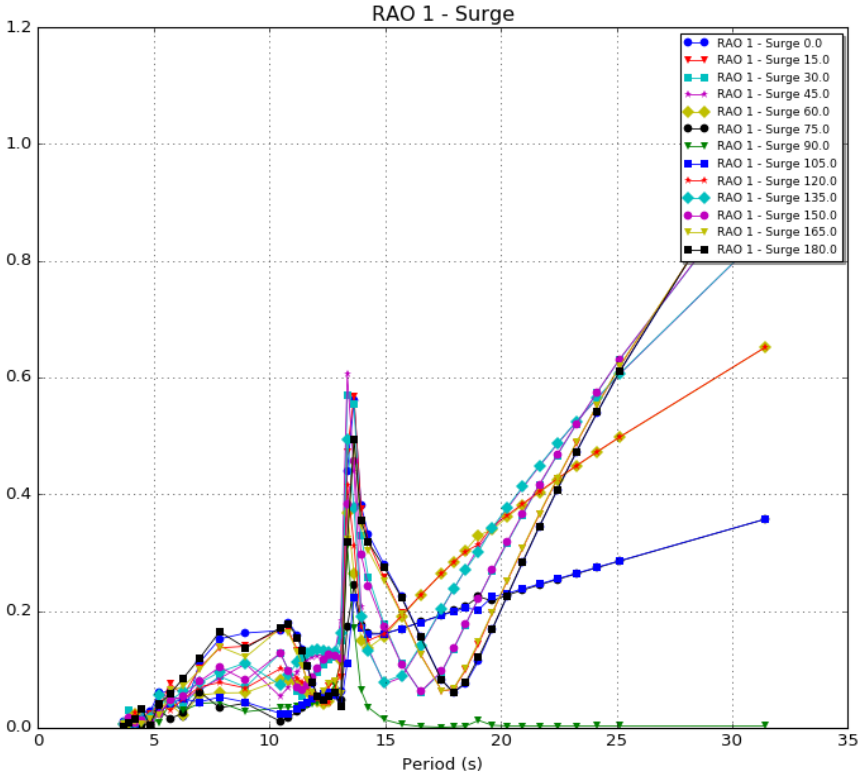

Figure B.1: Response Amplitude Operatior for surge motion

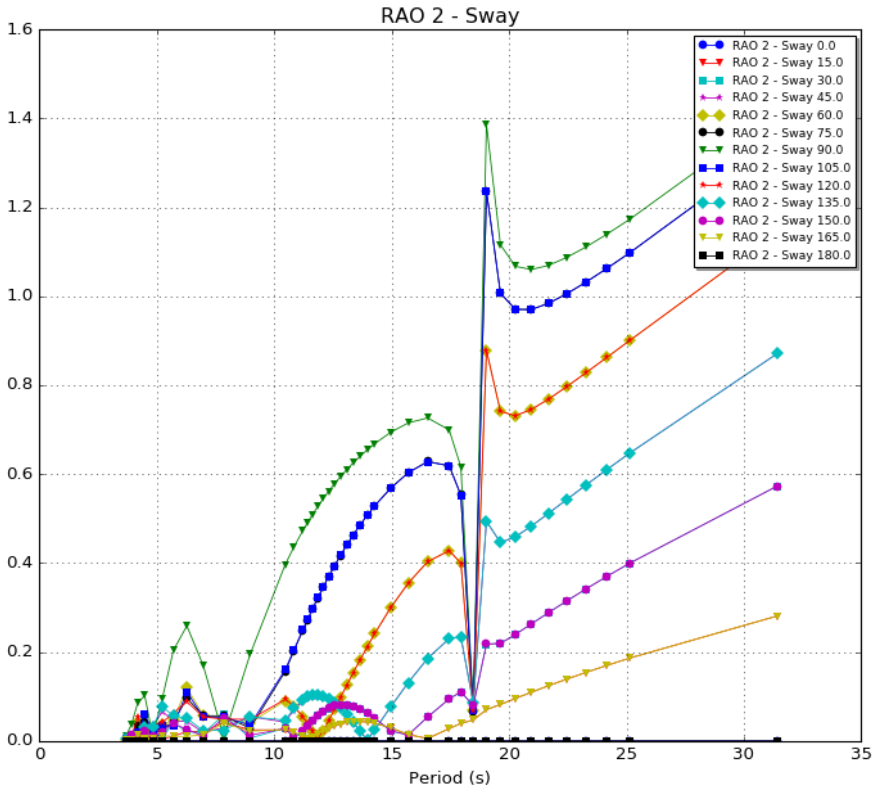

Figure B.2: Response Amplitude Operatior for sway motion

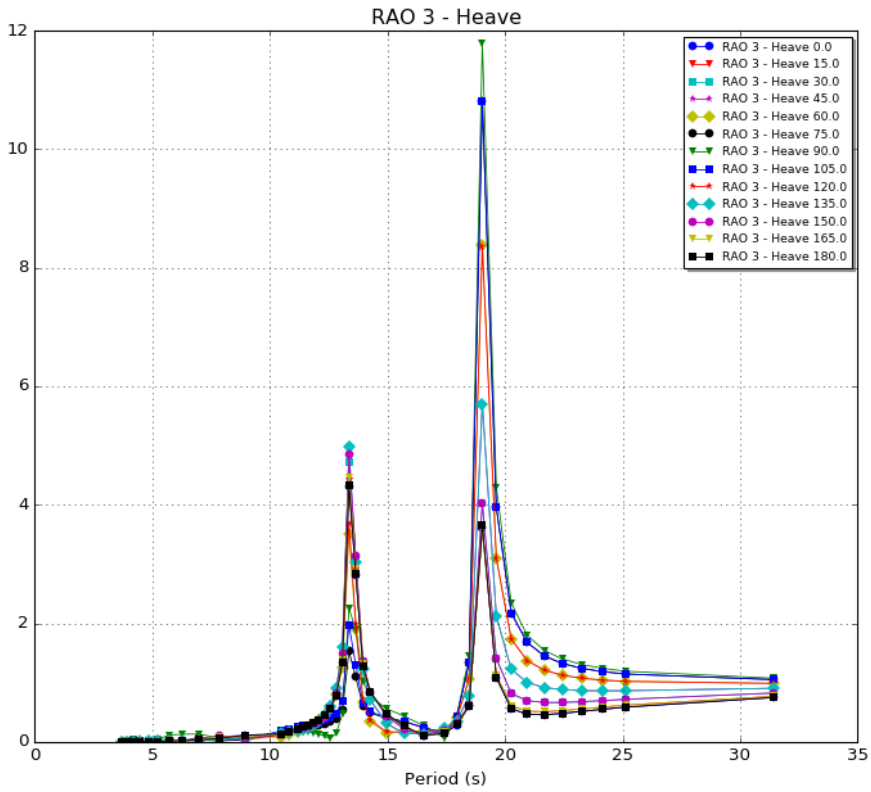

Figure B.3: Response Amplitude Operatior for heave motion

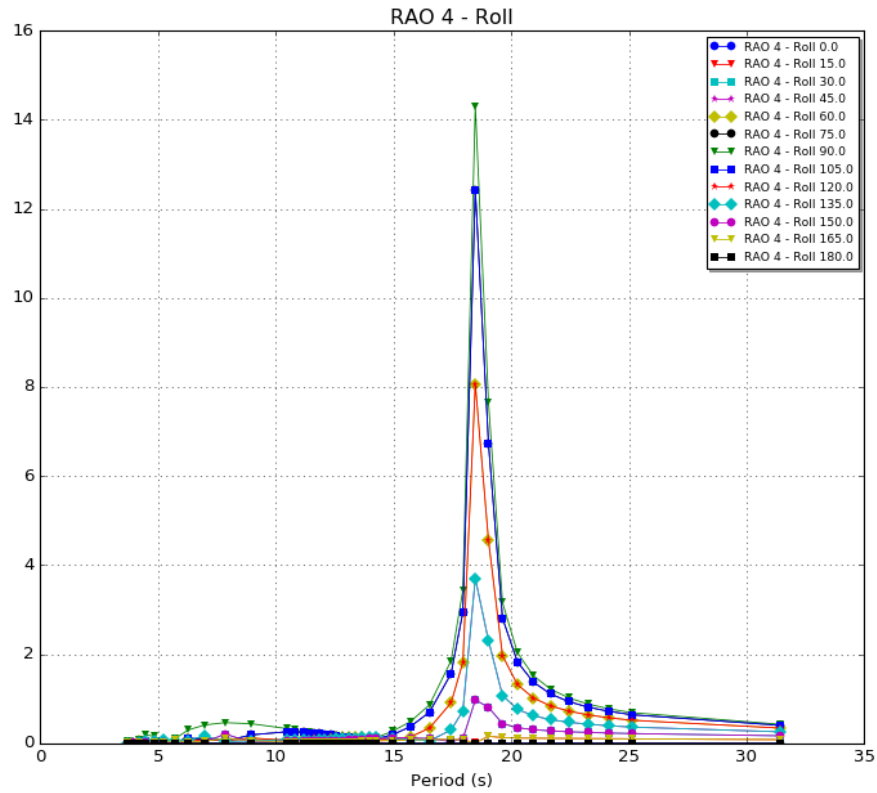

Figure B.4: Response Amplitude Operatior for roll motion

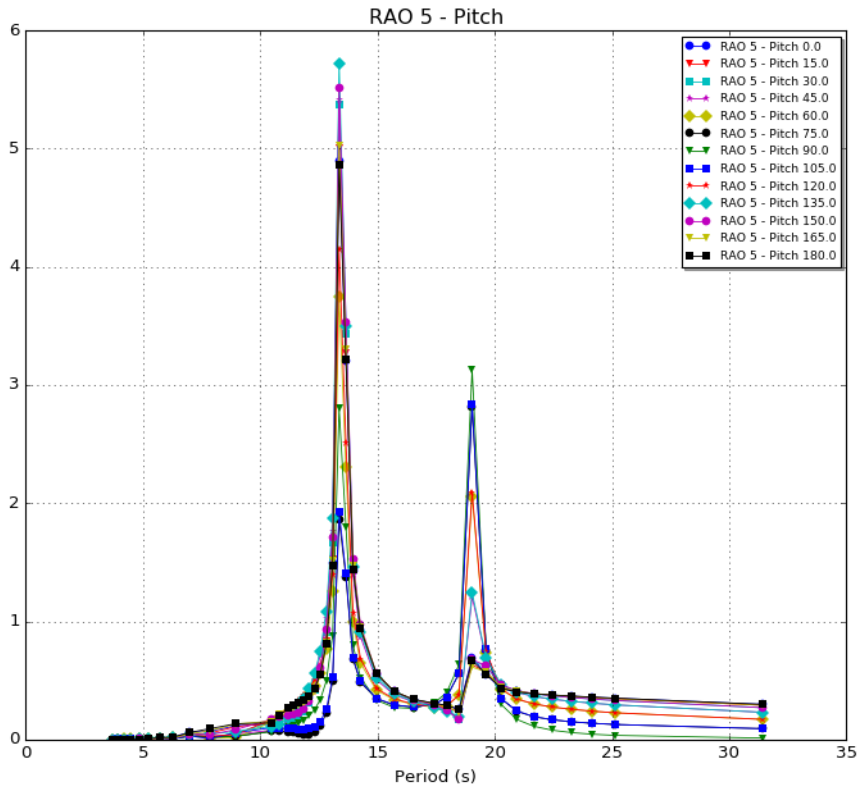

Figure B.5: Response Amplitude Operatior for pitch motion

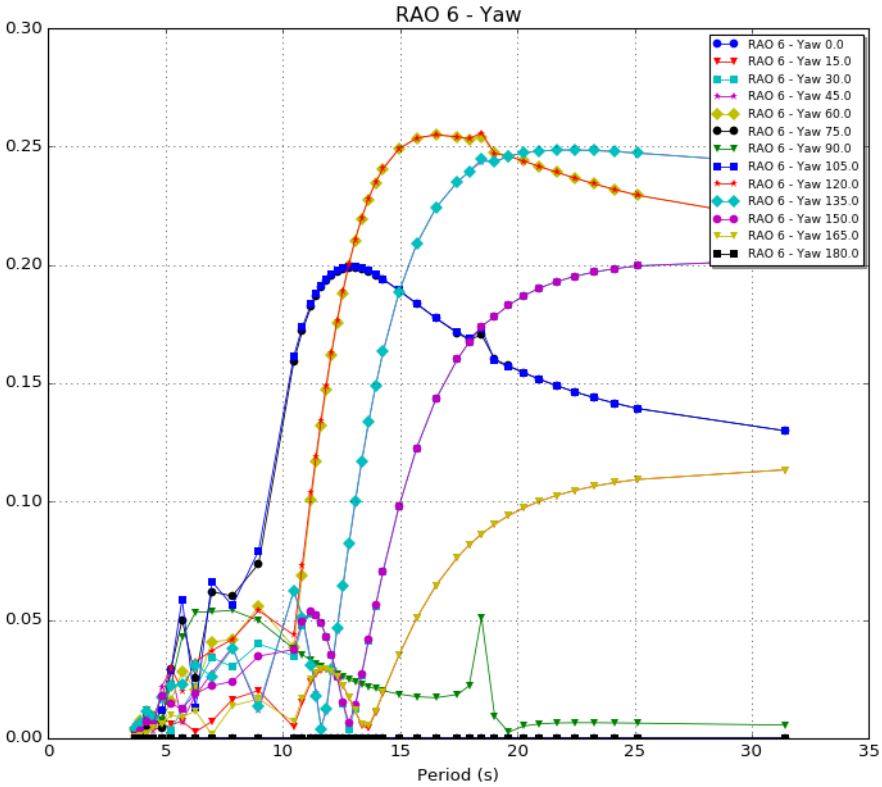

Figure B.6: Response Amplitude Operatior for yaw motion

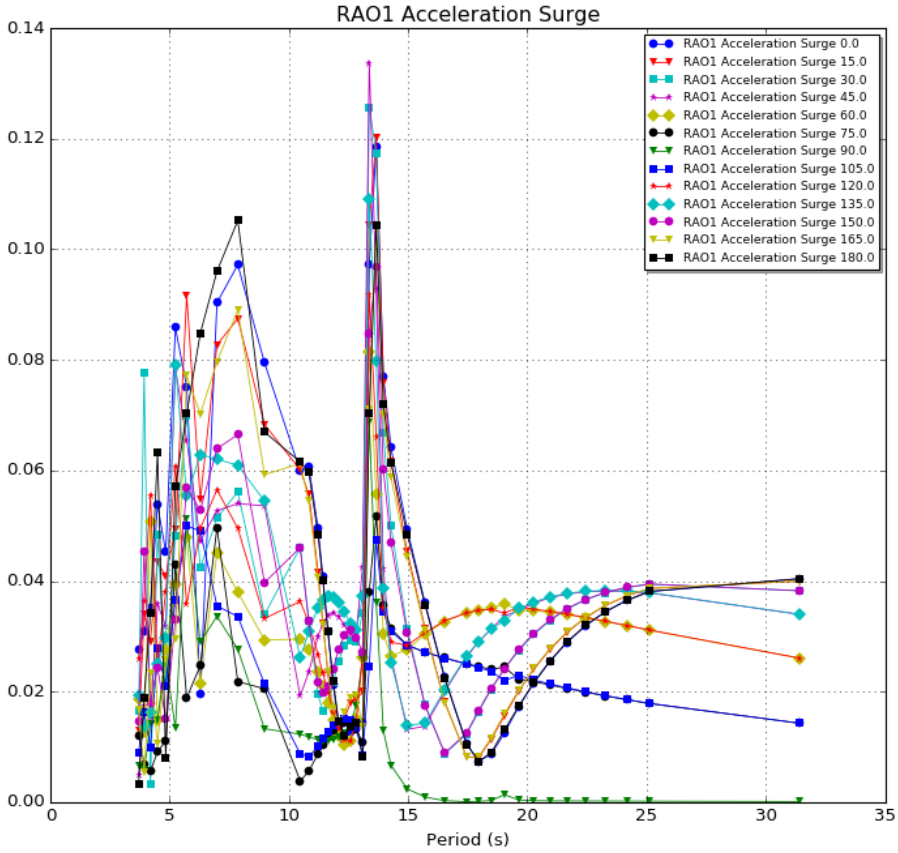

Figure B.7: Response Amplitude Operatior for surge acceleration

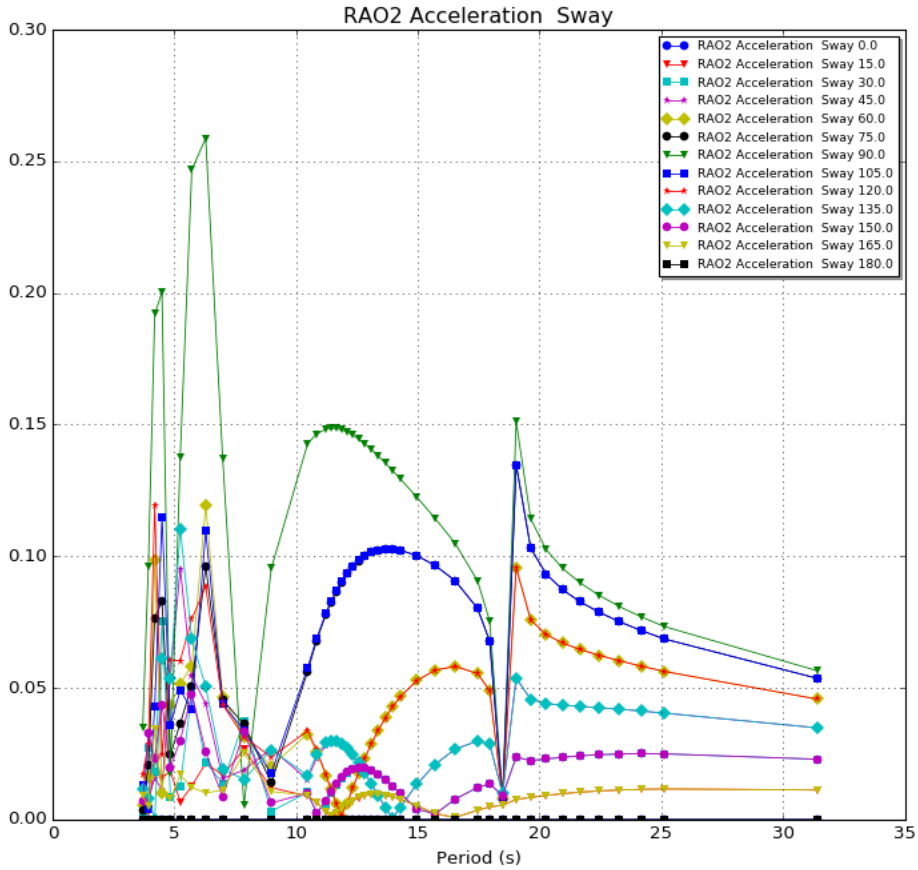

Figure B.8: Response Amplitude Operatior for sway acceleration

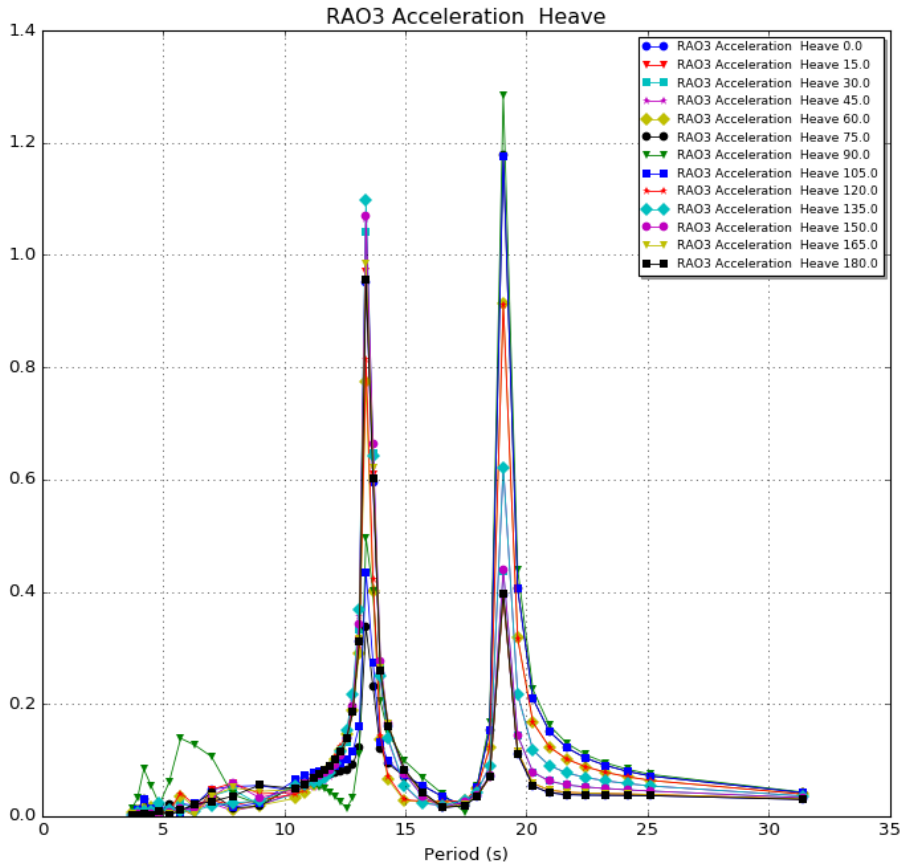

Figure B.9: Response Amplitude Operatior for heave acceleration

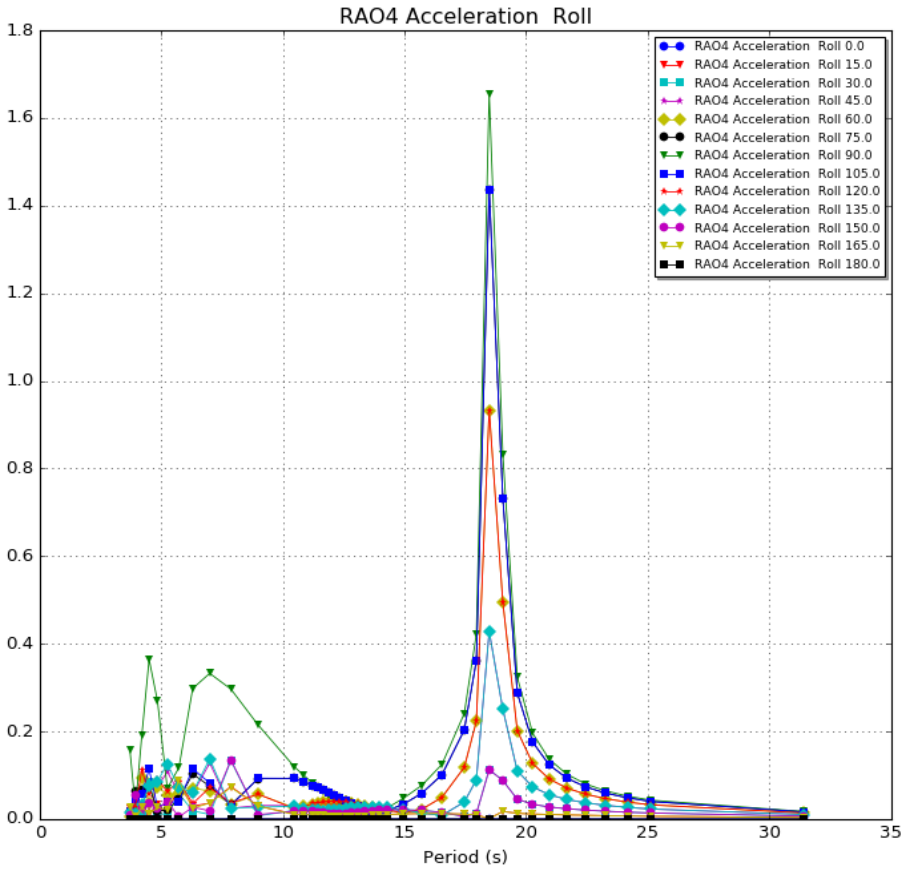

Figure B.10: Response Amplitude Operatior for roll acceleration

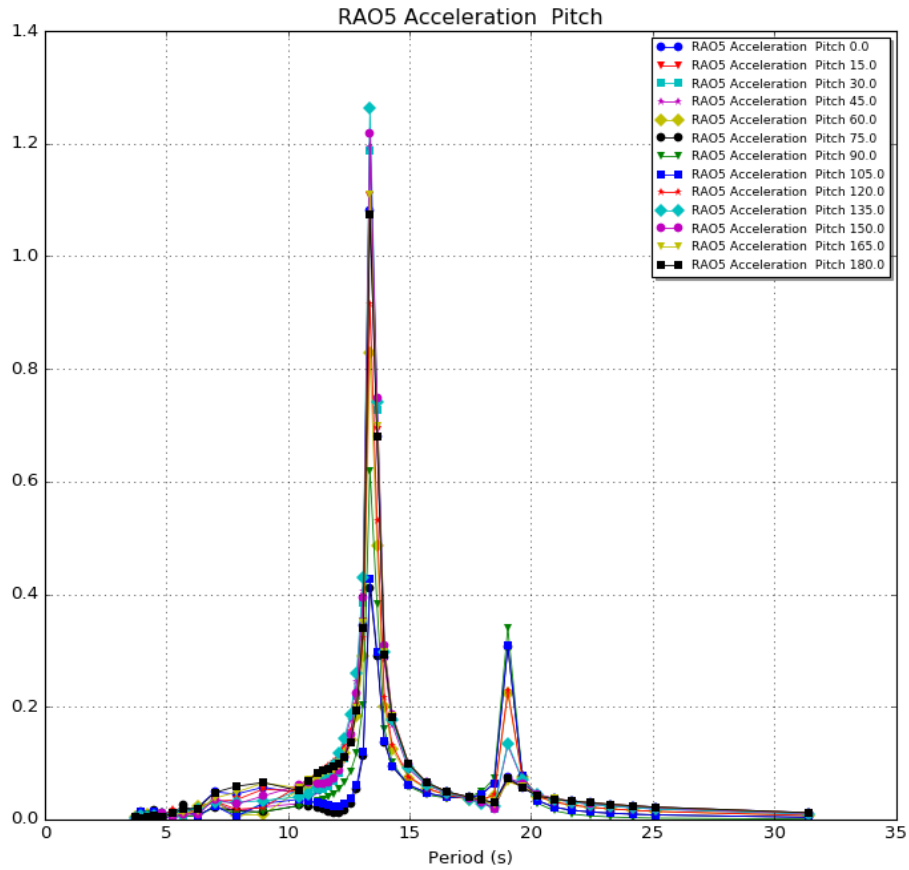

Figure B.11: Response Amplitude Operatior for pitch acceleration

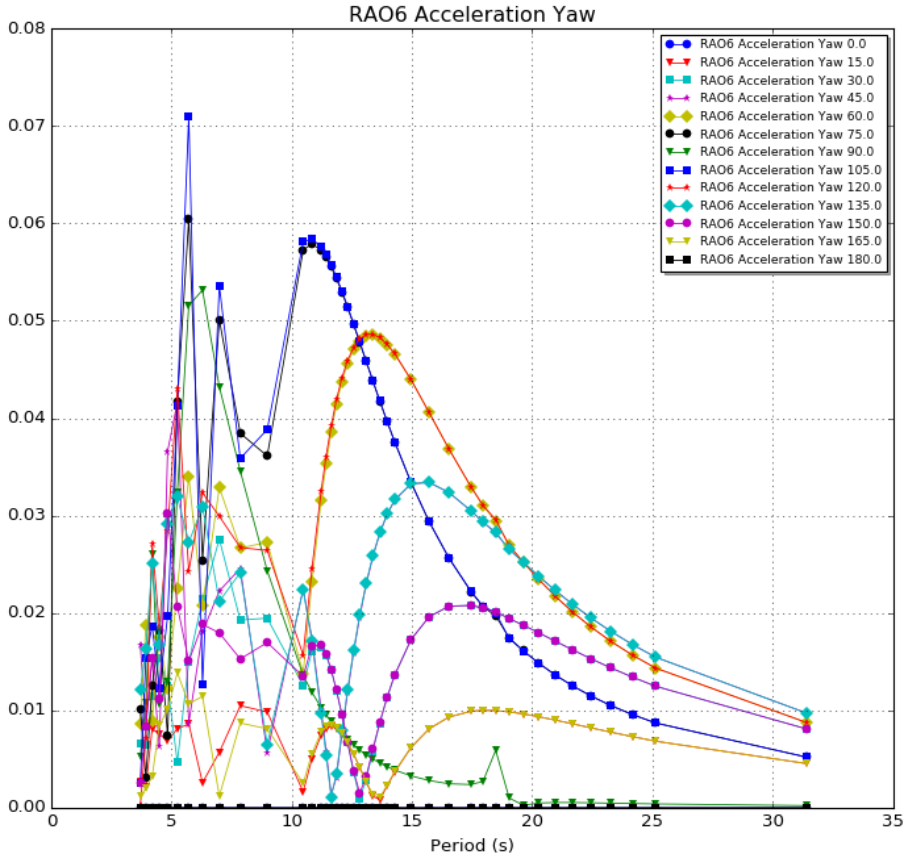

Figure B.12: Response Amplitude Operatior for yaw acceleration

Appendix C

Internal Load RAOs

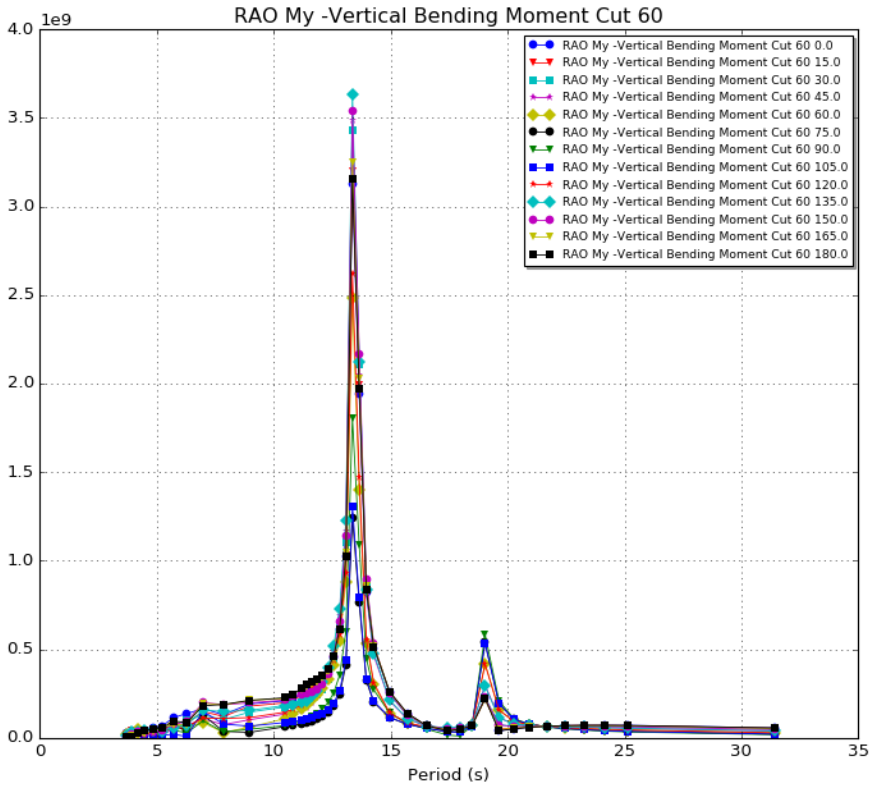

Figure C.1: Response Amplitude Operator for Vertical Bending Moment at cut 60, y-axis unit [Nm]

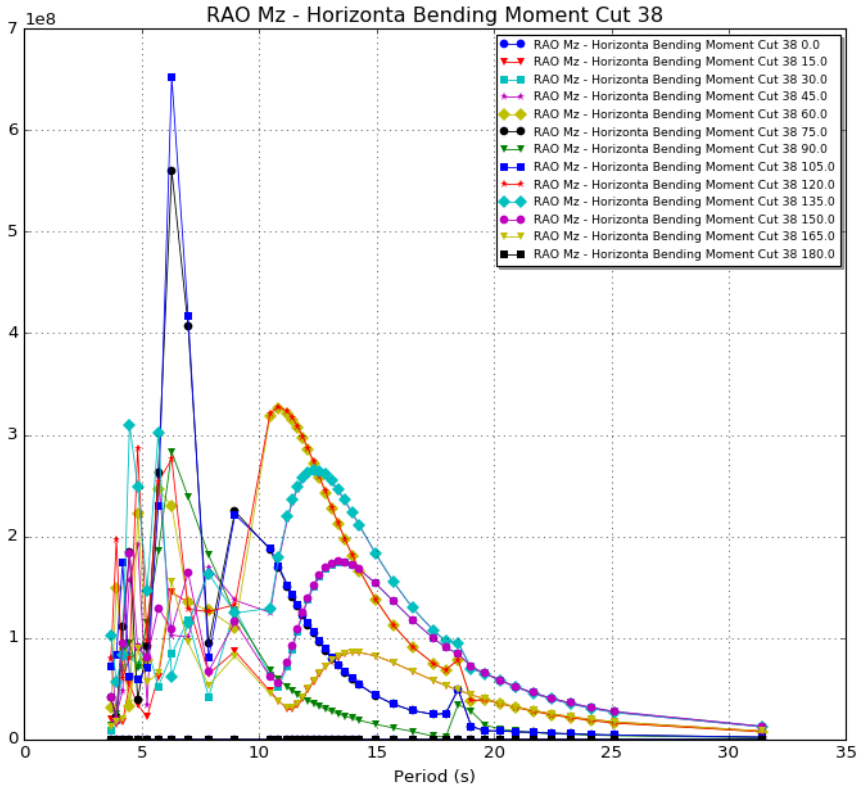

Figure C.2: Response Amplitude Operator for Horizontal Bending Moment at cut 38, y-axis unit [Nm]

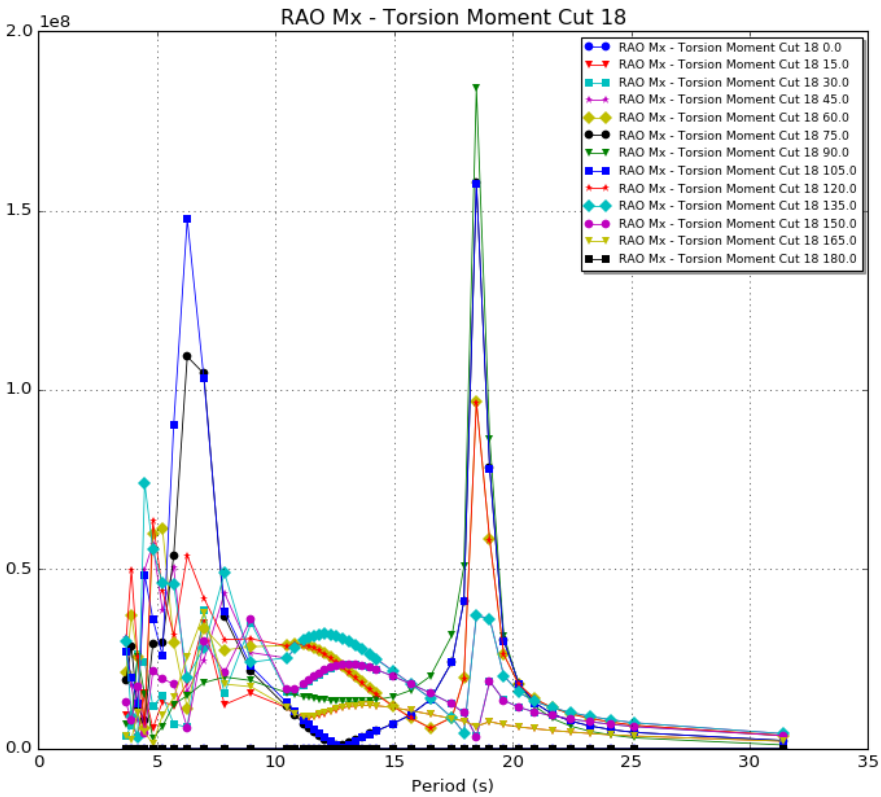

Figure C.3: Response Amplitude Operator for Torsional Moment at cut 18, y-axis unit [Nm]

Appendix D

Motion RAOs from NSK Ship Design

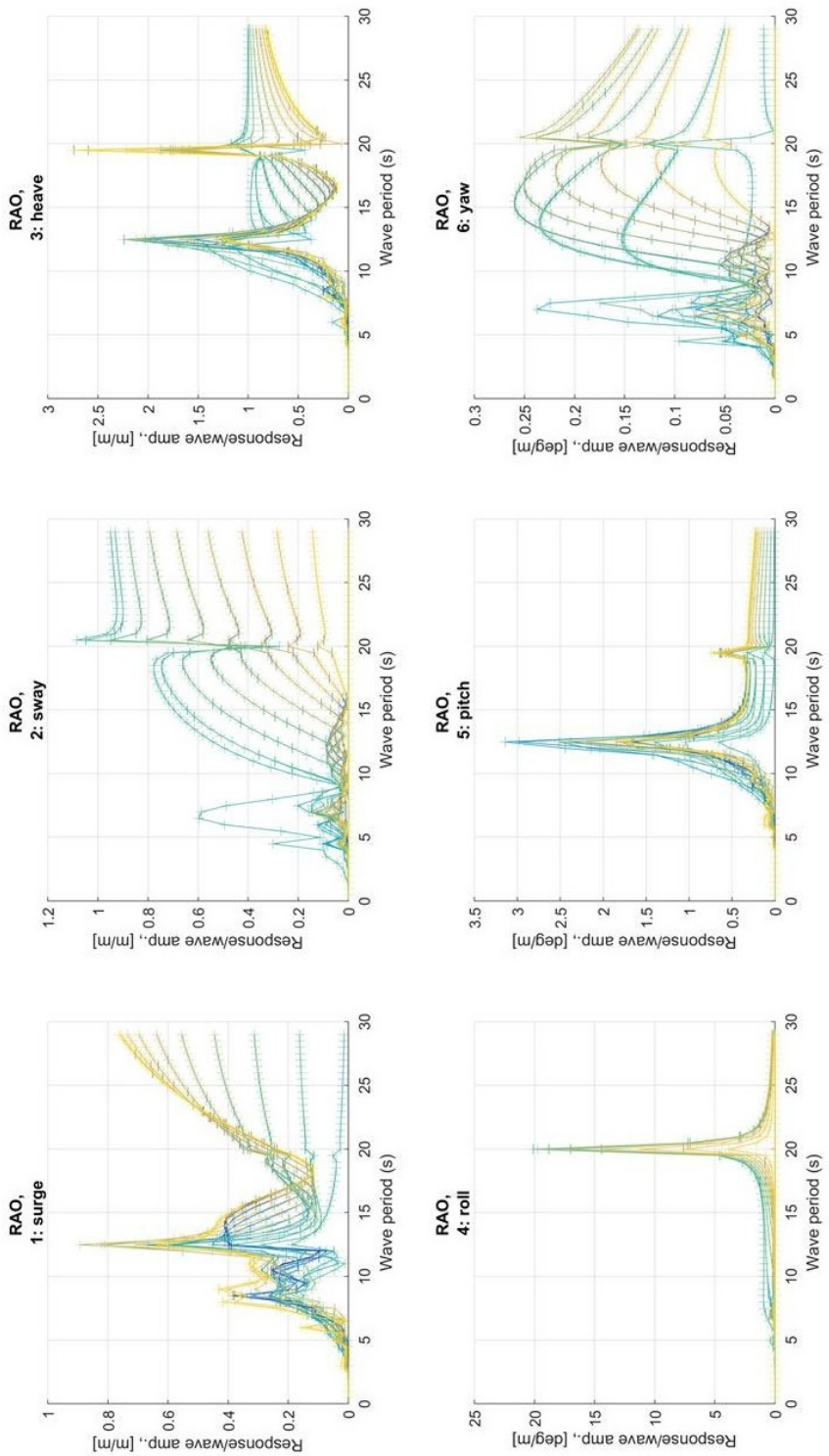
RAO,
1: surge
RAO,
2: sway
RAO,
3: heave
RAO,
4: roll
RAO,
5: pitch
RAO,
6: yaw
Response/wave amp., [m/m]
Response/wave amp., [deg/m]
Wave period (s)
0
10
20
30
40
50
60
70
80
90
100
110
120
130
140
150
160
170
180